The Dissertation Committee for Sean Gregory Trettel Certifies that this is the approved version of the following dissertation:

Grid cell co-activity patterns remain stable across different behavioral states and experiences

Committee:

Laura Lee Colgin, Supervisor

Ila Fiete

Daniel Johnston

Michael Mauk

Rick Aldrich

Grid cell co-activity patterns remain stable across different behavioral states and experiences

by

Sean Gregory Trettel

Dissertation

Presented to the Faculty of the Graduate School of

The University of Texas at Austin

in Partial Fulfillment

of the Requirements

for the Degree of

Doctor of Philosophy

The University of Texas at Austin

December 2017

Dedication

To my friends and family, who have supported me through everything.

Acknowledgements

There are many people who have supported me and my work through the years. First and foremost, I would like to thank Dr. Laura Lee Colgin, my supervisor and mentor, who's continued support and encouragement saw me through to the end. Dr. Ila Fiete has been a second mentor to me, and has always been there to help and encourage me. I would also like to thank the other members of my committee – Drs. Daniel Johnston, Rick Aldrich and Michael Mauk – for their guidance and suggestions. This project wouldn't be what it was without them.

I would next like to thank my lab-mates for many great and interesting discussions, their invaluable help, and unwavering support. They have all lent hands when I needed it and been there to celebrate the successes and forget the failures.

I want to thank my friends and family, who's unwavering support has meant so much to me over the years. To my parents in particular -- you have done so much to help me, and asked for nothing in return but that I do my best. To my best friend Daniel -- You have helped so much in keeping my spirits high when things get difficult, been there to celebrate the victories and never once questioning whether I could achieve anything I put my mind to.

Finally, I want to pay special thanks to my fiancée Kylie. You have done so much to keep me going. Your understanding and kindness during the long nights of recording or writing, picking up dinner when there wasn't time to cook, and making sure I remembered to take a break every once in a while, all mean the world to me.

Grid cell co-activity patterns remain stable across different behavioral states and experiences

Sean Gregory Trettel, Ph.D.

The University of Texas at Austin, 2017

Supervisor: Laura Lee Colgin

Grid cells in the medial entorhinal cortex have been well studied while animals are exploring their environment; however, what they do when an animal is not navigating is less clear. Other cell types in the entorhinal-hippocampal network appear to have memory-related activity when an animal is inactive, so what grid cells do during quiescence is an important question. If grid cells show activity similar to place cells during rest and sleep, then it would imply that grid cells play an active role in memory functions rather than simply providing current sensory information to the hippocampus. Models have been proposed that make testable predictions about grid cell activity when spatial input is absent. The continuous attractor network model of grid cell pattern formation posits that grid cell patterning is a result of network connections between grid cells. As a result of this connectivity, these models hypothesize that grid cell co-activity patterns should be

the same during sleep as during active navigation. In my first study, I investigated how spike time correlations between grid cell pairs during sleep compared to spike time correlations between the same grid cell pairs during waking activity. I found that the same correlation patterns were present regardless of whether spatial information was available to grid cells (i.e., during active navigation) or whether sensory input was absent (i.e., during sleep). These results support the continuous attractor network model hypothesis. In my second study, I examined whether novel experience changed grid cell co-activity patterns during active waking behaviors, rest, and sleep. I found that spike time correlations between grid cell pairs remained stable across behavioral states regardless of experience. In my last study, I looked at organized sequences of firing in grid cell ensembles to examine whether small changes in correlations led to detectable changes in more complex ensemble representations of experience. I found that grid cell ensemble activity did not appear to be influenced by different behaviors or novel experience. Taken together, these results suggest that grid cells are part of a low-dimensional, continuous attractor network and that grid cell activity patterns during sleep reflect connections in the grid cell network rather than representing specific experiences.

Table of Contents

List of Tables

List of Figures

Chapter 1: Introduction

A major question in neuroscience research is “How do we remember what we’ve experienced?” There have been a number of theories and studies investigating the origin of memories, how memories are strengthened and stored after experience, and what regions of the brain are required for memories to form and persist. One of the primary regions implicated in the formation of new memories of experiences is the hippocampus. In humans, much of what is known about the role of the hippocampus in memory formation resulted from studies of patient H.M. (Corkin 1965; Milner et al 1968; Scovile & Milner, 1957), who had bilateral removal of much of his hippocampus to treat drug-resistant epileptic seizures. While patient H.M. could remember many of the experiences he had long before his surgery, he was unable to form memories of new experiences (Scovile & Milner, 1957). The bilateral excision of his hippocampus also resulted in significant spatial memory deficits, more so than patients with a single lobe of the hippocampus removed (Corkin 1965; Smith & Milner, 1981). Later studies using MRI to verify the extent of patient H.M.’s lesions showed extensive damage to the entorhinal cortex as well (Corkin et al. 1997).

Studies of the hippocampus in rodents have found that hippocampal neurons show a strong response to an animal’s position in an environment (O’Keefe & Dostrovsky, 1971), suggesting a role for the hippocampus in coding of spatial locations. Also, lesion studies in primates (Parkinson et al. 1988) and rodents (Morris et al, 1982; Moser et al. 1993) have supported a requirement for the hippocampus in spatial learning and memory.

Less work has been done to understand whether the major cortical structure that provides input to, and receives output from, the hippocampus, the medial entorhinal cortex (MEC), plays a role in memory. However, neurons that fire in specific spatial locations, namely grid cells (Hafting et al, 2005), have been found in the medial entorhinal cortex, suggesting that the medial entorhinal cortex plays a role in representing space and perhaps also in the processing of spatial memories.

It has been theorized that hippocampal firing patterns during active behaviors store memory traces that are temporary and that consolidation of these memories into long-term storage sites in the neocortex occurs during sleep (Buzsaki 1996; Squire & Zola-Morgan 1991). However, this theory remains controversial, in part because it lacks much direct experimental support (Rasch and Born, 2013). For example, the entorhinal cortex is the interface between the hippocampus and the neocortex, and yet little to nothing is known about whether neuronal representations of earlier experiences are activated in the entorhinal cortex during sleep.

In the studies described herein, I set out to fill this gap in knowledge by recording from ensembles of grid cells in the medial entorhinal cortex during awake spatial exploratory behaviors and overnight sleep. I investigated the extent to which correlations between grid cell firing patterns during sleep were explained by specific co-activity patterns during earlier waking experiences. The pattern of results suggests that grid cell co-activity patterns do not change as a result of specific behaviors or experiences. Instead, the results suggest that a grid cell network is a low-dimensional attractor network: low-dimensional because the grid cell activity co-varies as the animal moves through

space, and an attractor because the grid cell response is stable across long time scales, environments, and behavioral states.

1.1 – THE MEDIAL ENTORHINAL CORTEX CIRCUIT

The main brain area containing grid cell networks is the medial entorhinal cortex. I begin this chapter by explaining its anatomical organization. An understanding of the connectivity of the medial entorhinal cortex is necessary for developing plausible theories regarding the potential role of grid cell networks in spatial memory operations.

1.1.1 Entorhinal-cortical connections

The rat MEC receives a majority of its cortical input from the postrhinal, secondary motor, and secondary sensory areas (Burwell & Amaral 1998a,b). From these areas the MEC receives highly processed sensory information, with a large portion of the inputs coming from the visual associational areas and the primary visual cortex (Burwell & Amaral 1998a). The MEC also receives a significant amount of input from the primary and secondary somatosensory areas and the retrosplenial cortex (Burwell & Amaral 1998a). Similar findings have been reported in the primate as well (Insausti et al. 1987; Van Hoesen et al 1972). These cortical inputs primarily land in the superficial layers of the MEC (layers II and III). Because of these diverse sensory inputs coming in to the areas which then project on to the hippocampus, it is believed that the medial entorhinal cortex provides current, highly processed, sensory information to the hippocampus. In addition, the deep layers of the entorhinal cortex process much of the output of the hippocampus and then project back to the neocortex, primarily back to associational

areas, particularly the parietal and occipital cortices, and to the frontal and prefrontal cortices (Insausti et al 1997).

1.1.2 Entorhinal – hippocampal connections

The entorhinal cortex projects to all areas of the hippocampus (Figure 1.1). In particular, layer II projects to the dentate gyrus and CA3, while layer III projects directly to CA1 (Steward & Scoville 1976). Layer II projections to the dentate gyrus and CA3 travel along the perforant path, landing in stratum lacunosum moleculare (SLM) in CA3,

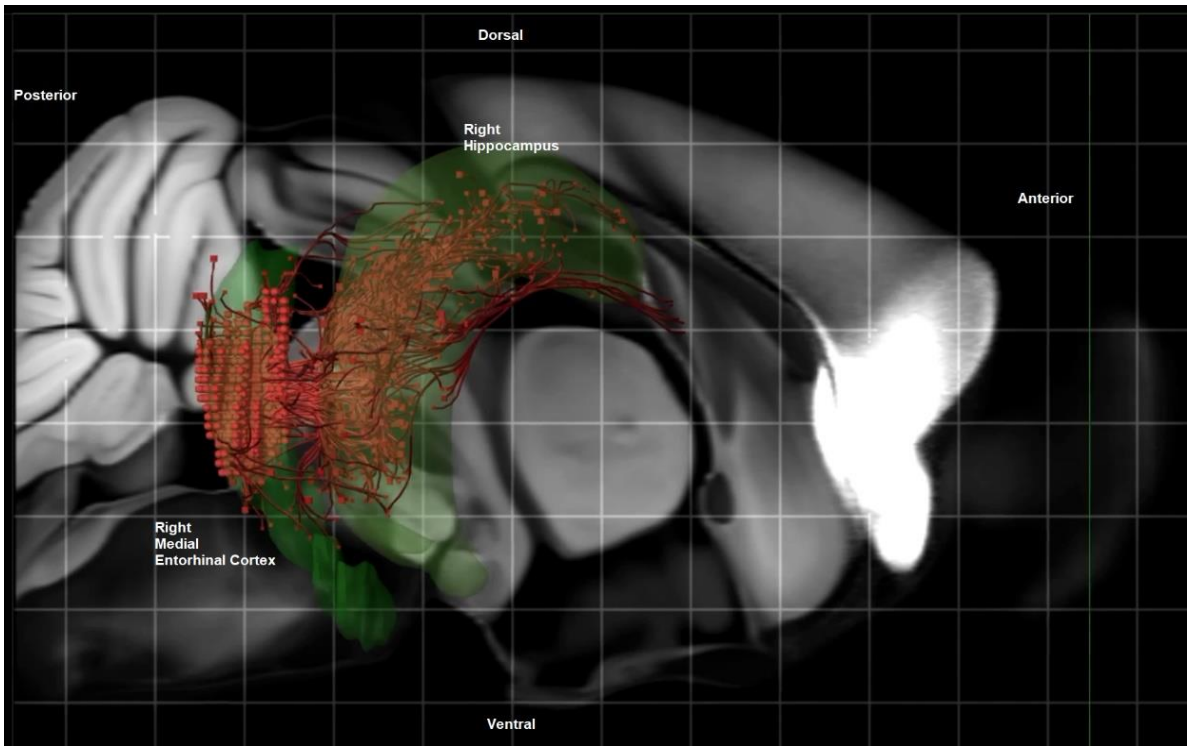

Figure 1.1 – Anatomical connections from MEC to the hippocampus. The MEC has many connections throughout the hippocampus, as illustrated here. The MEC is the green region to the left, and the hippocampus is the larger lighter green region to the right. The spheres in the MEC represent the origin of the projections to both the ipsilateral and contralateral hippocampus. The red/orange lines represent the connections between the MEC and the hippocampus.

the distal region of the dendrites, and the outer stratum moleculare of the dentate gyrus (Schwartz & Coleman, 1981; Steward & Scoville, 1976). Layer III projections to CA1 also project through the perforant path and land in SLM of CA1 (Steward & Scoville 1976). Each region of the hippocampus thus receives information directly from MEC, and CA3 and CA1 receive MEC inputs that have been further processed by the dentate gyrus or CA3, respectively.

The hippocampus also projects back to the entorhinal cortex. Specifically, subiculum and CA1 project primarily to layer V, with some additional projections to layer III (Saunders & Rosene, 1988; Van Groen et al, 1986; Van Groen & Wyss, 1990; Witter et al. 2000). Projections from both CA1 and the subiculum generally appear to land on cells in the entorhinal cortex that do not project back to the hippocampal formation (Witter et al. 2000). The intrinsic connections of the MEC close the circuit between the superficial layer projections to the hippocampus and the hippocampal projections to the deep layers of the MEC (Canto & Witter 2012; Dolforo & Amaral 1998). The deep layers of the MEC project widely throughout the superficial MEC, while the superficial layers project to more localized areas in the superficial MEC (Dolorfo & Witter, 1998; Köhler, 1986).

1.1.3 Functional interactions between the hippocampus and MEC

Studies of hippocampal and entorhinal function have also shown a strong interdependent relationship between the hippocampus and entorhinal cortex. The entorhinal cortex, particularly the MEC, is required for the stability and specificity of hippocampal place representations and spatial learning (Hales et al. 2014). Lesions of the entorhinal cortex lead to unstable hippocampal representations of space after

repeated exposure to the same environment (Hales et al. 2014; Van Cauter et al. 2008). In addition, animals were less able to learn the Morris water maze task, and were less able to adapt to water maze reconfiguration after learning (Hales et al. 2014). In addition, inactivation of the hippocampus leads to a reduction of the spatial specificity of MEC grid cells, with grid cells becoming selective for head direction (Bonnevie et al. 2013).

1.1.4 Coordinating communication between the hippocampus and MEC: local field potential oscillations of the hippocampal circuit

There are several important oscillation patterns in the local field potential of the hippocampal circuit. These oscillations are thought to organize communication between different areas by providing a mechanism by which populations of cells have coordinated periods of relatively heightened excitability. Therefore, inputs during these periods are more likely to elicit temporally coordinated spikes across different cells (Colgin et al, 2009; Mizuseki et al. 2009). During active exploratory behavior, there is a strong, sustained ~6-10 Hz oscillation in the local field potential called the theta oscillation (Figure 1.2a). Theta is also prominent during REM sleep (Figure 1.2b). The occurrence of theta is hypothesized to indicate periods when the hippocampus is taking in information from the entorhinal cortex (Buzsaki 1989).

During periods when theta is absent, the hippocampal formation has short, punctate, irregularly occurring periods of heightened cellular activity and large amplitude local field potentials (LFPs), characterized by a single sharp deflection followed immediately by a high-frequency (~180-250 Hz) “ripple” oscillation (sharp-wave ripple, or SWR). These SWRs are most prominent during awake rest and NREM sleep, although

they do occur during grooming, drinking, and eating as well (Buzsaki et al. 1983). SWRs are believed to play a role in learning and memory consolidation. Disruption of waking SWRs leads to decreased spatial learning (Jadhav et al. 2012), and SWRs have been shown to correlate with synchronized reactivation of learning related patterns in the hippocampus and prefrontal cortex (Peyrache et al. 2009). SWRs are believed to originate in CA3 and propagate through the entorhinal-hippocampal network to the superficial layers of the entorhinal cortex (Chrobak & Buzsaki 1996; MEC SWR shown in

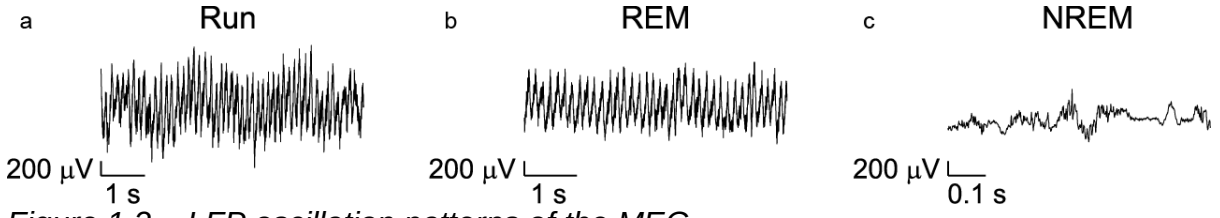

Figure 1.2 – LFP oscillation patterns of the MEC.

a) Theta oscillations (6-10 Hz) during exploratory activity, recorded in the superficial layers (II / III) of the MEC.
b) Theta oscillations during REM sleep are slightly lower frequency, on average, when compared to waking activity.
c) Entorhinal sharp wave recorded in layer II of the MEC.

Figure 1.2c). Also, SWRs have been observed to co-occur with cortical sleep spindles (Sirota et al. 2003) and are thought to coincide with the hippocampal output to cortex (Buzsaki 1989).

1.2 – PLACE CELLS, GRID CELLS, AND OTHER SPATIALLY RESPONSIVE CELLS IN THE ENTORHINAL-HIPPOCAMPAL CIRCUIT

1.2.1 Place cells

Place cells are spatially responsive cells located in the hippocampus that are active in one or a very small number of locations in an environment (O'Keefe & Dostrovsky,

1971). Place cells can have fields in multiple different environments, but relationships between place cells are not static across environments (Muller & Kubie 1987). This results in a high-dimensional representation of an environment through the firing of a unique subset of place cells. Place cells' firing is sensitive to even small changes in an environment, with small changes of parts of an environment leading to changes in firing rate (called "rate remapping") and more significant changes to the environment leading to complete changes in field location or even cells losing or gaining fields (called "global remapping") (Anderson & Jeffery, 2003; Bostock et al. 1991; Muller & Kubie 1987).

A linear track environment can be used to make place cells generate a specific and repeatable firing sequence, as an ensemble of place cells will have fields spanning the length of the track and will therefore fire sequentially as an animal traverses the track trajectory. Such sequences have been used to investigate the potential role of place cells in memory consolidation by looking for repetition of firing sequences from waking behaviors during later periods of sleep and rest (Foster & Wilson, 2006; Lee & Wilson, 2002; Louie & Wilson 2001; Nadasdy et al. 1999). Such reactivation of sequences believed to represent earlier experiences has been called "replay", and replay has been hypothesized to be a mechanism for consolidating recently acquired memories (Bendor & Wilson, 2012; Ego-Stengel & Wilson, 2010; Girardeau et al. 2009; Jadhav et al. 2012; Lee & Wilson, 2002; Nadasdy et al. 1999).

1.2.2 Grid cells

Grid cells are a spatially responsive functional cell type located in the MEC (Hafting et al. 2005). They have multiple regions in space in which they are active, and these regions (firing fields) are organized in a triangular grid pattern across the environment (Figure 1.3). Grid cells are located throughout the MEC but are most highly concentrated in the superficial layers, particularly layer II (Sargolini et al. 2006). Grid cells are part of discretized modules, which share the same grid orientation (orientation angle of the grid with respect to the environment) and the same field size and spacing (spatial period) (Stensola et al. 2012). Where the grid cells of a module differ is the position of their fields in relation to the environment (termed "spatial phase"). Cells in the same module, therefore, would look like copies of each other, shifted in the X and/or Y directions. The modules are organized along the dorso-ventral axis of MEC, with modules with the

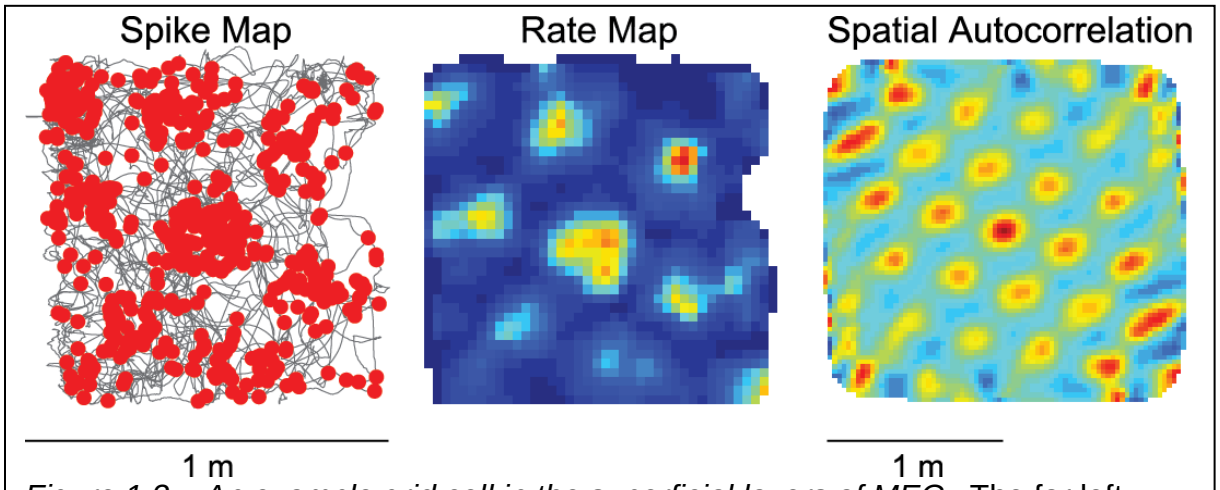

Figure 1.3 – An example grid cell in the superficial layers of MEC. The far left panel shows the spike map of the example grid cell, with each red dot representing the animal's location where a spike occurred, while the gray line represents the animal's trajectory over a 20 minute session in the open field. The middle panel shows the firing rate map, binned into 3 cm bins with spike counts in each bin normalized by the time spent in that bin. The right panel shows the spatial autocorrelation map, in which the rate map of a cell is compared to shifted versions of itself, highlighting periodic spatial patterns in its firing fields.

smallest grid spacings located the most dorsally. Many grid cells, particularly in MEC layers III and V, additionally have significant head direction selectivity (Sargolini et al. 2006). Also, grid cells that do not normally show head direction responsiveness will begin to respond to head direction when excitatory drive from the hippocampus (Bonnevie et al. 2013) or cholinergic inputs from the medial septum (Brandon et al. 2011; Koenig et al. 2011) are reduced.

1.2.3 Head direction cells, speed cells, time cells, and border cells

There are several other functional cell types located in the hippocampal and parahippocampal circuit that are important for navigation. These include head direction cells (Sargolini et al. 2006; Taube et al. 1990), speed-modulated cells (Ahmed & Mehta 2012; Kropff et al. 2015; Sun et al. 2015; Zheng et al. 2015), and border cells (Solstad et al. 2008). Together, these cells make up a circuit that is believed to be important for spatial navigation. All of these cell types can be found in the MEC, though border (Solstad et al 2008) and head direction cells (Taube et al 1990) are also present in other neighboring regions, such as the postsubiculum (both head direction and border cells) and the thalamus (head direction cells). Models of grid cells hypothesize that grid cells require head direction and speed information to maintain the network (Burak & Fiete 2008), and, accordingly, many grid cells code head direction and speed information (Figure 1.4). Border cells have been hypothesized to provide error correction information to grid cells (Hardcastle et al 2015).

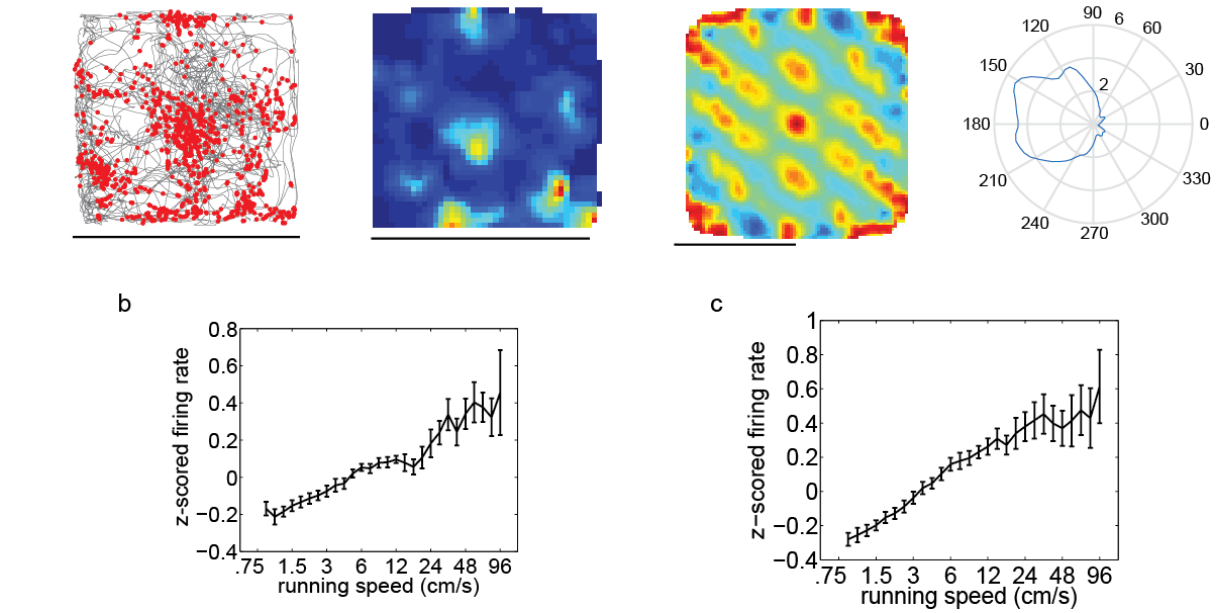

Figure 1.4 – Speed and head direction sensitive grid cells.

A) An example of a conjunctive grid-head direction cell, showing both grid patterning (left three panels) and head direction selectivity (right panel). Scale bars in the left three panels are 1 m. The right-most plot shows the average firing rate as a function of head direction, with radial lines indicating head direction in degrees and circles indicating firing rate in Hz.

B) Grid cells in superficial layers of MEC exhibit firing rate increases with running speed. Modified from (Zheng et al. 2015).

C) Interneurons in the superficial layers of the MEC also increase their firing rate as running speed increases (Zheng et al. 2015).

1.3 – GRID CELL MODELS

1.3.1 Continuous attractor models of grid field formation

One of the primary models to describe the formation of grid cell patterning is a continuous attractor, or network, model (Burak & Fiete 2009). This model postulates that the formation of grid cell firing patterns is a result of large scale, patterned, recurrent connectivity. Grid cells with similar spatial fields have either excitatory or a lack of

inhibitory connections, while grid cells with more divergent spatial selectivity will have stronger inhibitory connections. The connectivity pattern of continuous attractor networks makes specific predictions of how the neurons in the network are active both with and without strong input (Amari, 1977).

Continuous attractor network models depend on specific connectivity patterns between cells to stabilize the response of the cells in the network. The cells respond to a subset of the range of possible responses that the population of cells acting independently could exhibit (Amari, 1977; Taylor, 1999). Rather than each neuron representing the input independently, connections between neurons bias connected cells towards responding to similar input, enforcing a measure of structured correlations across the network of neurons (Amari, 1977; Taylor 1999). This can, depending on the structure of the correlations, have the added effect of increasing the accuracy of the network's representation of the input (Abbott & Dayan, 1999; Hu et al. 2014). The correlations can also confer stability and robustness to noise in the response, automatically correcting the response when noise perturbs it beyond its normal range (Burak & Fiete 2009; Hu et al. 2014). The cost of this stability is that the neurons in the network have a smaller set of responses that are exhibited, reducing the range of representations possible for a given number of neurons. Low-dimensional continuous attractor models therefore have stable, robust representations of the network input, at a cost of having many more neurons than variables the network can represent. The resistance to noise and stability of the representation makes the continuous attractor model a compelling possibility for describing grid field formation (Burak & Fiete 2009).

Attractor network models of grid cells predict specific relationships between the relative location of grid cell firing fields and pairwise spike time correlations, as well as how those relationships are maintained during sleep. Because cells with similar grid firing fields have either a shared lack of inhibition or recurrent excitation, one would predict that cells with similar grid fields would have high spike time correlations on a short time scale. Cells with much less overlap, however, would have little correlation, or even anti-correlation, between their spike trains. Furthermore, these correlations, because they are a result of connectivity in the network, would be present even during non-spatial activity such as sleep. These correlations, if present, would be a confounding factor for identifying experience-dependent replay in grid cells, and would require verification of the effect of experience on detected replay to confirm that grid cell reactivation is experience-dependent and not an artifact of pre-existing connectivity.

1.3.2 Oscillatory interference models of grid field formation

One alternative model of grid field formation involves interference between local field potential oscillations and cellular membrane potential oscillations (Burgess et al. 2007). This model was able to account for some of the distinct attributes of grid cells, namely theta phase precession and the variation of membrane potential oscillation frequency along the dorso-ventral axis of MEC. However, the discovery of grid cells in the absence of theta oscillations (Yartsev et al. 2011), as well as the absence of evidence of theta interference in intracellular recordings of putative grid cells (Domnisoru et al. 2013; Schmidt-Hieber & Häusser 2013), have made it unlikely that the oscillatory interference model on its own provides a full description of grid cell dynamics.

1.4 - THE ROLE OF THE NAVIGATION CIRCUIT DURING NON-SPATIAL ACTIVITY

1.4.1 Hippocampal place cells replay waking experience during sleep and rest.

In addition to firing during active exploratory behaviors, place cells of the hippocampus have been shown to be active during rest and sleep (Ranck 1973). Pairs of place cells show increased spike train correlations during rest and sleep following novel experiences (Wilson & McNaughton, 1994, Kudrimoti et al. 1999). Moreover, ensembles of place cells have been shown to repeat sequences of activity from earlier active behaviors during both REM (Louie & Wilson 2001) and NREM sleep (Nadasdy et al. 1999; Lee & Wilson 2002). This reactivation or "replay" is believed to serve a function in maintaining and strengthening recently acquired memories, as well as possibly transmitting hippocampal memory representations to higher cortical areas for long term storage (Buzsaki 1996; Giradeau et al. 2009; Squire & Zola-Morgan, 1991).

1.4.2 Grid cell reactivation and its relationship to experience.

Interactions between sensory cortices and hippocampal areas during sleep indicate that not only hippocampal place cells exhibit replay. Both auditory (Rothschild et al. 2016) and visual cortex (Ji & Wilson 2007) have been reported to reactivate patterns of waking activity during subsequent sleep, with cortical cells often reactivating immediately prior to hippocampal replay (Rothschild et al. 2016; Ji & Wilson 2007). These reports raise the question of whether grid cells show replay, considering that the medial entorhinal cortex transmits highly processed visual information to the hippocampus (Burwell & Amaral 1998a). In addition, the question of whether grid cells play a role in

offline memory functions during sleep, in addition to their role in representing an animal's location in space during active behaviors, remains largely unanswered.

Two recent reports have reported grid cell reactivation, in both deep (Ólafsdóttir et al. 2016) and superficial layers (O'Neill et al. 2017) of MEC. Superficial layer grid cells did not appear to reactivate in a coordinated fashion with hippocampal place cells, however, while deep layer grid cells were reported to show coordinated reactivation with place cells. A critical component lacking from these two studies, however, is a determination of whether the observed reactivation was specific to a particular experience or simply reflected stable patterns of network connectivity that persist across all experiences and behavioral states.

1.5 - DISSERTATION OVERVIEW

Several hypotheses relevant to the question of whether grid cells play a role in offline memory processing are investigated in this dissertation. In Chapter 2, I first examine the hypothesis that grid cell firing patterns are shaped by network connections during both spatial (online) and non-spatial (offline) behaviors. The activity of grid cells during both REM and NREM sleep, recorded across the duration of the rats' overnight sleep cycle, was investigated together with grid cell activity during active waking behaviors. The relationship between short-term spike time correlations and spatial field overlap between grid cells was examined in an attempt to answer the question of whether similar relationships exist across all behaviors, as predicted by continuous attractor network models of grid cell formation.

Chapter 3 describes an investigation of whether novel experience changes co-activity relationships between grid cells during novel waking experience as well as during sleep and rest periods immediately following the novel experience. If changes in grid cell co-activity patterns are induced by learning of a novel trajectory, then one would expect to see changes in grid cell co-activity patterns during novel exploration and during sleep or rest following the novel experience, but not during sleep or rest preceding the novel experience. Furthermore, such changes in grid cell co-activity patterns would not be expected to be observed during or after a familiar experience. Pairwise correlations alone are not enough to fully rule out whether experience-dependent replay is occurring however. One would also need to look at the cell ensemble level to see if complex cell firing sequences are replayed after experience.

Finally, Chapter 4 investigates the extent to which sequences of grid cells that fired during waking behaviors are reactivated during subsequent sleep and rest. In contrast to pairwise correlation methods used in earlier chapters, this chapter employs template-matching methods that have been used in the field previously to identify putative replay events in ensembles of hippocampal place cells (Louie & Wilson 2001). Bootstrapping methods are also employed to determine the likelihood of sequential events during waking and sleep being strongly correlated by chance.

Chapter 2: Grid cell co-activity patterns during sleep reflect spatial overlap of grid fields during active behaviors[1]

2.1 - INTRODUCTION

Grid cells of the medial entorhinal cortex (MEC) (Hafting et al. 2005) together with place (O'Keefe & Dostrovsky, 1971), head direction (Sargolini et al. 2006; Taube et al. 1990), border (Solstad et al. 2008), speed cells (Kropff et al. 2015), and cells that simultaneously code multiple navigational variables (Hardcastle et al. 2017), convey information about the evolving location and orientation of mammals as they move through 2D open fields, run on 1D linear tracks, or fly through 3D space (Yartsev et al 2013). Grid cells are defined by regular, periodic responses to an animal's 2D spatial location. Each grid cell's multiple spatial receptive fields ("grid fields") form a characteristic geometric pattern well-described by a lattice of equilateral triangles.

Several different classes of models seek to explain grid cell activity and function (Burak & Fiete, 2009; Burgess et al. 2007; Fuhs & Touretzky, 2006; Grossberg & Pilly,

---

[1] This work was previously published on BioRXiv.org in 2017.

Trettel, S. G., Trimper, J. B., Hwaun, E., Fiete, I. R., & Colgin, L. L. (2017). Grid cell co-activity patterns during sleep reflect spatial overlap of grid fields during active behaviors. *bioRxiv*, 198671. Dissertator contributed to the conception, design, data collection, analysis, interpretation and writing of the study.

2012; Navratilova et al. 2012; Moser et al. 2014). One of the principal models is based on continuous attractor dynamics that emerge through pattern formation in networks with strong lateral connectivity (Burak & Fiete, 2006; Burak & Fiete, 2009; Fuhs & Toretzsky, 2006). In such continuous attractor network models, connectivity between cells tightly constrains their patterns of co-activation, and thus connectivity is closely related to relationships in spatial tuning. Specifically, these models predict that cell pairs with strong short-time correlations should exhibit similar spatial tuning phases, whereas most pairs with weak short-time correlations or negative correlations should exhibit offset or anti-phase spatial tuning. Moreover, these correlations should be preserved across states because the circuit dynamics are always shaped by the same recurrent connectivity in the network. This prediction can be tested in recordings of the same grid cell ensembles across active waking, quiescent, and sleep states.

Other spatially responsive cells appear to have structured activity patterns during sleep. During waking rest and non-REM sleep (NREM), place cells show a transient increase in their spike time correlations that is related to the firing patterns of the place cells during exploration (Karlsson & Frank, 2009; Kudrimoti et al. 1999; O'neill et al. 2008; Wilson & McNaughton, 1994). Head direction cells have been shown to exhibit structured activity during sleep states as well (Brandon et al. 2012; Peyrache et al. 2015). Considering that place cells, head direction cells, and grid cells are part of a larger navigational and spatial memory system, and that grid cells in the superficial layers of the MEC provide input to place cells (Canto et al. 2008; Fyhn et al. 2007; Steward & Scoville 1976; Zhang et al. 2013), it is possible that grid cells in the superficial layers of MEC drive hippocampal place cell reactivation during sleep. However, little is known about

superficial layer MEC grid cell firing patterns across overnight sleep, and a recent study suggested that coordinated reactivation typically does not occur between place cells and grid cells in the superficial layers of MEC (O'Neill et al. 2017).

The central question of this paper is to ask whether, and to what extent, states in the grid cell circuit across sleep resemble those during waking. These findings will help to better understand the potential role of the grid cell circuit in driving dynamics of the larger navigational and spatial memory system. Grid cells are hypothesized to integrate velocity cues as an animal navigates through an environment, thus obtaining a continuously updated estimate of location even when spatially informative external cues are unavailable (Hafting et al. 2005; McNaughton et al. 2006; Welinder et al. 2008). Also, grid cells have more recently been shown to play a role in non-spatial tasks, namely measuring the passage of time (Kraus et al. 2015) or creating a map of the visual field (Killian et al. 2012). Although grid cells have been characterized as exhibiting grid-like responses during both spatial and non-spatial tasks, the presence or stability of relationships between grid cell pairs across both spatial and non-spatial tasks has not been examined. Thus, it remains unclear whether the cell-cell relationships predicted by the continuous attractor network models persist across spatial and non-spatial behaviors.

Here, we examined spike time cross-correlations in large numbers of MEC grid cell pairs in freely behaving rats during exploratory behaviors and across several hours of overnight sleep. Hippocampal circuits have been shown to exhibit preserved patterns of very recent past experience during the first 20 mins of sleep (Kudrimoti et al 1999; Wilson & McNaughton 1994). In contrast, we examine a prediction of low-dimensional continuous attractor models, namely that patterns of activity during sleep in grid cells exhibit a

preserved structure across hours of overnight sleep. We found that spike-time and spike-rate correlations between grid cells were related to the degree of overlap in their spatial tuning curves and that, remarkably, these relationships persisted during rapid eye movement (REM) and non-REM (NREM) sleep. Moreover, the preserved patterns of co-activity during sleep were not explained by theta entrainment of spike times or analogous hippocampal co-activity patterns.

2.2 - RESULTS

2.2.1 Activity of grid cells during waking and sleep

To examine the structure of the grid cell circuit responses during sleep, we simultaneously recorded multiple single units in MEC over several hours as rats (n=6) ran in open field and across the entirety of their overnight sleep cycle. From these ensembles, we identified putative grid cells using a gridness score (Sargolini et al. 2006) (see Methods) calculated from three twenty-minute open field sessions. Grid cell recordings were only obtained from MEC superficial layers (i.e., II and III). Grid cells were only included if they remained stable across active waking recordings, subsequent overnight sleep recordings, and additional open field recordings the next morning (see Methods). From a total of 157 putative grid cells and 417 possible putative grid cell pairs, 226 grid cell pairs from 6 animals passed our inclusion criteria (see Methods; Table 2.1). The criteria for beginning an experimental session was detecting a minimum of four grid cells; thus, there were more grid cell pairs than individual cells.

Animal	Number of Grid Cells	Number of Grid Cell Pairs Used	Number of Recording Days
Rat 20	33	57	5
Rat 26	24	52	4
Rat 29	5	9	1
Rat 74	20	10	7
Rat 78	24	78	5
Rat 109	52	75	7

Table 2.1. Grid cell counts per animal.

Grid cells were active during spatial exploration of open field environments and during both REM and NREM stages of sleep (Figure 1). However, firing rates were significantly different across the three behavioral states (157 grid cells; RUN: 2.04 +/- 0.10 Hz, REM: 1.08 +/- 0.06 Hz, NREM: 0.76 +/- 0.04 Hz, $F(2, 468)=89.6$, $p < 0.0001$; 1-way ANOVA; Figure 2.1b-c). Firing rates during REM and NREM were significantly lower than during waking behaviors ($p < 0.0001$ in both cases, post hoc Tukey's HSD test). In addition, REM firing rates were significantly higher than NREM firing rates ($p = 0.004$, post hoc Tukey's HSD test).

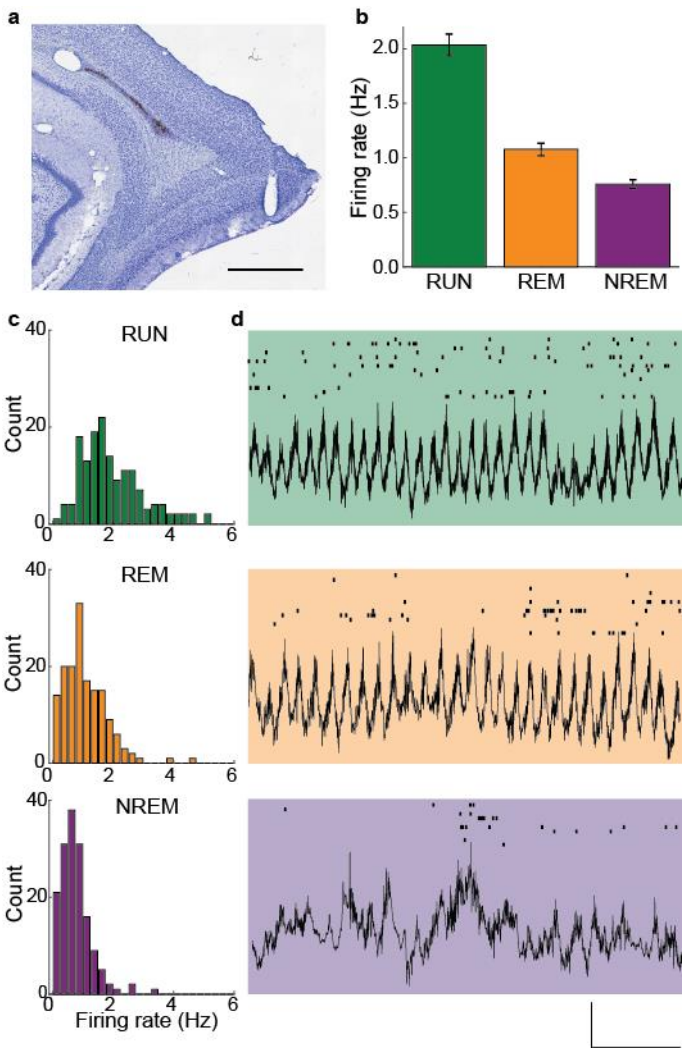

Figure 2.1 - Grid cell firing rates varied across active and sleep states

(a) An example histological section shows a tetrode track in the superficial layers of the medial entorhinal cortex. Scale bar is 1 mm.

(b) Grid cell firing rates differed significantly across behavioral states. Firing rates (mean +/- SEM) were highest during active ambulation and lowest during NREM sleep.

(c) Histograms show the distributions of firing rates across grid cells segregated by behavioral state.

(d) Representative examples of LFP epochs are presented with simultaneous spike rasters from an example ensemble of grid cells plotted above each trace. Each row of the raster plots corresponds to a single grid cell. Activity from the same ensemble of grid cells is shown in each behavioral state. Vertical scale bar is 500 µv, horizontal scale bar is 1 s.

2.2.2 Patterns of co-activation in individual grid cell pairs were maintained across active and sleep states

We next investigated whether co-activity patterns of pairs of grid cells were related to overlap in their spatial tuning properties, as predicted by attractor network models of

grid cells (Burak & Fiete 2006; Burak & Fiete 2009; Fuhs & Touretzky 2006). Cross-correlograms between pairs of grid cell spike trains showed structure related to the spatial overlap between the cells' grid fields (Figure 2.2). During running (Figure 2.2b-c, left column), grid cell pairs with highly overlapping grid fields (sorted to correspond to higher cell pair IDs in Figure 2.2) showed high cross-correlations between their spike trains at zero or near zero lags. Grid cell pairs with only partially overlapping grid fields tended to show moderately low correlations at short time lags, whereas grid cell pairs with anti-phase spatial tuning (corresponding to lowest cell pair IDs in Figure 2.2) showed the lowest correlations at short time lags. Remarkably similar correlated and anticorrelated activity patterns were observed for the same set of grid cell pairs during REM and NREM states (Figure 2.2a-c, middle two columns and right column). The overall widths of the short-time lag peaks and dips in the cross-correlograms were narrower during NREM than during waking and REM, suggesting that grid cell network dynamics operate on a faster (by a factor of approximately 5) time scale during NREM. This finding is consistent with temporal compression of spike sequences previously observed during NREM in networks of head direction cells (Peyrache et al 2015) and place cells (Lee & Wilson 2002; Nádasdy et al. 1999). Nevertheless, the general relationship between NREM spike-time correlations and spatial rate map correlations was qualitatively the same as that seen during waking and REM, as is particularly apparent for NREM correlations shown on a magnified time scale (Figure 2.2a-c, right column).

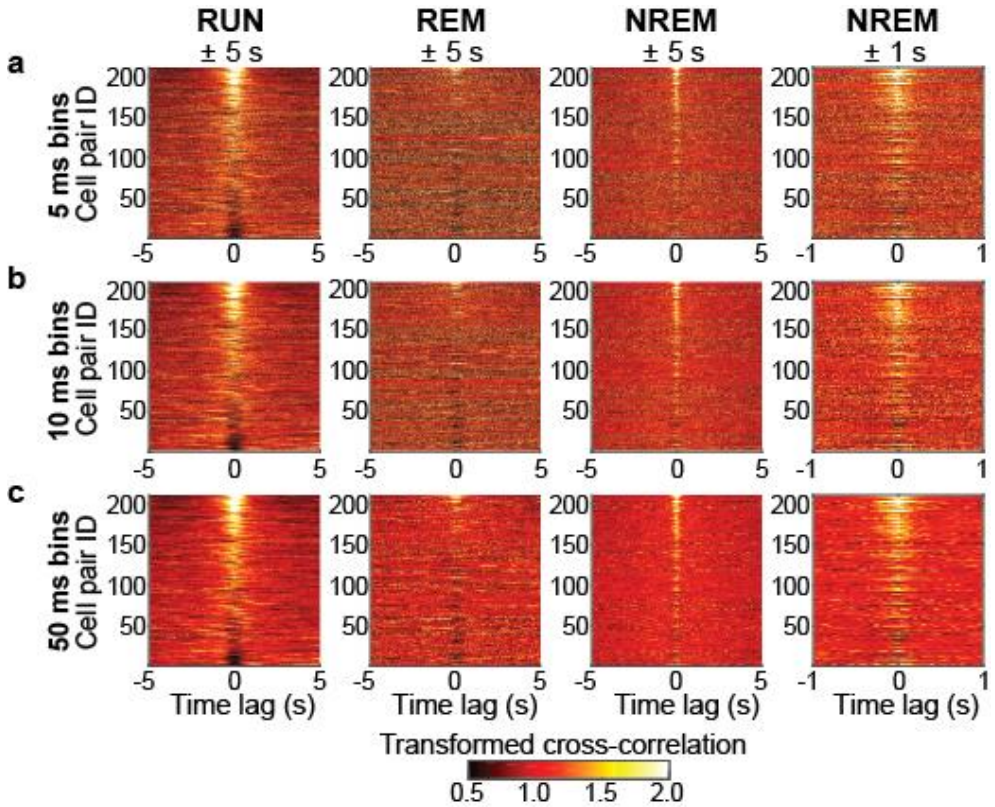

Figure 2.2 - Cross-correlations between grid cell spike times were related to the degree of overlap in grid cell rate maps across active waking behaviors and sleep.

(a-c) Each panel shows color-coded spike time cross-correlations (divided by their average; see Methods) for all pairs of grid cells sorted from highest rate map correlation coefficient (highest Cell Pair ID) to lowest rate map correlation coefficient (lowest Cell Pair ID) (See Methods). The leftmost three columns show results for RUN, REM, and NREM and are plotted across time lags of +/- 5 s. The rightmost column shows results for NREM plotted across time lags of +/- 1 s. Note that similar qualitative relationships between spike time cross-correlations and grid cell rate map correlations are maintained across all three behavioral states and for spike trains binned with varying degrees of temporal resolution (i.e., 5 ms bins in a, 10 ms in b, and 50 ms in c).

To quantify the qualitative trends seen in the patterns of pairwise cross-correlograms, we summed the spike time cross-correlograms within +/-5 ms time lags to obtain a single short-time cross-correlation estimate for each grid cell pair. We then compared these estimates to their associated rate map correlations to determine the extent to which temporal correlations between grid cells' spike trains were predicted by overlap between their rate maps across the three behavioral states (Figure 2.3a). Not surprisingly, grid cells' spike train cross-correlation estimates were significantly related to their rate map correlation values during active exploration (significant regression for RUN: $F(1,209) = 235.25$, $p < 0.0001$, $R^2 = 0.53$), with higher spike train cross-correlation values associated with higher rate map correlations. Remarkably though, rate map correlation values from active behaviors also significantly predicted temporal correlations between grid cells during sleep states (significant regressions for REM: $F(1,209) = 52.53$, $p < 0.0001$, $R^2 = 0.20$; and NREM: $F(1,209) = 93.81$, $p < 0.0001$, $R^2 = 0.31$) . Therefore, despite a lack of sensory input driving the system during sleep, the relationship between cell pairs' spike-time cross correlations and rate-map cross-correlations observed during active behaviors persisted during sleep. This finding strongly suggests that temporal correlations during both waking and sleep states result from connectivity in the grid cell network.

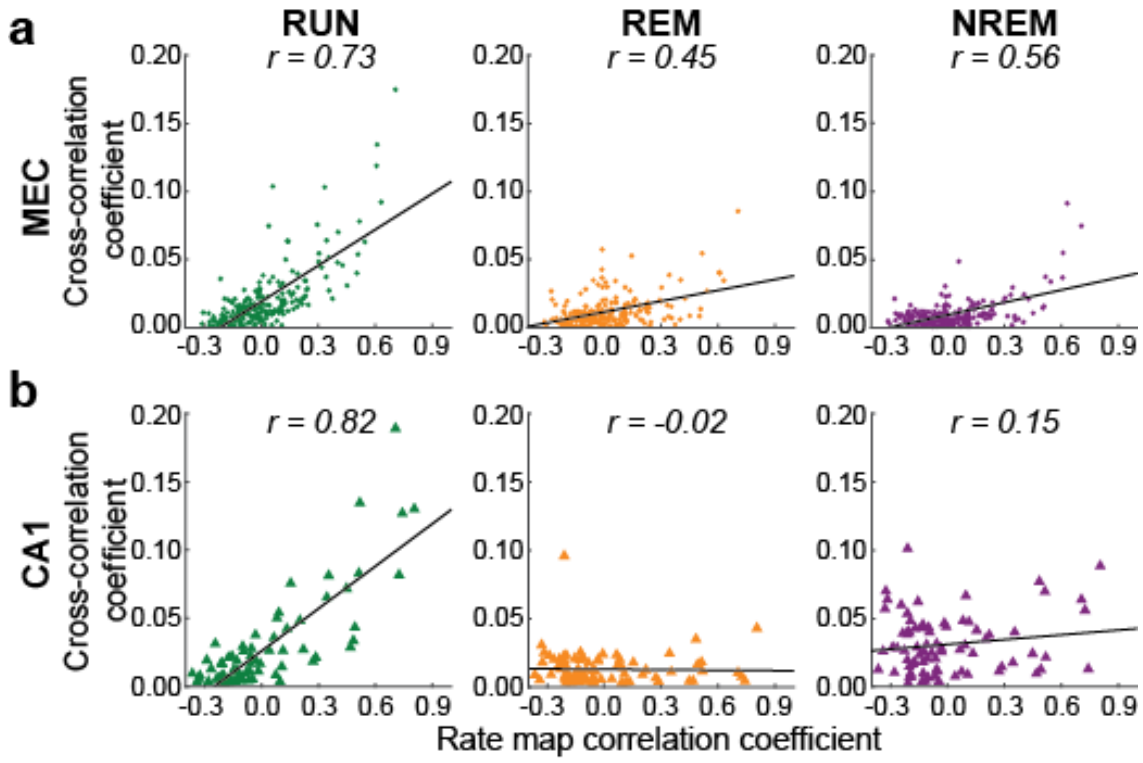

Figure 2.3 - The relationship between spatial overlap and spike-time cross correlations was preserved across waking and sleep states for grid cell pairs but not CA1 place cell pairs

Spike time cross-correlation coefficients were summed across a +/- 5 ms time lag. Each dot in a scatterplot represents a grid cell pair's rate map correlation coefficient and summed spike train cross-correlation coefficient. Each plot also shows the best-fit line in black and the associated correlation coefficient, r.

(a) For all grid cell pairs and across all three behavioral states, positive correlations were observed between spike time cross-correlations and grid cell rate map correlation coefficients.

(b) Pairs of CA1 place cells exhibited a significant positive correlation between summed spike time cross-correlation coefficients and place cell rate map correlation coefficients during active waking behaviors, but that relationship was not maintained during REM or NREM sleep.

2.2.3 Preserved correlation structure in grid cells during sleep was not explained by hippocampal place cell correlation structure during sleep

With the goal of evaluating the possibility that preserved grid cell correlation relationships across awake spatial exploration and sleep were driven by place cells (Bonnevie et al. 2013), we next tested whether place cells' spike time correlations during sleep were related to the overlap of their spatial fields during awake exploration. For recordings obtained during active running on a circular track (i.e., RUN), temporal correlations between 78 place cell pairs' spike trains were significantly related to the correlation of their firing rate maps (Figure 2.3b (left); significant regression for RUN: $F(1,76) = 160.55$, $p < 0.0001$, $R^2 = 0.68$), with temporal correlations between place cells increasing as a function of their rate map correlations. However, this relationship was not preserved in REM and NREM overnight recordings of the same place cell ensembles (Figure 3b (right panels); non-significant regressions for REM: $F(1,76) = 0.04$, $p = 0.84$, $R^2 = 0.001$; and NREM: $F(1,76) = 1.78$, $p = 0.19$, $R^2 = 0.023$). Accordingly, there was a significant interaction between brain region (CA1 or MEC) and behavioral state (RUN, REM, or NREM) on spike time cross-correlation values (significant multiple regression model: $F(4,862) = 94.91$, $p < 0.001$; significant interaction term: $\beta = 0.42$, $p < 0.001$), indicating that CA1 place cell pairs' temporal correlations were not related to field overlap across behavioral states in the same manner as was observed for MEC grid cells. That is, the degree of place field overlap during track running only predicted the strength of place cell pairs' temporal correlations during active waking behaviors, but not during REM or NREM sleep. Differences in relationships between MEC and CA1 field overlap and spiking co-activity across behavioral states were not explained by qualitative differences

in firing rates across behavioral states. That is, CA1 firing rates between active waking behaviors and sleep followed a roughly similar pattern as MEC grid cell firing rates, with significantly lower firing rates in CA1 during REM and NREM than during active wakefulness (41 place cells; RUN: 1.61 +/- 0.25 Hz, REM: 0.85 +/- 0.14 Hz; NREM: 0.88 +/- 0.13 Hz; $F(2, 120)=5.434$, $p = 0.006$; 1-way ANOVA; $p = 0.012$ for RUN vs REM, $p = 0.016$ for RUN vs NREM, no significant difference between REM and NREM, post hoc Tukey's HSD tests).

2.2.4 The relationship between grid cells' relative spatial phases and spike time correlations was maintained across active and sleep states

The results shown in Figures 2 and 3 suggest that spatial map correlations are reflected, putatively through recurrent connectivity, in spike-time correlations across states. However, spike time correlations computed per cell pair are noisy, and spatial map correlations are not a perfect measure of spatial tuning relationships between pairs of grid cells. We therefore used a more detailed measure of spatial tuning relationships between cells and, to reduce noise, combined spike time cross-correlation estimates for cell pairs with similar spatial tuning offsets (see Methods). Briefly, we obtained the relative spatial phase for a given pair of cells by estimating the offset from the origin of the central peak in their spatial cross-correlogram, similar to a previous study (Yoon et al. 2013) (Figure 2.4a) (see Methods). This value was then used to sort cell pairs into ($\Delta\varphi_X$, $\Delta\varphi_Y$) relative phase bins. For each cell pair, we summed the temporal cross-correlogram in a +/- 5 ms window about zero time-lag, as in Figure 3. We then averaged this value across all pairs in a bin and plotted average spike-time cross-correlations against relative spatial phase

(Figure 4b, left column). This process was repeated using a broader time window of +/- 50 ms about zero in the temporal cross-correlogram to obtain a temporally coarser spike-rate cross-correlation estimate across relative spatial phases (Figure 2.4b, right column). We then performed the same cross-correlation computations for REM and NREM periods. To account for differing firing rates across states, we scaled each surface according to its maximum average cross-correlation value. Comparing the left and right columns of Figure 2.4b reveals the same general pattern at both short (spike-time) or long (spike-rate) timescales. That is, there was a strong relationship between relative spatial phase values and temporal correlations, with low relative spatial phases associated with high temporal correlations. This relationship persisted across all states regardless of whether the behavior was spatial (RUN) or not (REM and NREM).

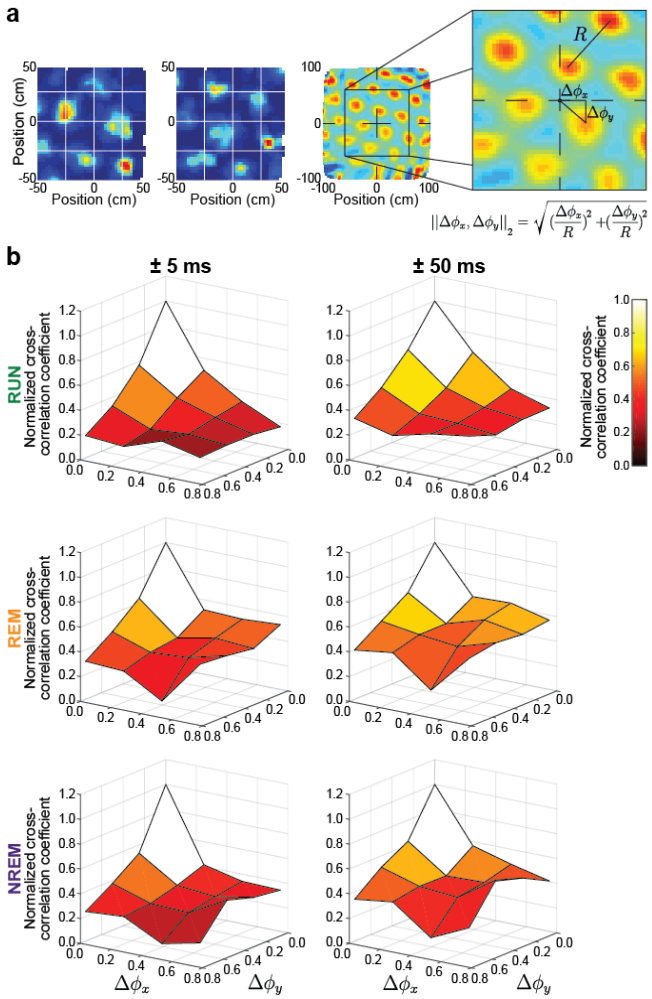

Figure 2.4 - Grid cell spike time correlations during waking behaviors and sleep were predicted by spatial phase offsets between grid fields

(a) The method used to calculate the relative spatial phase between grid cells is demonstrated with this illustrative example. Color-coded rate maps for a pair of grid cells are shown in the left two panels. The third panel shows the rate map cross-correlation for the grid cell pair. The grid cell rate map cross-correlation peak nearest to the plot origin was used to estimate ΔφX and ΔφY offsets (see right panel). Each offset was then normalized by the spatial period (R), which was assumed to be the same between all peaks in the rate map cross-correlation.

(b) The relationship between grid cell pairs' relative spatial phases and their spike time cross-correlations is shown. Spike time cross correlation values were summed across time lags of +/- 5 ms (left column) or +/- 50 ms (right column) and averaged within each (ΔφX, ΔφY) bin. Data from RUN (top), REM (middle), and NREM (bottom) states show maximal spike train cross-correlation values at low relative spatial phases (i.e., high overlap of grid fields) and weaker spike train cross-correlation values at high relative spatial phases (i.e., low overlap of grid fields). The plots were scaled by their peak value to compare across behaviors with different spike rates. Normalized cross-correlation coefficient values are plotted in color scale for ease of plot interpretation.

We further compressed and reduced noise in the results by collapsing the x and y components of relative spatial phase into a one-dimensional relative spatial phase magnitude (Figure 2.6a for normalized cross-correlation coefficients; see Figure 2.5a for non-normalized version). This transformation to one-dimensional relative spatial phase

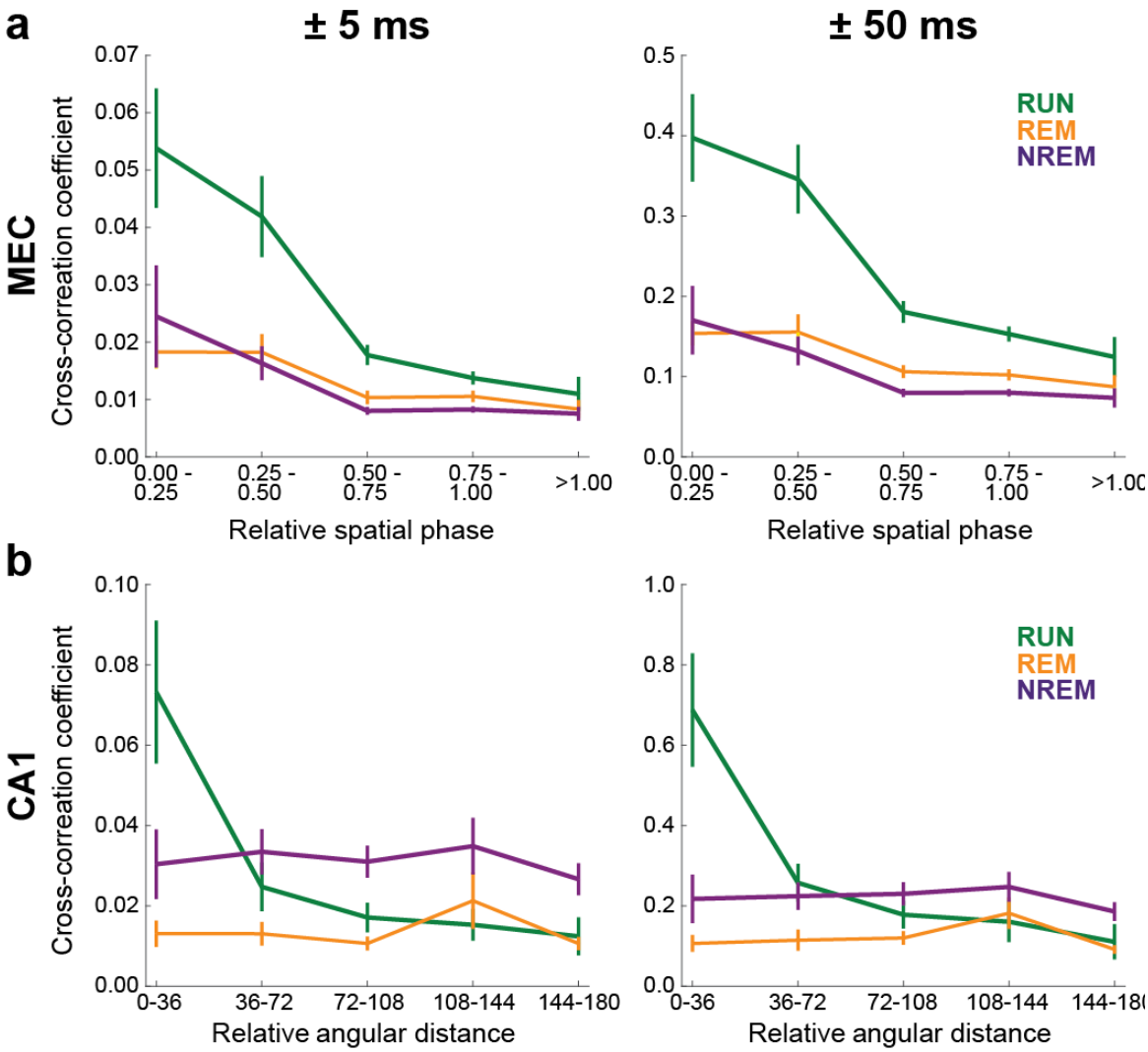

Figure 2.5 - Across all behavioral states, grid cell pairs' cross-correlation coefficients decreased with increasing relative spatial phase. Place cell pairs' cross-correlation coefficients decreased with increasing distance between place fields during RUN, but a similar relationship was not observed during NREM or REM. These plots are the same as those in Figure 2.6 except that spike time cross-correlation coefficients were not normalized according to maximum values within each behavioral state.

was also done to compare grid cell relative spatial phase plots to analogous metrics for CA1 place cell pairs recorded on a circular track (Figures 2.6b and Figure 2.5b). Across all three behavioral states, grid cells' spike time correlations decreased as their relative spatial phase magnitudes increased. Temporal correlations during REM exhibited a qualitatively similar, but quantitatively weaker, functional dependence on the magnitude of relative spatial phase compared to waking and NREM states (Figure 2.5 shows non-normalized plots for comparison of magnitudes). Higher noise in REM states (as is visible in Figure 2.2, second column) may explain this quantitative difference.

In contrast to grid cells, CA1 place cell pairs' cross-correlation coefficients during waking behaviors decreased with increasing distance between place fields, but cross-correlations during REM and NREM states did not reflect place field overlaps from the preceding spatial exploration session (Figures 2.6b and Figure 2.5b). Taken together with the results shown in Figure 2.3b, these results suggest that stable relationships between grid field overlap and grid cell co-activity patterns across waking and sleep states are not caused by inputs from place cells.

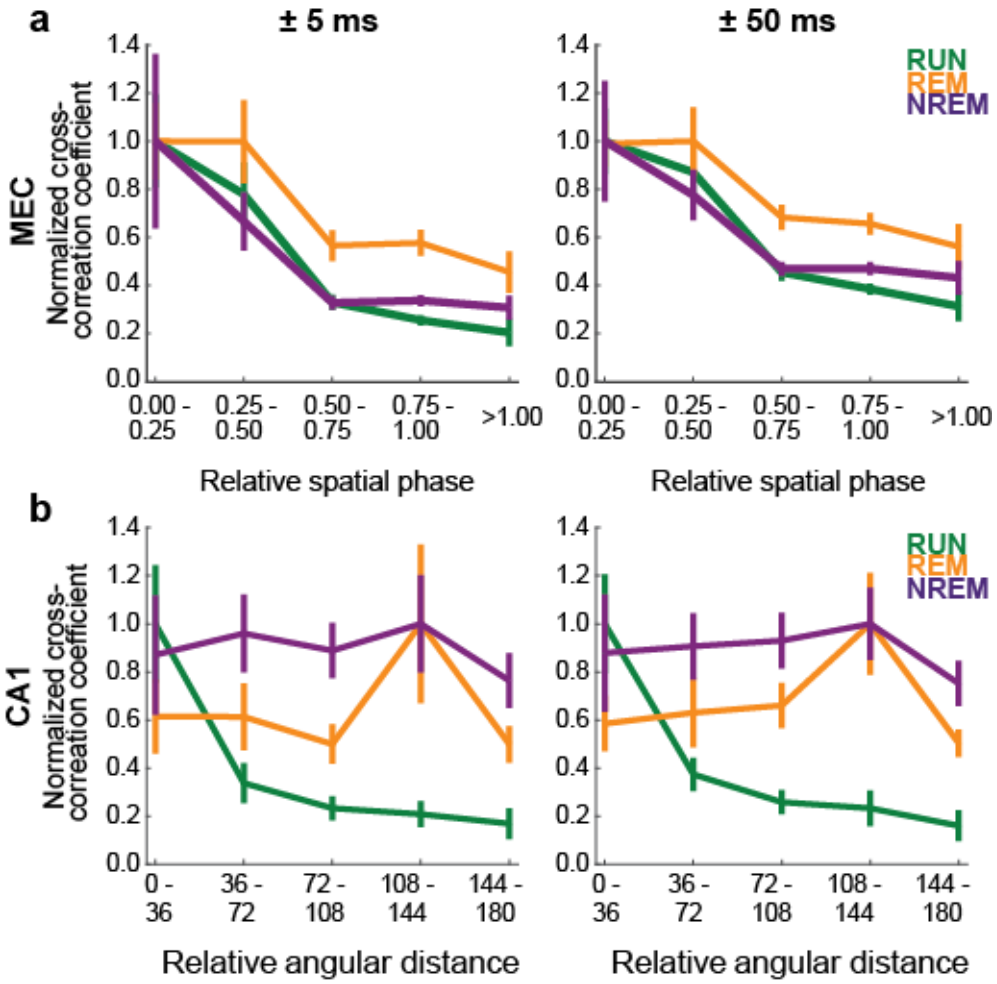

Figure 2.6 - Grid cell spike time correlations decreased with relative spatial phase magnitude across behavioral states, while CA1 spike time correlations were related to distance between place fields only during active running

In this figure, spike time cross-correlation coefficients for each behavioral state were normalized by dividing by the bin with the greatest average spike time cross-correlation coefficient (see Figure 2.5 for non-normalized versions).

(a) In these plots, the two-dimensional relative spatial phase values depicted in Figure 4B were collapsed to a single dimension (magnitude) by calculating the Euclidean distance of ΔφX and ΔφY. In all three behavioral conditions, spike time cross-correlations summed over +/- 5 ms (left) and +/- 50 ms time lags (right) decreased as the magnitude of relative spatial phase increased.

(b) In this plot, we calculated the relative angular distance between place field centers on the circular track and compared that distance to spike time cross-correlations summed over +/- 5 ms (left) and +/- 50 ms time lags (right). Place cells' spike time cross-correlations decreased as distance between place fields increased during active waking behavior (i.e., RUN) but not during sleep states (i.e., REM and NREM).

2.2.5 Observed grid cell correlation patterns were not explained by theta coordination

The preserved relationship between grid field overlap and spike time correlations during NREM periods is noteworthy because, unlike during active wakefulness and REM sleep, theta oscillations are not present during NREM. In other words, the preserved relationship between spatial tuning and NREM coactivity patterns cannot be attributed to coordinated theta phase relationships between grid cells (Hafting et al. 2008). Moreover, spike-time correlations were higher for cell pairs with overlapping fields than pairs with largely non-overlapping fields across both theta-associated states (i.e., RUN and REM) when theta phase effects were present and when they were removed ($N = 26$, overlapping fields group, $N = 12$, non-overlapping fields; $F(1,36) = 7.6$, $p = 0.009$, repeated measures ANOVA; Figure 2.7). Thus, the preservation of relationships between relative spatial phase of grid fields and spike time cross-correlations across sleep states does not appear to be explained by a shared theta modulation of cell pairs' spikes.

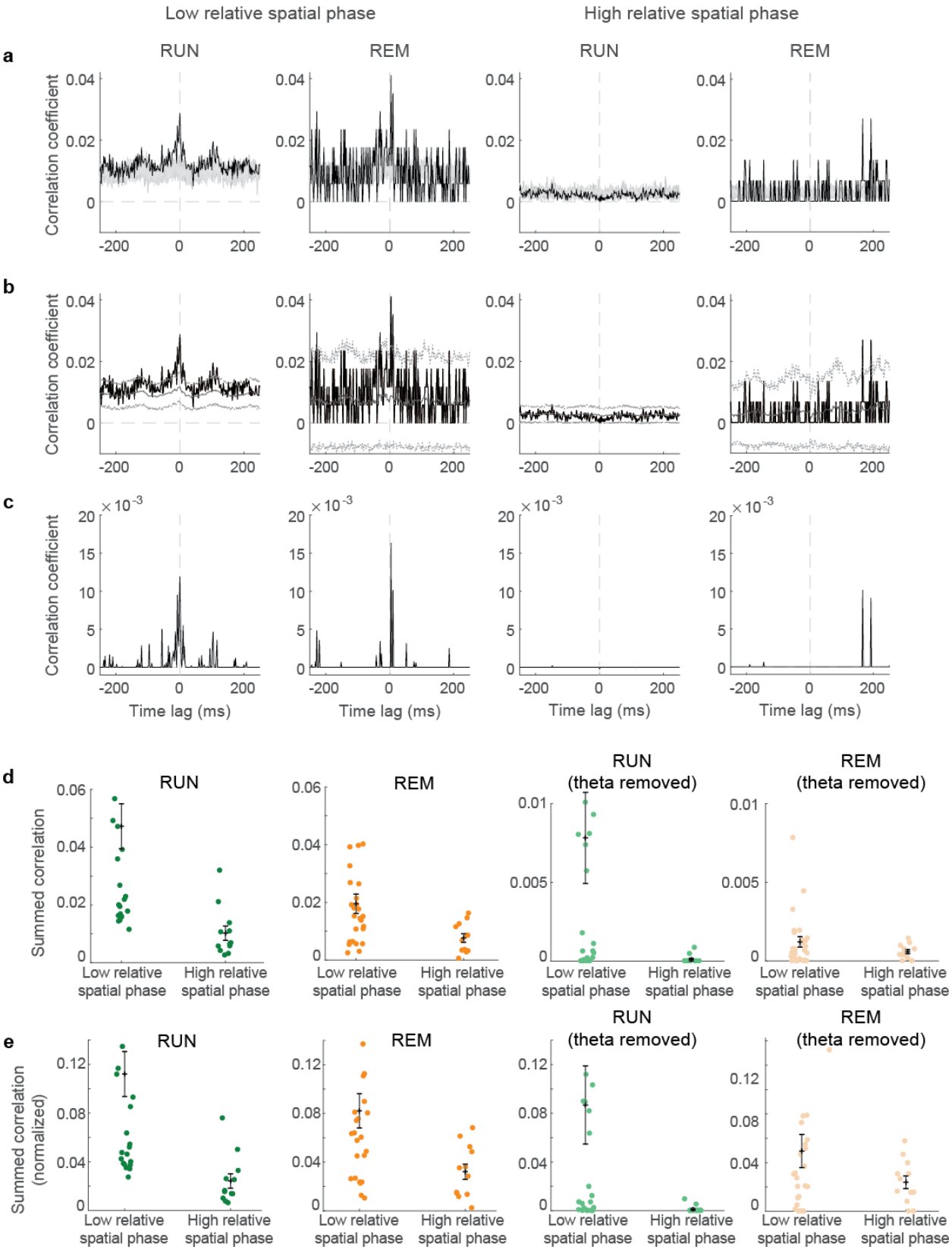
Low relative spatial phase
High relative spatial phase
a
RUN
REM
RUN
REM
Correlation coefficient
0.04
0.02
0
-200
0
200
b
c
×10^-3
20
15
10
5
Time lag (ms)
d
RUN
REM
RUN (theta removed)
REM (theta removed)
Summed correlation
0.06
0.01
0.005
Low relative spatial phase
High relative spatial phase
e
Summed correlation (normalized)
0.12
0.08

Figure 2.7 - Short-time spike time correlation patterns of grid cell pairs with overlapping grid fields maintained across behavioral states when the effect of theta phase modulation of spiking and other slow influences was removed. To determine the extent to which spike time cross-correlation results were explained by shared theta phase preferences of spike times and other slow modulations in spike rate, spikes were temporally shuffled two hundred times within 500 ms moving windows, while keeping the theta phase of each spike time fixed. Spike time cross-correlations were then re-calculated using shuffled trains (See Methods). This analysis was only done for RUN and REM spike trains, given that NREM is characterized by an absence of theta.

a) Shown are original spike time cross-correlations (black) overlaid on 10 (out of 200) randomly selected examples of shuffled cross-correlations (gray) for an example grid cell pair. Cross- correlograms for an example grid cell pair with highly overlapping fields (i.e., low relative spatial phase magnitude) are shown for RUN (first column) and REM (second column). Also shown are RUN (third column) and REM (fourth column) cross-correlograms for an example grid cell pair with largely non-overlapping grid fields (i.e., high relative spatial phase magnitude).

b) The average theta-determined component of the correlation (gray, solid) with 98% confidence intervals (gray, dotted) and associated original spike time cross-correlogram (black). Columns are as in A.

c) The correlogram remaining after removal of the theta-modulated components. Note that substantial peaks around zero lag were still present in the low relative spatial phase plots (left two columns) but not in the high relative spatial phase plots (right two columns).

d) Cell pairs were split into low and high relative spatial phase groups as in Figure 6, and their correlation was summed over the +/- 5 ms lag window. The average correlation sum was calculated across each subpopulation for both RUN (first column) and REM (second column). The same calculation was done on the theta-removed correlations in the two columns to the right.

e) The same as in D, but with values normalized by the Euclidean norm of the population of summed correlations before sorting into near or far groups. This was done to aid visual comparison between RUN and REM conditions, and between original and theta-removed groups

2.2.6 Grid cell pairs with different relative spatial phase magnitudes exhibited different distributions of spike time correlations

In addition to looking at average relationships between relative spatial phase magnitude and temporal correlations across all grid cell pairs, we categorized individual grid cell pairs according to their relative spatial phase magnitudes and plotted the associated distributions of spike time cross-correlations. We expected that the distribution of spike time correlations for cell pairs with a low relative spatial phase magnitude (i.e., high grid field overlap, example in Figure 2.8a) would have more mass at higher values compared to the spike time cross-correlation distribution for high relative spatial phase magnitude pairs (i.e., low grid field overlap, example in Figure 2.8b). Indeed, this pattern was observed when we sorted grid cell pairs into three categories according to the degree of overlap in their grid fields. Across all three behavioral conditions, the spike time correlation distributions for the low relative spatial phase magnitude group (i.e., high grid field overlap) exhibited tails containing relatively high correlation values (Figure 2.8c, left column). In contrast, the correlation distributions for the high relative spatial phase magnitude group (i.e., low grid field overlap; Figure 2.8c, right column) were more sharply peaked at lower values, across all three behavioral states. Grid cell pairs with intermediate grid field overlap showed distributions of spike time cross-correlations across all states that were intermediate between the corresponding distributions observed for high and low overlap groups (Figure 2.8c, middle column). Taken together with results described above, these results show that correlated grid cell activity patterns across waking and sleep reflect the degree of grid field overlap during active exploratory behaviors.

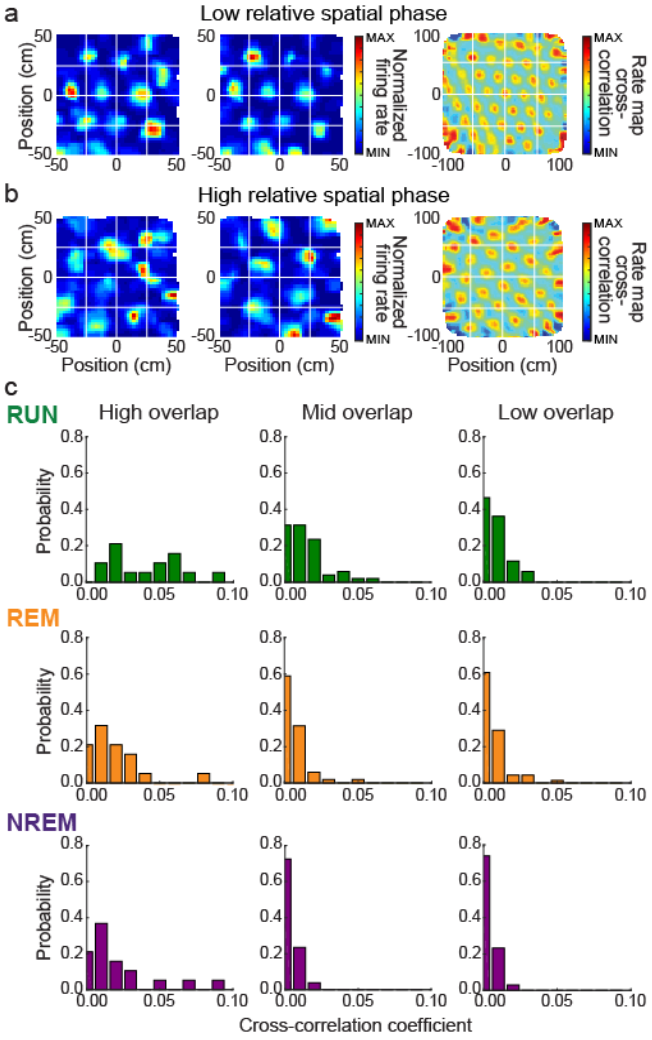

Figure 2.8 - Grid cell pairs with overlapping grid fields exhibited a greater proportion of high spike time cross-correlations across active and sleep states.

a) Color-coded rate maps (left two columns) and rate map cross-correlation (right column) for an example grid cell pair with low relative spatial phase (i.e., high grid field overlap).

b) Same as A but for an example grid pair with high relative spatial phase (i.e., low grid field overlap).

c) Probability density functions for normalized spike time cross-correlation coefficients summed over +/- 5 ms time lags. Grid cell pairs were sorted into High Overlap (left column), Mid Overlap (center column), or Low Overlap (right column) categories, corresponding to low, moderate, and high relative spatial phase magnitude values, respectively. For all three behavioral conditions, grid cell pairs in the High Overlap category were more likely to exhibit relatively high spike time cross-correlations, and grid cell pairs in the Low Overlap category were more likely to exhibit low spike time cross-correlations.

2.3 - DISCUSSION

We examined whether the spatial tuning relationships of grid cells influence their spike-time correlations during non-spatial sleep states. We found that cells with strong spike-time correlations have similar spatial tuning, whereas cells with minimal spatial tuning overlap exhibit weaker or negative spike-time correlations. Further, these patterns of spatial-tuning based correlation are preserved across REM and NREM sleep states during which there is no spatial behavior. These results could not be accounted for by theta modulation, since the pattern of correlations in NREM, when theta was absent, matched that found during REM sleep and waking exploration, when theta was strong. The across-state preserved pattern of correlations as a function of spatial tuning was also not explained by hippocampal place cell inputs from CA1, since these cells did not exhibit unchanged patterns of correlation across states. Thus, the pattern of correlations is likely to originate within the entorhinal cortex rather than being inherited, through feedforward projections, from circuitry in the hippocampus. Taken together, our results suggest that recurrent connectivity is likely a major determinant of grid cell activity across awake navigation and non-spatial sleep states, consistent with continuous attractor network models of grid cells (Burak & Fiete 2006; Burak & Fiete 2009; Fuhs & Touretzky 2006). In grid cell models, the recurrent connectivity may involve both excitatory and inhibitory connections (Burak & Fiete 2009) or inhibitory connections alone (Burak & Fiete 2009; Couey et al. 2013). While we have seen some evidence for short-latency positive spike-time correlations between cells with high spatial overlap, with the correlation peaks preserved across states (suggesting the possibility of direct excitatory coupling between grid cells of similar phase), our evidence is not sufficient to clarify which types of

connections underlie the present results, given that anatomical studies have shown both patterns of connectivity exist within the MEC superficial layers (Couey et al. 2013; Dhillon & Jones, 2000; Fuchs et al. 2016; Pastoll et al. 2013).

It is notable that MEC grid cell correlation patterns from waking appear to be better preserved in sleep than are CA1 place cell correlations patterns. This result may seem surprising at first glance, considering that CA1 place cells replay activity patterns during sleep that resemble activity patterns from earlier waking behaviors (Kudrimoti et al. 1999; Lee & Wilson 2002; Louie & Wilson 2001; Nádasdy et al. 1999; Wilson & McNaughton 1994;). However, our results examined correlation structure across an entire night's sleep, while correlations between CA1 place cell spiking during active waking behaviors and subsequent NREM sleep notably decay within the first hour of sleep (Kudrimoti et al 1999; Wilson & McNaughton 1994). Moreover, the relationship between place cells' field overlap and spike time correlations is stronger during awake rest than during sleep (Karlsson & Frank 2009). It should also be noted that different correlated spiking patterns in CA1 associated with different environments can reactivate within the same sleep episode (Kudrimoti et al 1999)[17], suggesting that place cells exhibit multiple patterns of coactivation during sleep that reflect different experiences. Thus, the lack of preserved correlated activity between CA1 place cells across sleep states is consistent with higher-dimensional dynamics in the hippocampus during waking, which allow for globally remapped representations of different environments (Colgin et al. 2008). It is possible that hippocampal sleep states explore this higher-dimensional space, activating multiple representations that reflect waking trajectories from a variety of different environments. By contrast, the states in one grid module maintain the same low-dimensional dynamics

across non-active and sleep states that they exhibit during awake exploratory behaviors in novel and familiar environments of different shapes and configurations (Fyhn et al. 2007; Yoon et al. 2013; Yoon et al. 2016). This rigid confinement of the dynamics of grid cells in a module, across behaviors and states, implies and predicts that the grid cells will likely exhibit the same preserved cell-cell relationships during other modes of behavior, such as during navigation through non-spatial and other conceptual spaces (Aronov et al. 2017; Kraus et al. 2015; Killian et al. 2012). This prediction is readily testable, using simultaneously recorded co-modular grid cells. Indeed, all models of grid cells that are based on integrating a velocity signal to generate an updated estimate of grid phase (these include continuous attractor models and oscillatory interference models [Burgess et al. 2007; Grossberg & Pilly 2012; Navratilova 2012; Welinder et al 2008]) are applicable to navigation through non-physical continuous spaces, so long as the velocity input to the grid cells reflects the time-derivative of the corresponding continuous variable. However, the predictions of preserved low-dimensional structure through conserved cell-cell relationships during non-spatial navigation follow specifically from low-dimensional attractor models (Amari, 1997; Burak & Fiete 2009; Welinder et al. 2008; Yoon et al. 2013).

Within the class of continuous attractor models are networks with different types of recurrent connectivity and topology. One possibility is that the grid cell network supports the activation of one local group of interacting neurons (an activity bump) in the neural sheet and that connectivity is global (single-bump networks [Guanella & Verschure, 2006]). Another is that the connectivity is local (according to some proper rearrangement of neurons) and that activity consists of multiple activity bumps on the

cortical sheet (Burak & Fiete 2009; Welinder et al 2008). In the former network, co-active neurons are recurrently coupled and should always show high correlations. In the latter, co-active neurons in different bumps may share no direct coupling, and thus the distribution of correlations given the same tuning phase should be bimodal. The slight hint of bimodality in the correlations of cells with high spatial tuning overlap (far left column in Figure 6c, particularly during RUN) may be suggestive of a multi-bump network. However, additional experimentation with circuit perturbation techniques will be required to determine which connectivity pattern most accurately describes the system (Widloski et al. 2015).

The finding that grid cell co-activity during sleep resembles co-activity during waking behaviors raises the possibility that superficial-layer MEC grid cells play a role in offline memory processing. This hypothesis is consistent with reports involving recordings from other cortical areas. For example, neuronal activity in primary visual cortex (Ji & Wilson, 2007), auditory cortex (Rothschild et al. 2016), and medial prefrontal cortex (Euston et al. 2007), as well as grid cell activity in deep layers of MEC (Ólafsdóttir et al. 2016), has been reported to correlate with hippocampal place cell activity during replay events, which are hypothesized to play a role in memory consolidation. However, the present results only involve grid cells recorded from MEC superficial layers. An initial study of grid cell replay in MEC superficial layers reported that grid cells rarely show coordinated reactivation with hippocampal place cells (O'Neill et al. 2017), a result that seems inconsistent with the hypothesis that superficial layer grid cells drive consolidation of hippocampal memory representations during sleep.

The present results emphasize a need for caution when searching for evidence of replay in superficial-layer grid cells during sleep. That is, the extent to which replay occurs in the superficial layer grid cell network may be overestimated due to the structured nature of instantaneous activity patterns that reflect stable, long term network connections rather than plasticity induced by earlier experiences. Investigations of replay in superficial layer grid cells would therefore be strengthened by the inclusion of additional behavioral controls, such as comparisons of co-activity patterns during sleep to co-activity patterns during subsequent exploration of a novel environment. Grid cell simulations would also be helpful to determine the extent to which it is possible to distinguish between co-activity due to long-term network connections versus more recent experience-dependent reactivation. Such simulations would likely provide useful information about the number of simultaneously recorded superficial layer grid cells necessary to reliably detect experience-dependent reactivation. Future experiments, designed to determine whether sleep-associated reactivation of correlated firing patterns in ensembles of superficial layer MEC grid cells is experience-dependent, are key to achieving a deeper understanding of neural and network mechanisms of memory consolidation in the entorhinal-hippocampal network during sleep.

2.4 – METHODS

2.4.1 Behavioral training of CA1 rats

Rats implanted with drives in CA1 were initially part of a different study, and thus different behavioral training protocols were used. Prior to surgery, CA1 implanted rats were trained to run on a circular track with a diameter of 100 cm and a track width of 10

cm. Small pieces of sweet cereal were placed on opposite ends of the circular track as food reward. Once the rats reliably ran at least ten laps on the track in a 10-minute session, hyperdrive recording devices were implanted. Following one week of recovery, rats were re-trained to run on the circular track. Each training day consisted of three 10-minute running sessions interleaved with four 10-minute rest sessions. All CA1 implanted rats received a minimum of three days of training on the circular track before data collection began.

On each recording day, CA1 implanted rats ran on the circular track for four 10-minute running sessions with intervening 10-minute rest sessions. Upon completion of the circular track task (~8pm), rats were placed in a 60 cm x 60 cm open field enclosure, with water and food provided along with cloth bedding and enrichment items, for overnight sleep recordings.

2.4.2 Place cell firing rate map calculation

Given that CA1 place cells were recorded while rats performed laps around an elevated circular track, rather than ambulating throughout an open field environment as with grid cell recordings, the procedure for rate map calculation was different for place cells than for grid cells. For CA1 recordings on the circular track, rats' positions were first converted from two-dimensional Cartesian coordinates to a one-dimensional measure of angular position along the track. The sequence of angular coordinates corresponding to a rats' position at each video frame time were then sorted into 5-degree bins spanning from 0 to 360. Rate maps were calculated by dividing the total number of spikes occurring while the rat was actively ambulating within each radial bin by the total amount of time

that the rat spent actively moving within that bin. They were then smoothed with a Gaussian kernel 25 degrees wide.

2.4.3 Relative distance between pairs of place cells

The relative angular distance between the firing locations of two CA1 cells on the circular track was defined as the length of the minor arc between their fields. Only place cells with peak firing rates exceeding 1 Hz were included in this analysis. Each cell pair was sorted into one of five bins based on the relative angular distance (each bin spanned a range of 36 degrees), and the average spike time correlation across all pairs within a group was calculated (Figure 2.5). Similar to Figure 2.6a, spike time correlations for each behavioral state were then normalized by the maximum average spike time cross-correlation coefficient for that behavioral state (Figure 2.6b).

2.4.4 Grid cell firing rate estimation

Grid cell firing rates during each RUN, REM, and NREM period were calculated by dividing the total number of spikes by the duration of the detected behavioral period, averaged across periods for each behavioral state (Figure 2.1c, histograms), and then averaged across units (Figure 2.1b).

2.4.4 Removal of theta contribution to spike time cross-correlations

One possible explanation for the relatively high spike time cross-correlations observed for some grid cell pairs, aside from network connectivity, is that spikes from those grid cells tended to occur at the same theta phase. To address this possibility, the observed spike time cross-correlations in each behavioral period (RUN or REM) were

compared to distributions containing 200 spike-time cross-correlations computed from shuffled spike train pairs, based on a method reported previously (Geisler et al. 2007). In these shuffled spike trains, the times of each spike for each grid cell were shuffled independently. Each spike was moved randomly to a new time that satisfied two conditions: the new time fell within a +/- 500ms window around its original spike time and was associated with a theta phase within 5 degrees of the original spike time's associated theta phase. Thus, theta-induced correlations and other correlations on a time-scale slower than 500 ms in the shuffled data were preserved, while short-latency correlations were eliminated. Examples of individual cross-correlations for shuffled spike trains are shown in Figure 2.7 together with the corresponding original cross-correlation. The average of the cross-correlations for all shuffled spike trains was presumed to represent the portion of the cross-correlation explained by theta phase co-modulation alone (Figure 2.7). To visualize the temporal correlations of spikes that were not attributable to theta phase modulation of spike times, the magnitude of the observed cross-correlation that fell within the 98% confidence interval of shuffled distribution was reduced by the amount attributable to theta or other slow correlations (Figure 2.7). To do so, first, any lag bins of the original correlogram with values that fell within the confidence interval were set equal to zero. Next, in any time lag bins in which the correlogram was greater than the upper bound of the confidence interval, the correlogram was reduced by the value of the upper confidence interval bound in that bin (e.g. if the correlogram in a bin was equal to 0.1 and the upper confidence interval bound was 0.06, the new correlogram value would be 0.04). Values of the correlogram which fell below the lower bound of the confidence interval were reduced by the value of the lower bound (e.g. if the correlogram bin was equal to

0.02 and the lower confidence interval bound was 0.03, the new correlogram value would be -0.01).

For each cell pair, the average theta-removed cross-correlation across all sessions of a given behavior was calculated by taking the theta-removed cross correlation for each individual behavioral session and then averaging across sessions. The area of the cross-correlogram between +/- 5 ms lag was calculated ("summed correlation", as in Figures 2.3, 2.4B left, 2.5 and 2.6C and A2.1) and used as a measure of short-latency correlation in Figure 2.7. The population average of the summed correlation was used in Figure A2.2 to look at differences between low and high relative spatial phase groups, calculated as in Figure 2.8. The relationship between relative spatial phase and the summed correlation or the summed, theta-subtracted correlation (Figure 2.7) was tested using repeated measure ANOVA.

2.4.5 Statistics

Unless otherwise noted, all analyses were performed in MATLAB 2017a (The MathWorks, Inc., Natick, Massachusetts) using custom-written software. However, standard built-in MATLAB functions were used (e.g. "xcorr," "corrcoeff," etc.) whenever possible.

The SPSS Statistics Subscription (build 1.0.0.781, IBM) software package was used for the statistical analyses in this paper. This includes the statistics describing firing rate differences across behaviors (as shown in Figure 2.1 for MEC), the statistics comparing the relationships between rate map correlation coefficients and the spike time correlation values (calculated from the sum of the correlations within the +/- 5 ms lag

window) for data in Figure 2.3, as well as the statistics used to analyze the effects of removing theta phase influences (Figure 2.7).

Chapter 3: Grid cell pairwise correlations were not detectably changed by experience

3.1 Introduction

As shown in the previous chapter, network correlations appear to play a major role in shaping the firing patterns of grid cells in the superficial medial entorhinal cortex. Grid cells pairs with similar spatial patterning were shown to exhibit functional connectivity during both spatial behaviors and non-spatial behaviors such as sleep, as predicted by the continuous attractor model of grid cell pattern formation. We found this to be the case during both REM sleep, when theta rhythms dominate LFP recordings, and NREM sleep and rest, when theta is absent. During all examined behaviors, short time scale correlations between grid cells were related to the relative spatial orientation of their grid fields during active behaviors, suggesting that grid cells' grid pattern formation is a network phenomenon. These findings have important implications for the study of grid cells in general, and particularly for investigations of experience-dependent reactivation of grid cell activity patterns.

One of the implications of the strong influence of these network connections on grid cell firing is that it complicates studies aimed at determining the extent to which grid cell reactivation during sleep relates to specific experiences. Specifically, because spike time correlations between cells appear to result largely from stable network connections, spontaneous activation of the network by random noise may be difficult to distinguish from patterns of activation that are biased by structured input or previous experience (Ikegaya et al 2004; Tsodyks et al 1999). Given that reports of replay in grid cells are available

(O'Neill et al. 2017, Ólafsdóttir et al. 2016), the question now becomes whether this reported "replay" reflects novel experiences or is a result of grid cell network connectivity irrespective of specific experiences.

Replay of waking experience is believed to be a mechanism for memory consolidation after learning (Dragoi & Buzsaki 2006; Foster & Wilson 2006; Nádasdy et al. 1999), so understanding the extent to which experience-dependent replay occurs, and in which brain regions it occurs, would provide insight into the systems and mechanisms underlying the formation of memories. Hippocampal place cells, particularly in area CA1, have been shown to exhibit experience-dependent replay (Foster & Wilson 2006; Lee and Wilson 2001; Louie & Wilson 2001; Nádasdy et al 1999). Grid cells are believed to provide input to place cells (Canto et al. 2008, Fyhn et al. 2007, Zhang et al. 2013), and so answering the question of whether grid cells are involved in experience-dependent replay would help to clarify the potential role of the medial entorhinal cortex in offline memory processes. Furthermore, primary sensory areas, such as V1 and primary auditory cortex, have been shown to exhibit coordinated replay with place cells (Ji & Wilson, 2007, Rothschild et al. 2017). Considering that much of the sensory information that is fed into the hippocampus is processed by the MEC and postrhinal cortex (Burwell & Amaral 1998a, Burwell & Amaral 1998b), these coordinated replay results raise the question of whether grid cells also reactivate in an experience-dependent manner.

If grid cell reactivation is experience-dependent and important for memory formation, then one would expect to see an increased amount of reactivation during sleep and rest following novel experiences compared to familiar experiences (Kudrimoti et al. 1999, Wilson & McNaughton 1994). One would also expect that the correlations between

activity patterns present during novel experience, and activity patterns present during reactivation in the sleep or rest periods following that experience, to be greater than the correlation between those behavioral activity patterns and the activity patterns observed during periods of rest prior to that experience (Kudrimoti et al. 1999, Wilson & McNaughton 1994). This comparison of novel activity patterns to the activity patterns in the rest and sleep periods prior to the novel behavior is what hereafter will be called ‘‘pre-activation”.

In this chapter, I investigate whether novel experience changes the relationship between grid field overlap and spike time correlations in pairs of grid cells observed in chapter 2. If grid cell reactivation is experience dependent, one would expect to see changes in the correlation patterns between grid cell spike time correlations and grid field overlap, indicative of the presence of experience-dependent changes in network connections. Additionally, I show preliminary results regarding reactivation of grid cell firing patterns during sleep following a novel waking experience, and how that reactivation compares to both reactivation during sleep following a familiar experience and pre-activation during sleep preceding the novel experience. The prediction under the hypothesis that grid cell reactivation is experience dependent would be to see a greater amount of reactivation following novel experience compared to reactivation of a familiar experience, as has been observed for hippocampal place cells (Cheng & Frank 2008). What is found, however, is no apparent changes in the relationship between grid cell spike time correlations and grid field overlap, which is indicative of a lack of plasticity in the grid cell network in response to novel experiences. This lack of plasticity is also supported by the observation that grid cells can stably represent a novel environment by the first lap

along a novel linear track configuration. Finally, preliminary results indicate that grid cell reactivation after novel experience may be no greater than reactivation after familiar experience. This pattern of results suggests that grid cell reactivation likely results from pre-existing network connections rather than plasticity occurring during specific experiences.

3.2 RESULTS

3.2.1 A novel linear track orientation produces changes in individual grid cell firing rate maps.

To investigate whether reactivation during sleep and rest of grid cell firing patterns from waking was changed by a novel experience, I first confirmed that a novel trajectory changed grid cell firing patterns compared to a familiar trajectory. Specifically, I used two different orientations of a 2 m long elevated linear track. The first, familiar orientation extended from one corner of the video camera's field of view to the opposite corner. In the second, novel configuration the track was rotated to span the other major diagonal (approximately 112 degrees rotation). In addition to the track rotation, the flower pot in which the animal rested between sessions was moved to a different location in the recording room. The distributions of population rate map correlation coefficients (see Methods) between pairs of laps from the familiar track orientation (Figure 3.1a) or pairs of laps from the novel track orientation (Figure 3.1b) were skewed toward positive values. In contrast, the distribution of population rate map correlation coefficients between

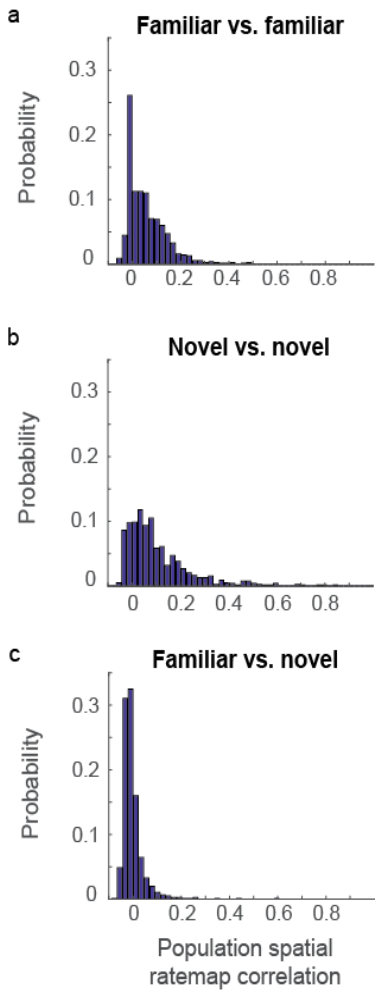

Figure 3.1 – Rate maps for a novel track configuration are significantly different than those for a familiar track configuration. The distributions of population rate map correlation coefficients between familiar and novel laps was significantly different than distributions of correlation coefficients between two laps on the familiar track or two laps on the novel track.

a) The distribution of population rate map correlations between lap pairs on the track in the familiar orientation.
b) The distribution of population rate map correlations between lap pairs on the track in the novel orientation.
c) The distribution of population rate map correlations between lap pairs on the track in the familiar and novel configurations.

familiar-novel lap pairs was clustered around zero (Figure 3.1c), indicating that grid cell rate maps were largely dissimilar between familiar and novel track orientations. The three distributions were significantly different (1-way ANOVA, $p < 0.0001$, $F(2,2310) = 242.7$), with the familiar-familiar and novel-novel, but not the novel-familiar, distributions having means above zero (familiar-familiar distribution: 0.058 +/- 0.003, novel-novel distribution: 0.103 +/- 0.005, familiar-novel: -0.003 +/- 0.002). Therefore, I used grid cell recordings from the novel and familiar track orientations

to investigate whether novel experience changed correlation patterns found between grid cell pairs.

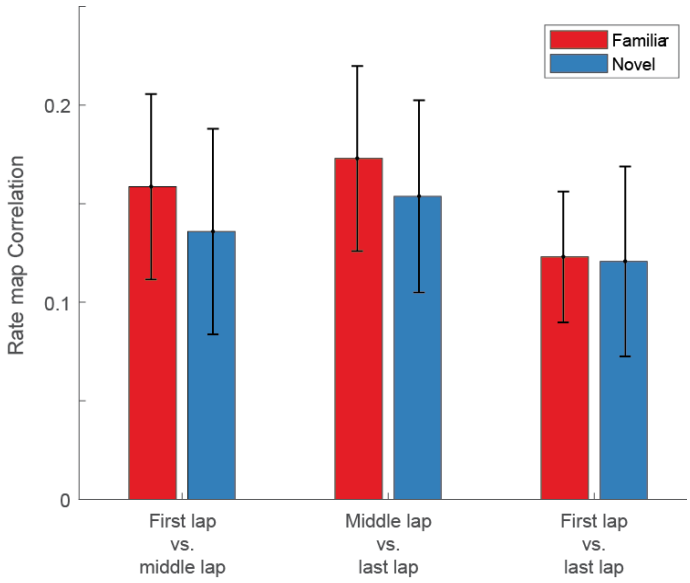

Figure 3.2 – Grid cell rate maps were immediately stable during the first experience of a novel trajectory. Grid cell firing rate maps were compared from the first, middle and last lap of the first session of both familiar and novel track experiences. Rate maps between first and middle, middle and last, and first and last laps were similarly correlated during both familiar and novel track traversals. Directions on the track were treated as independent laps, as grid cell rate maps differ depending on the direction of travel (Hafting et al. 2008). The same cells were used for both novel and familiar track calculations. Error bars show mean +/- SEM, and n=26 laps each for novel and familiar track sessions.

3.2.2 Grid cell representations of a novel track configuration emerge immediately upon initial experience.

I next examined whether grid cells represented the novel linear track orientation in a stable manner. Prior studies have found varying changes in grid field stability during a first experience with a novel environment, reporting either changes in grid orientation but not scale (Fyhn et al. 2007) or changes in both grid orientation and scale (Barry et al. 2012). I found that grid cell representations of a novel track configuration were stable starting from the first lap along the novel trajectory. Moreover, as described above, grid cell firing patterns representing the novel trajectory differed from grid cell representations of the familiar trajectory. In Figure 3.2, I quantified the average (+/- S.E.M.) rate map correlation coefficient between the first and middle laps,

middle and last laps, and first and last laps during the first session of each day with either the familiar or the novel track configuration. Neither first and middle, middle and last, or first and last lap rate map correlation comparisons showed a difference between familiar track (Figure 3.2: red, left) or novel track (Figure 3.2: blue, left). Moreover, in Figure 3.3, I show example spike rasters of grid cells during the first five laps in one direction during the first behavioral session of a recording day for three different animals. Note that grid cell firing did not appear to vary more between the first and fifth lap for the novel (2^{nd}, 4^{th}, and 6^{th} rows) track configuration compared to the familiar (1^{st}, 3^{rd}, and 5^{th} rows) configuration.

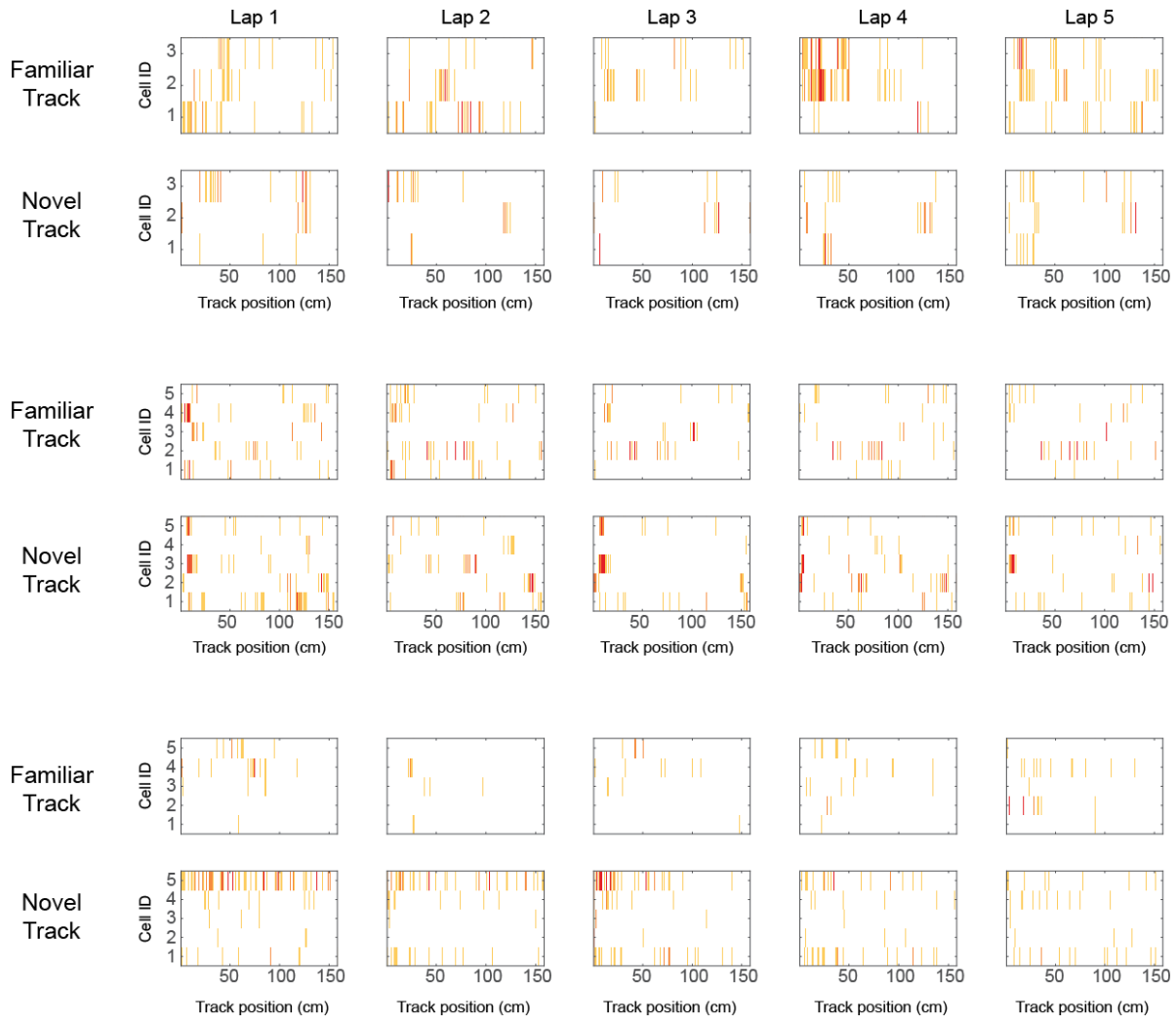

*Figure 3.3 – Example spike rasters from grid cells during initial traversals of linear track***.** Grid cells do not appear to be particularly unstable during the initial traversals of a novel linear track configuration compared to the first experience in a day of the familiar configuration. Within each panel, rows show spikes from different simultaneously recorded grid cells on the familiar track (top panels) and novel track (bottom panels). While some variability is observable in both familiar and novel configurations, grid cell representations of a novel trajectory appear to emerge immediately upon an animal's first experience.

3.2.3 Spike time correlations between grid cells in overnight recordings were unchanged after a novel experience.

I next investigated whether the relationship between spike time correlations and grid field overlap of grid cell pairs during sleep were changed by a novel experience. To

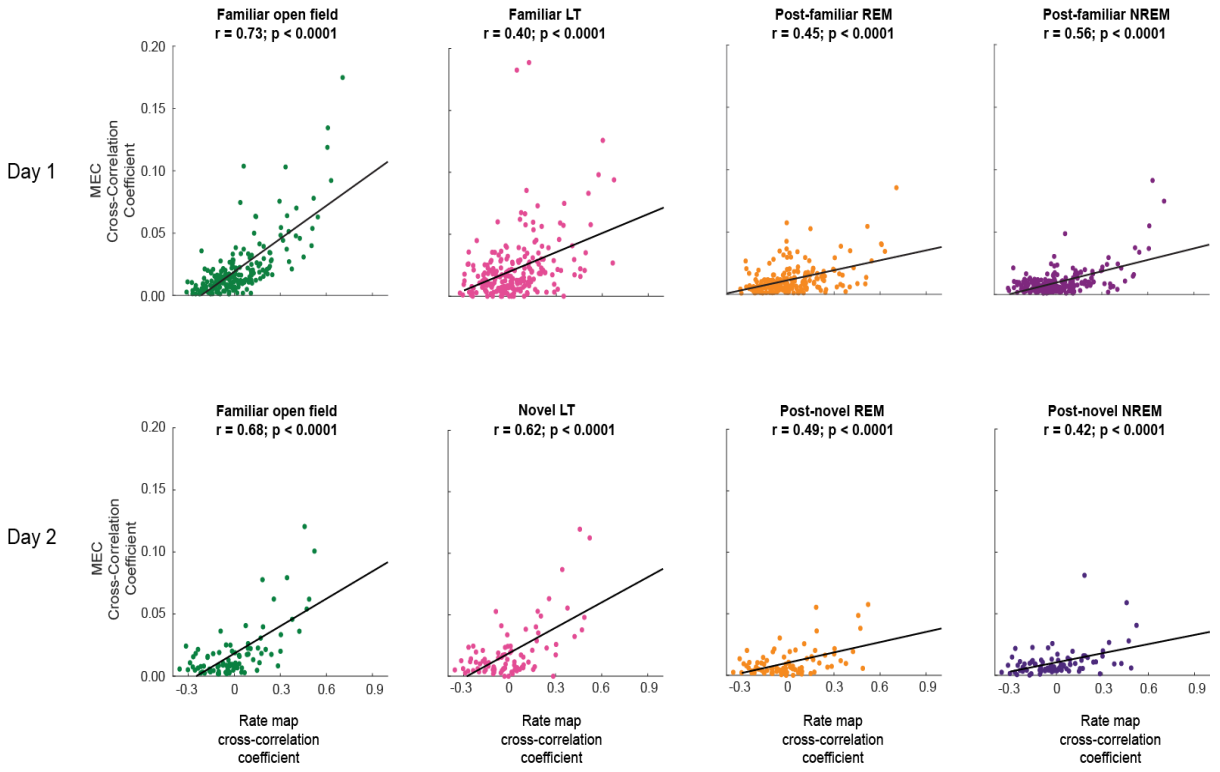

Figure 3.4 – Novel experience does not impact the relationship between rate map correlations and short-timescale spike time correlations. Spike time correlations between pairs of grid cells show the same relationship with their rate map correlation coefficients on the linear track as they do in the behaviors examined in chapter 2 (top row, columns 1, 3, and 4 are taken from Figure 2.3). This relationship between rate map correlation coefficients and spike time cross-correlations was not changed due to novel experience. The rate map cross-correlation coefficients plotted on the x-axis in each plot were measured from that day's open field sessions. The upper row shows the data from the first day, which included familiar linear track and open field sessions. The bottom row shows results from the second day, which included another run in the familiar open field environment as well as sessions on the novel linear track orientation. The sleep sessions on day one occurred after the familiar track exploration, and the sleep sessions on day two occurred after the novel linear track experience (n=211 cell pairs on day one, n=87 cell pairs on day two).

address this question I used two of the methods described in chapter 2: the relationship between grid cells' rate map correlations and spike time correlations (Figure 3.4) and the comparison of grid cells' relative spatial phase magnitudes and spike time correlations (Figure 3.5). I found that, for the relationships with both the rate map correlation coefficient and the relative spatial phase magnitude measures, there was no change in the relationship between spatial overlap and spike time correlations after novel experience. In the top row of Figure 3.4, the same scatter plots are shown as in Figure 2.3a, with the additional inclusion of results from a familiar linear track. The bottom row of Figure 3.4 shows the relationship between open field rate map correlations and spike time cross-correlations calculated on day two, the day when the animal experienced the novel track configuration. In the day two results, no changes in the relationship between spatial correlations and spike time correlations were seen for any behavior. There was no interaction effect or main effect of day on the regression (Multiple regression model: $F(5,1186) = 3.26$, $b = -0.14$, $p=0.07$, day * spatial correlation; $F(5,1186) = 0.35$, $b = 0.06$, $p = 0.55$, day * behavior; $F(5,1186) = 0.26$, $b = -0.03$, $p = 0.61$, day), indicating that the relationship between spatial correlation and spike time correlation was not affected by the novel experience and did not change from day to day. Significant correlations were present in all behaviors on day 1 (RUN: $F(1,209) = 235.25$, $p < 0.0001$, $R^2 = 0.53$; Familiar linear track: $F(1,209) = 38.0$, $p < 0.0001$, $R^2 = 0.15$; REM: $F(1,209) = 52.53$, $p < 0.0001$, $R^2 = 0.20$; and NREM: $F(1,209) = 93.81$, $p < 0.0001$, $R^2 = 0.31$) and day 2 (RUN: $F(1,85) = 72.4$, $p < 0.0001$, $R^2 = 0.46$; Novel linear track: $F(1,85) = 52.9$, $p < 0.0001$, $R^2 = 0.38$; REM: $F(1,85) = 26.5$, $p < 0.0001$, $R^2 = 0.24$; and NREM: $F(1,85) =$

18.4, $p < 0.0001$, $R^2 = 0.18$). Thus, the results did not indicate functional plasticity in the grid cell network connections in response to a novel experience.

Figure 3.5 shows the relationship between grid cell pairs' relative spatial phase magnitude and spike time correlations during open field, linear track, REM sleep, and NREM sleep and rest. The top row of Figure 3.5 shows the results from the first day, when rats ran on the familiar track configuration, while the bottom row shows the results for day two, when rats ran on the novel track configuration. For both days, the same pattern in the relationship between relative spatial phase and spike time correlation was seen as in Chapter 2, namely that the lower the relative spatial phase magnitude the greater the spike time correlation. These results are apparent for both short (+/- 5 ms, left panels) and relatively long(+/- 50 ms, right panels) timescales. Like the results shown in Figure 3.4, these results suggest an absence of changes in the functional connectivity of the grid cell network in response to novel experiences.

3.2.4 Grid cell reactivation is not correlated with behavioral experience.

We used a partial correlation analysis that has been used previously to investigate reactivation of correlated place cell activity from waking behaviors during subsequent sleep (Kudrimoti et al., 1999) to determine whether grid cell pairwise correlations between waking and sleep recordings increased selectively after a novel experience. If

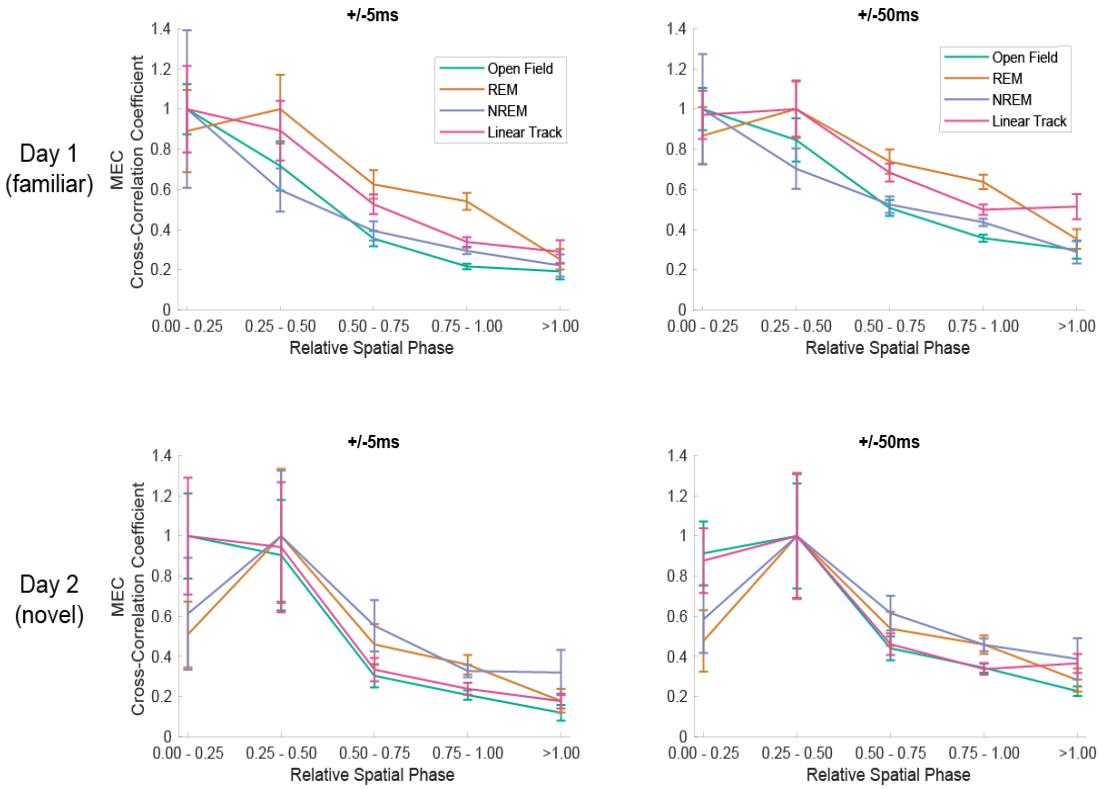

Figure 3.5 – Relationships between grid cell pairs' spike time correlations and relative spatial phase magnitude were not affected by novel experience. To examine the stability of the relationship between grid fields' relative spatial phase and grid cells' spike time correlations, we looked at grid cell pairs during open field running, linear track running, and both REM and NREM sleep. As in Figure 2.4, we look at both +/- 5 ms and +/- 50 ms windows, and again results were similar for the two window sizes. In the top row are the results for grid cell pairs (n=226) recorded on day one, which consisted of experiences in familiar environments. The bottom row shows grid cell pairs (n=87) recorded during and after exposure to a novel trajectory. No apparent differences can be seen between results for familiar and novel conditions, indicating that experience in a novel environment did not change the relationship between grid cells' grid field overlap and spike-timing across behavioral states.

reactivation of grid cell activity patterns is experience-dependent, then one would expect correlations observed during novel experience to be poorly described by correlations observed during familiar experience. How well correlations recorded during behavior can be explained by network correlations alone can be measured by looking at partial correlations. Partial correlations estimate the amount of correlation between grid cell activity patterns during novel behavior and the following sleep periods, while controlling for spike time correlations during open field foraging in a familiar environment, recorded the next morning. The ”explained variance”, calculated as the square of the partial correlation, is the variance explained by specific experiences rather than general network correlations presumably reflecting pre-existing network connectivity (Kudrimoti et al 1999). The explained variance can be compared to “pre-activation” (i.e., the correlation between co-activity during the novel experience and the preceding sleep period) conditioned on the previous day’s open field session. If the explained variance is no different between reactivation and pre-activation, then the explained variance is likely not measuring experience-induced change in correlations.

To test the hypothesis that grid cell activity patterns are more strongly reactivated during sleep after novel experience, we first focused on REM sleep in overnight recordings. The amount of variance in the grid cells’ correlation pattern in REM sleep that was explained by the grid cells’ correlation structure during earlier traversals on the novel track was estimated, after controlling for the general correlation pattern observed during exploration of a familiar open field environment the following morning. These explained variance estimates for REM sleep following exposure to the novel track fell within the range of analogous explained variance estimates for REM following traversals of the

familiar track (Figure 3.6a). The explained variance estimates for REM sleep following exposure to the novel track were also similar to explained variance estimates for REM that preceded experience on the novel track (Figure 3.6a). However, these results are highly preliminary and should be interpreted with caution because REM recordings following a novel experience were only obtained from two animals. Still, these preliminary results do not support the conclusion that reactivation of grid cell firing patterns during REM sleep reflects specific waking experiences, such as exposure to a novel environment.

I also examined NREM sleep epochs in overnight recordings to assess whether grid cell reactivation occurred during NREM sleep. Hippocampal place cell reactivation during NREM sleep (Wilson & McNaughton 1994, Skaggs & McNaughton 1996, Kudrimoti et al 1999) has been more thoroughly investigated than reactivation during REM (Louie & Wilson 2001). Moreover, previous grid cell studies have reported reactivation of grid cell activity patterns during NREM sleep and awake rest (O'Neill et al. 2017, Ólafsdóttir et al. 2016). However, these grid cell studies did not investigate whether reactivation of grid cell activity during sleep was changed by experience in a novel environment nor did they assess whether pre-activation of grid cell activity during sleep was observed prior to experience in a novel environment, which are important controls necessary to exclude the possibility that grid cell correlations are pre-existing, fixed, and unrelated to specific experiences. To look for evidence of grid cell reactivation during NREM that is specific to novel experiences, I again calculated the explained variance using partial correlation analyses, as was done above for REM sleep. The amount of variance in the grid cells' co-activity patterns in NREM sleep that was explained by the grid cells' co-activity

patterns during earlier experience on the novel track was estimated, after controlling for general correlations observed during exploration of the familiar open field (Figure 3.6b). Explained variance estimates for NREM sleep following novel track sessions spanned a wide range but did not appear to be strikingly different than explained variance estimates for NREM sleep following sessions on the familiar track (Figure 3.6b) or estimates for NREM sleep preceding novel track sessions (pre-activation control; Figure 3.6b).

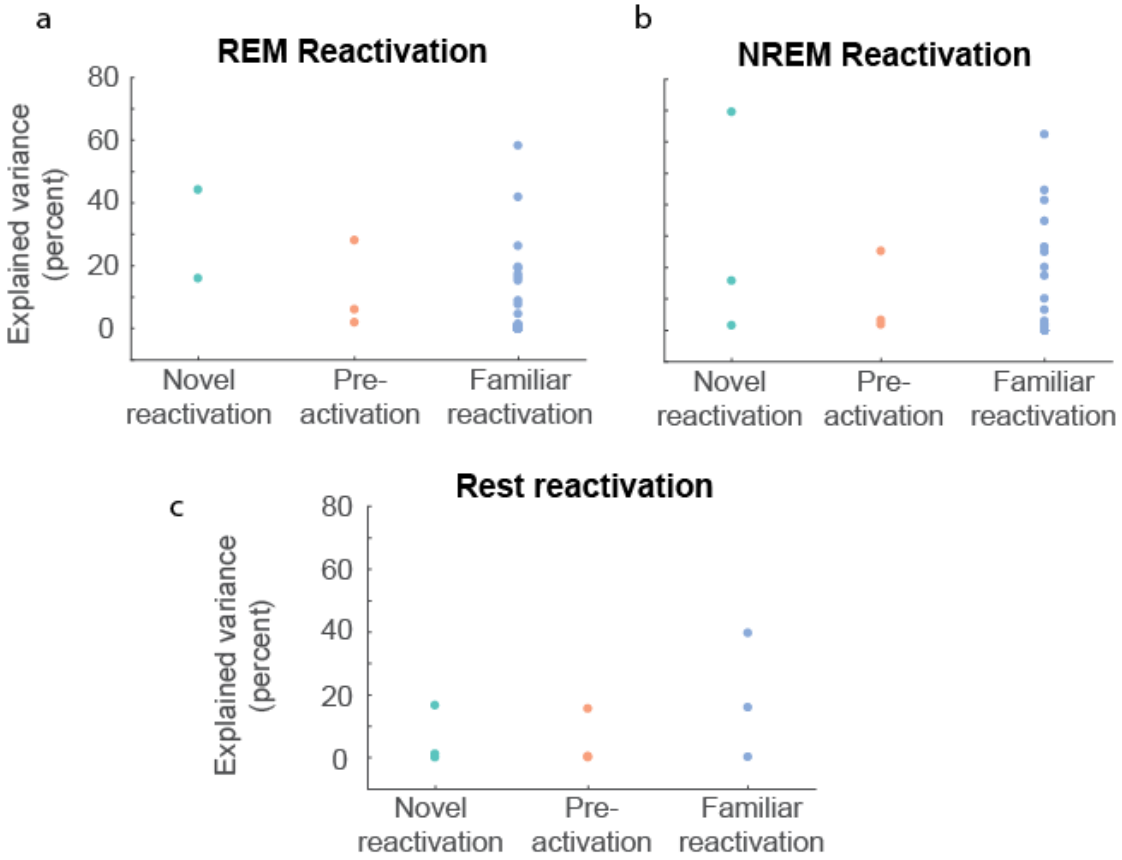

Figure 3.6 – Evidence of grid cell reactivation during sleep and rest following experience in a novel environment was not obtained. Explained variance computed using partial correlation analyses (see Methods) is shown for reactivation of grid cell co-activity patterns on a novel track configuration during subsequent REM ("Novel reactivation" in panel a), for pre-activation of grid cell co-activity patterns on the novel track during the previous night's REM ("Pre-activation" in panel a), and for reactivation of grid cell co-activity patterns on a familiar track during subsequent REM ("Familiar reactivation" in panel a). Analogous results are also shown for NREM (b) and waking rest (c).

However, as with REM results, these data are preliminary and should be interpreted with caution, given the low number of animals with grid cell recordings on the novel track configuration (n = 3 rats).

Finally, we examined post-behavior waking rest to test whether grid cells exhibit experience-dependent reactivation during waking rest shortly following a novel experience. These conditions are similar to those in which the strongest reactivation has been observed in place cells (Davidson et al 2009; Karlsson & Frank 2009; Kudrimoti et al 1999; Tang et al. 2017). Specifically, reactivation of hippocampal place cells during sleep and rest has been shown to be strongest in the first ten minutes of awake rest following exposure to an environment (Kudrimoti et al. 1999; Skaggs & McNaughton 1996; Wilson & McNaughton 1994). Therefore, if grid cells exhibit reactivation during sleep or rest, one would expect it to be most readily detected in quiet rest occurring shortly after active behaviors in a novel environment. However, using analogous analysis methods and comparisons as described above for REM and NREM, we observed no evidence for significant reactivation of grid cell activity in waking rest following novel experience (Figure 3.6c). However, these results are, again, only preliminary, due to the low number of recordings, and thus strong conclusions cannot be made.

3.3 Discussion

3.3.1 Traversal of a novel trajectory produces immediately stable grid cell responses.

We first examined whether re-orienting an elevated linear track produced grid cell rate maps that were significantly different from those observed during traversal of a

familiar orientation of the track. These different grid cell rate maps may reflect a different slice through the grid cells' representation of the recording room (Yoon et al. 2016). In any case, rate maps recorded during exploration of the novel track configuration were as stable as the familiar track rate maps, consistent with the results of a prior study in which the same grid cells were recorded in different rooms or different environments in the same room (Fyhn et al. 2007). These results differ from another prior study, however, which showed an unstable expansion of the grid period upon exposure to a novel environment (Barry et al. 2012). Unlike our results, Barry and colleagues found that the grid period immediately expanded and then decreased over time as the animal explored a novel environment. Thus, the track orientation change in the present study may not have been sufficiently novel to cause the same grid period change and loss of gridness seen in Barry and colleagues' work (2012).

3.3.2 Novel experience does not change the relationship between grid cell pairs' spatial field overlap and spike time correlations.

As could be predicted from the results of chapter 2 as well as previous work (Fyhn et al. 2007; Yoon et al. 2013), the relationship between relative spatial phase and spike time correlations remained stable across multiple environments, as seen in the top row of Figure 3.4 and Figure 3.5. What was not so easily predictable, however, is that the exposure to a new environment did not change the relationship between spike timing and spatial similarity observed during REM and NREM sleep. The long-term stability of the relationship between relative spatial phase and spike time correlation between pairs of grid cells indicates that there is likely to be little functional plasticity occurring in the

superficial layer MEC grid cell network. While this result does not rule out the possibility that grid cells somehow participate in the experience-dependent reactivation that occurs in place cells soon after learning (Kudrimoti et al. 1999; Skaggs & McNaughton 1996; Wilson & McNaughton 1994), the lack of change in REM sleep does not match results observed in place cell ensembles during REM sleep (Louie & Wilson 2001). In REM sleep, Louie and Wilson (2001) observed the presence of replay occurring many hours after one of several repeated exposures to a familiar environment, whereas ensemble patterns from a novel environment were not observed until sleep periods that occurred after the initial exploration of the novel environment. The lack of change in spike time correlation patterns after novel experience observed here may indicate that different processes are occurring in MEC grid cells and hippocampal place cells during REM sleep.

3.3.3 No evidence of experience-dependent reactivation in grid cells of the superficial layers of MEC during overnight sleep was obtained.

Figure 3.6 shows results examining reactivation of grid cells during sleep and rest following a novel experience. Unfortunately, there was an insufficiently low number of recordings available to determine whether experience in a novel environment changed reactivation during sleep and rest. However, our preliminary results suggest that grid cell reactivation following experience in a novel environment differs from results from similar studies of reactivation in hippocampal place cells (Kudrimoti et al. 1999). In the earlier study, Kudrimoti and colleagues found that place cells showed a higher correlation between place cell co-activity observed during behavior in a novel environment and during the rest periods immediately following, compared to correlations between place

cell co-activity during the novel experience and rest preceding the novel experience. However, they did not have enough data during REM to assess whether reactivation occurred during REM sleep. On the other hand during NREM, they found, similar to other studies (Wilson & McNaughton 1994, Skaggs & McNaughton 1996), that the increase in pairwise correlations reflecting co-activity from waking experiences decayed rapidly, approaching the pre-experience baseline within approximately 30 minutes. The results reported here from the overnight sleep recordings are not directly comparable, therefore. Although preliminary, the results shown in Figure 3.6c are roughly on the same timescale as earlier place cell studies, and no evidence of differences between reactivation after novel experience, reactivation after familiar experience, or pre-activation of a novel experience was observed. A likely explanation for the lack of evidence of experience-dependent grid cell reactivation shown here is that grid cells are part of a relatively static network, which results in fixed spike time correlation patterns across different behaviors and experiences.

3.3.4 Other measures of experience-dependent reactivation may give different results.

The research described in this chapter did not address multi-unit measures, which may show different results from the pairwise measures investigated here. There may be replay of grid cell sequences that represent specific trajectories, which were not detected by the pairwise correlation measures just described. In the next chapter, I examine sequences of grid cell firing during waking behaviors and in sleep. I investigate whether replay of specific sequences during REM, NREM sleep, and rest from waking behaviors

after familiar experience occurs more often than ensembles of shuffled spike trains. I also show preliminary results investigating the rates of replay after novel experience, during REM, NREM sleep and rest, and compare those results to ensembles of shuffled spike trains.

3.4 METHODS

For general recording and analysis methods, please refer to Appendix 1.

3.4.1 Partial correlations

The explained variance was defined, as in (Kudrimoti et al. 1999), as the square of the partial correlation between spike time correlations during RUN (novel linear track or familiar linear track) and POST (the following sleep or rest period) conditioned on NET (the open field run correlations, recorded on the morning following the overnight recording). Pre-activation was calculated using the preceding sleep or rest period for POST and the open field from the preceding day for NET. The variable $r_{RUN,POST}$ is the correlation between the spike time correlations during RUN and the spike time correlations during POST, $r_{RUN,NET}$ is the correlation between the spike time correlations recorded during RUN and the spike time correlations during NET, and $r_{POST,NET}$ it the correlation between the spike time correlations recorded during POST and the spike time correlations recorded during NET. All correlation vectors were normalized by the product of the standard deviations of the two measures being correlated. The equation used was

$$EV = r^2_{RUN,POST|NET} = \left(\frac{r_{RUN,POST} - r_{RUN,NET}r_{POST,NET}}{\sqrt{1 - r^2_{RUN,NET}}\left(1 - r^2_{POST,NET}\right)}\right)^2$$

3.4.2 Population rate map correlation coefficient

The population rate map correlation coefficients used in Figure 3.1 were calculated via the builtin “corrcoef” MATLAB function (MATLAB 2017a, The MathWorks, Inc. Natick, Massachusetts). The two matrices, consisting of the linearized rate maps for each cell during a lap, were compared, and the off-diagonal value was reported. Only laps of the same left-to-right direction were compared.

Chapter 4: Grid cell ensemble co-activity remains unchanged regardless of specific behaviors or experiences

4.1 - Introduction

As was shown in Chapter 3, the functional connections between grid cell pairs remain stable regardless of behavioral state or experience. I observed that grid cells were able to immediately represent their environment upon initial exposure, even for novel trajectories that had not been run previously (Figures 3.2, 3.3). After novel experience, grid cell spike time correlations could be predicted by both rate map correlations (Figure 3.4) and relative spatial phase magnitudes (Figure 3.5). Thus, the grid cell firing patterns were stable across experiences and that stability could not be attributed to slow development of grid cell firing maps in a new environment. Up to this point, however, I have only examined pairwise correlations, which may not detect small changes that could be observed at the ensemble level.

Multi-unit sequences provide a more detailed measure of representation of space and experience, and therefore may provide different results. Previous studies have reported that sequences of grid cells from waking activity do reactivate in subsequent sleep and rest (Ólafsdóttir et al. 2016, O'Neill et al. 2017). However, grid cells in the superficial layers of MEC reportedly do not show replay that is coherent with replay in hippocampal place cells (O'Neill et al. 2017). In the deep layers of MEC, on the other hand, sequences of grid cells have been reported to reactivate coherently with replay in simultaneously recorded hippocampal place cell ensembles (Ólafsdóttir et al. 2016). Still, neither of these studies addressed whether replay in grid cells was experience-

dependent, the way place cell replay is reported to be across different stages of sleep (Nadasdy et al. 1999, Lee & Wilson 2002, Louie & Wilson 2001).

Place cells in the hippocampus are most likely to exhibit replay during awake rest immediately following activity (Davidson et al 2009; Karlsson & Frank 2009; Kudrimoti et al 1999; Tang et al. 2017), but they also show replay during NREM sleep (Nadasdy et al. 1999; Lee & Wilson 2002) and REM sleep (Louie & Wilson 2001). Louie and Wilson (2001) showed that during REM sleep, place cell sequences were replayed that matched those sequences activated during prior experience, both novel and familiar. Sequences matching those seen during novel behavioral experiences did not appear in sleep until after the novel experience. If grid cells in the superficial layers of MEC exhibit experience-dependent replay during sleep, then results analogous to those in place cells would be expected.

In this chapter, I investigated whether experience-dependent reactivation of grid cell ensemble activity from waking behaviors occurs during subsequent sleep and rest, or if, instead, functional connectivity in grid cell ensembles remains stable across different behaviors and sleep states, regardless of specific experiences. I examined the frequency of significant correlations between single-lap templates generated from grid cell ensemble spike trains recorded while an animal traversed an elevated linear track in both familiar and novel orientations (as described in Chapter 3). I then compared those results with results obtained using shuffled templates, as has been done previously for studies of hippocampal place cells (Louie & Wilson 2001).

4.2 - RESULTS

4.2.1 Grid cell ensembles do not appear to replay firing sequences from earlier waking activity during overnight NREM sleep.

Figure 2.1 (see Chapter 2) showed that grid cell firing rates during NREM sleep were significantly lower than firing rates during active behavior or REM sleep. Still, grid cells are active during NREM and during this time they may replay firing sequences from earlier waking behaviors. To test this idea, we examined grid cell ensemble activity during the first two periods of NREM sleep of the night. We restricted our search to NREM sleep occurring earlier in the night because NREM occurring soon after the onset of sleep has been proposed to be particularly important for memory (Plihal & Born 1997). We assessed whether firing sequences during NREM were significantly correlated with firing sequences during earlier waking trajectories on a familiar linear track (i.e., lap templates). Significance was determined by comparing correlations of lap templates and NREM firing sequences to correlations between the same NREM sequences and shuffled versions of the templates. To be categorized as significant, correlations between lap templates and NREM firing sequences were required to be greater than the 95th percentile of correlations between the NREM firing sequences and shuffled templates (see Methods).

I found that 62 +/- 13% of templates showed significant correlations with at least one NREM firing sequence (Figure 4.1a, n = 10 days of recording in 6 rats). To determine whether these correlations occurred more often than expected by chance, I produced surrogate data templates by circularly shifting each spike train independently by a random amount of time (see Methods). I found that 61 +/- 18% of surrogate templates also

showed significant correlations with at least one NREM firing sequence (Figure 4.1a). This indicates that the putative grid cell “replay” events observed during NREM sleep were not occurring more often than expected by chance and raises the question of whether sequence replay occurs in grid cell ensembles. The results may also reflect difficulties associated with applying methods used to assess sequence replay in CA1 place cells to grid cells, which fire periodically and are recurrently connected to each other (Gardner and Moser, 2017; Trimper et al., 2017).

Although the percentage of significant correlations found between templates and NREM firing sequences was no different than significant correlations found between surrogate templates and NREM sequences, it is still possible that correlation values may have been higher between the actual data templates and NREM firing sequences. To investigate this, I compared the distribution of significant correlation values for familiar track templates and NREM sequences to the corresponding surrogate template distribution (Figure 4.1b, left column). There were no obvious differences between the correlation values for the familiar track templates and the corresponding surrogate templates (Figure 4.1b, left column; Figure 4.1c), again providing no evidence of significant grid cell sequence replay using such template matching methods.

Using analogous methods as described above, I next compared whether significant correlations between grid cell ensemble firing sequences on the novel orientation of the linear track (“novel templates”) and NREM firing sequences were significantly greater than corresponding correlations for surrogate templates and NREM firing sequences. Again, no obvious differences between the distributions of correlation

values for novel templates and surrogate novel templates were seen (Figure 4.1b, right column).

An ANOVA was used to compare the four distributions of correlation values (for familiar templates, surrogate familiar templates, novel templates, and surrogate novel templates). The four distributions were significantly different ($F(3,3328) = 7.33$; $p < 0.0001$), but post-hoc analyses showed no differences between distributions for familiar templates and surrogate familiar templates (Tukey's HSD, $p=0.83$) or between novel templates and surrogate novel templates (Tukey's HSD, $p=0.92$). As there were only three animals with novel track experience, however, the novel track comparisons are preliminary and should be interpreted with caution.

As a final comparison, a Kolmogorov-Smirnov two-sample test was performed to determine whether the probability of high correlations between NREM sequences and familiar track activity was greater than the probability of high correlations between familiar surrogate templates and NREM sequences (Figure 4.1c). The likelihood of high correlation values between the familiar track templates and NREM activity was not larger than the likelihood of high correlation values between the surrogate templates and NREM activity (one sided, paired sample K-S test, $p = 0.89$, $D = 0.017$), again failing to provide evidence of grid cell sequence replay in NREM using methods previously used to detect place cell replay.

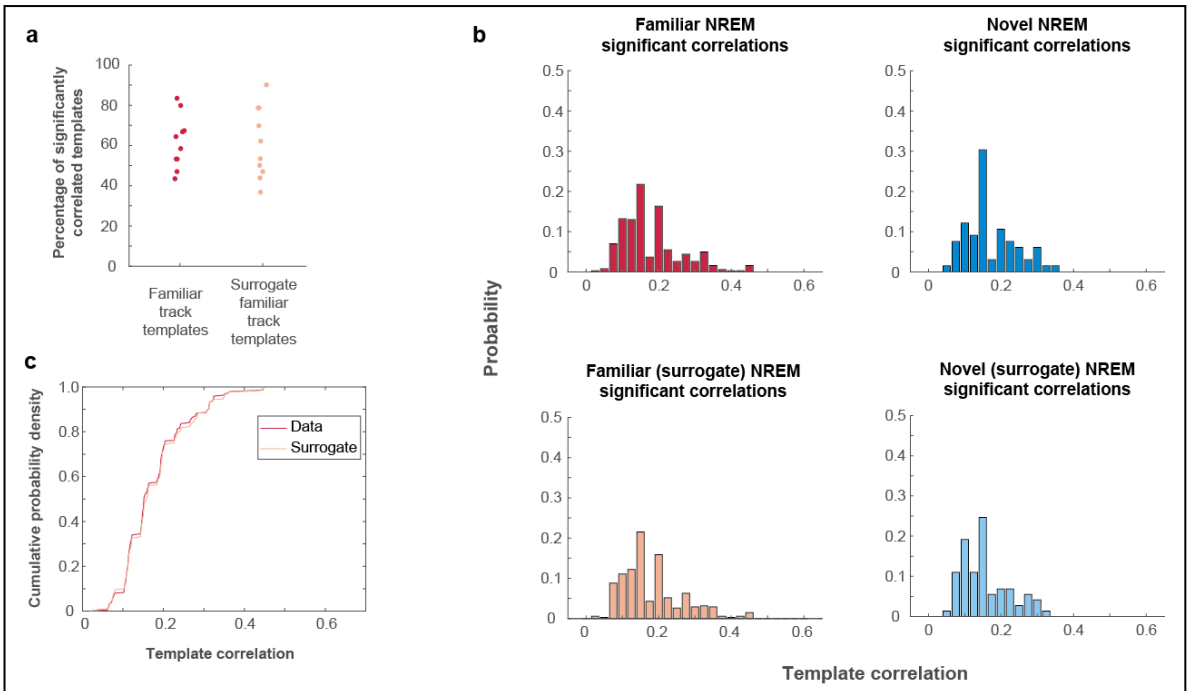

Figure 4.1 – Putative grid cell ensemble replay did not occur in NREM sleep more often than expected by chance.

a) This plot illustrates the percentage of templates that showed a significant correlation (see Methods) with at least one NREM firing sequence. There is no discernable difference between the familiar track templates (left) and the surrogate familiar templates (right; n = 10 days across 6 animals).

b) The distributions of significant correlations are shown for familiar templates (top left), surrogate familiar templates (bottom left), novel templates (top right), and surrogate novel templates (bottom right). There are no differences between the familiar and surrogate familiar distributions (left column) or the novel and surrogate novel distributions (right columns).

c) The cumulative probability density function (CDF) for the familiar and surrogate familiar correlation distributions is shown.

4.2.2 Grid cells do not appear to exhibit replay of firing sequences from earlier behavior during overnight REM sleep.

I next looked to see whether templates from familiar track traversals showed higher correlation to periods of REM sleep compared to surrogate controls. Prior studies have shown evidence of replay of familiar experiences in place cells during REM sleep multiple days after first experience, while sequences recorded during novel experience were not observed during sleep prior to the experience (Louie & Wilson 2001). Grid cells, however,

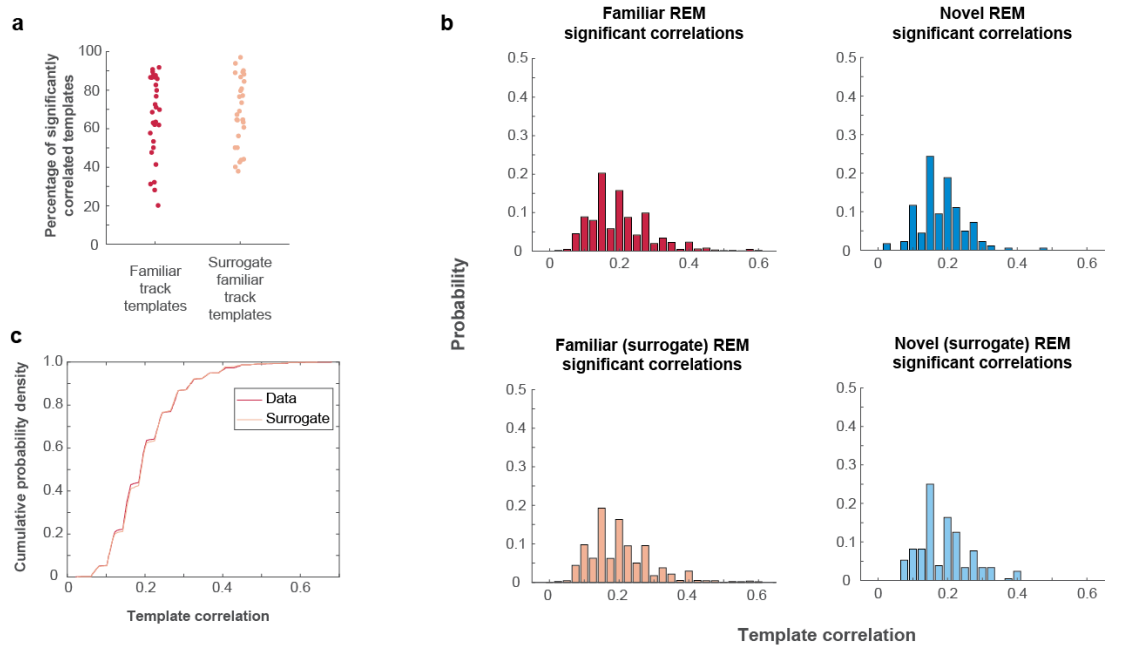

Figure 4.2 – There are no differences between the familiar templates or the surrogate familiar template correlations to firing sequences during REM sleep.

a) There is no difference between familiar track template and the surrogate familiar track template in the percentage of laps with detected replay (n=29 days across 6 rats).
b) The distribution of correlations that passed the criteria for being considered significant (see methods). The familiar and surrogate familiar distributions, as well as the novel and surrogate novel distributions were not significantly different, but the familiar and surrogate familiar distributions were significantly different from the novel track correlation distribution.
c) The CDF for the familiar and surrogate familiar track correlation distributions are shown.

appear to show no significant difference between familiar templates and surrogate controls in how often templates were significantly correlated with widnows of REM sleep (Figure 4.2a; average number of laps with detected replay on familiar track: 66 +/-21% , shuffled template: 68 +/-18%, n = 29 sessions across 6 rats).

The distribution of significant correlations between template and REM firing sequences of the four template groups (familiar templates, surrogate familiar templates, novel templates and surrogate novel templates; Figure 4.2b) were significantly different from each other (ANOVA: $F(3,6589) = 4.03$; $p = 0.007$), however there were no differences between familiar templates and surrogate familiar templates (Tukey's HSD, $p=0.97$) nor between novel templates and surrogate novel templates (Tukey's HSD, 0.84). As only two animals had REM sleep after the novel track experience, the novel template results are only minimally informative and are only for the sake of completeness.

To evaluate whether the distribution of significant correlations between familiar templates and REM firing sequences had a greater probability of higher correlation values than the distribution of significant correlations between the surrogate template and REM firing sequences, we again used the one-sided, paired sample Kolmogorov-Smirnov test. As illustrated in figure 4.2c, the distribution of significant correlation values from the familiar template comparison does not have a greater likelihood of high correlation values than the distribution of surrogate correlations (one sided, paired sample K-S test, $p = 0.66$, $D = 0.012$).

4.2.3 Grid cells do not appear to exhibit replay of firing sequences from earlier behavior during awake rest.

Finally, I looked at grid cell ensemble activity during the rest sessions following running on the linear track. Prior studies have reported place cell replay during rest sessions immediately following activity (Lee & Wilson 2002), so I looked at the first rest session following the first familiar or novel linear track run of the day and ran the same comparisons as in sections 4.2.1 and 4.2.2. Here, a much smaller percentage of lap

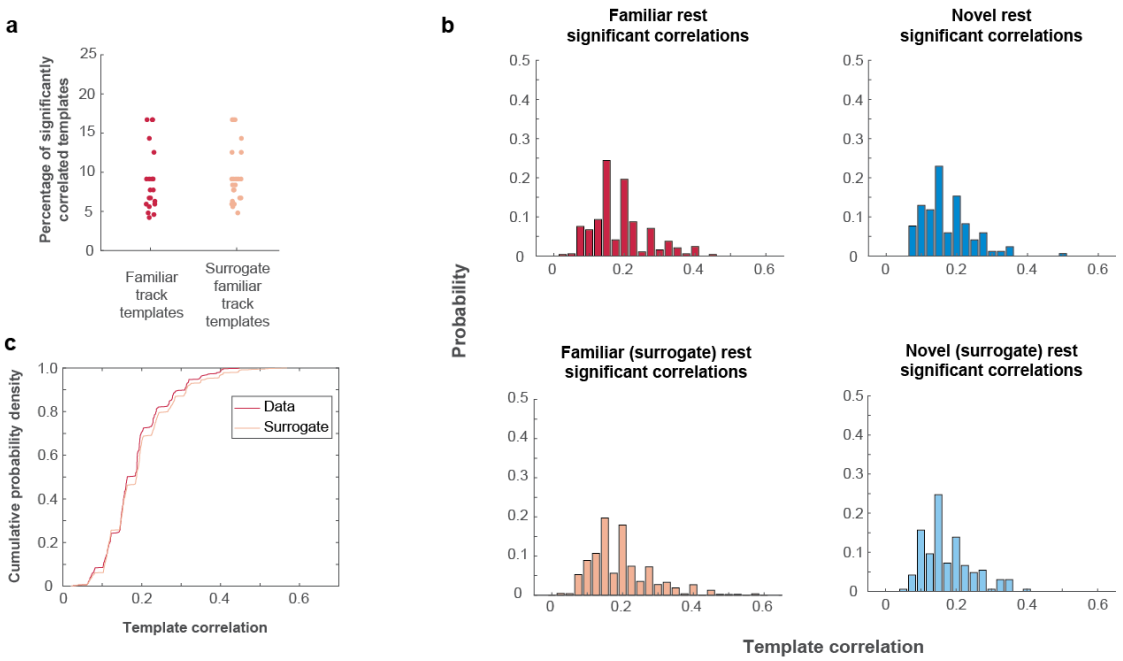

Figure 4.3 – There are no differences between familiar track and surrogate familiar track replay during post-activity rest.

a) There is no difference between the familiar and surrogate familiar templates with regard to the percentage of laps detected as having been replayed (n=20 days across 6 animals).
b) The distributions of significant correlations are shown for the familiar templates (top left), surrogate familiar templates (bottom left), novel templates (top right) and surrogate novel templates (bottom right). Neither the familiar and surrogate familiar template distributions nor the novel and surrogate novel template distributions were significantly different.
c) The CDF for the familiar (data) and surrogate familiar track templates are shown.

templates were found to show significant correlation with periods of awake rest, with 9 +/- 4% of the familiar templates (and 9 +/- 4% of the surrogate familiar templates) finding a significantly correlated firing sequence during the rest period (Figure 4.3a). Despite the reduced proportion of templates finding significant matches during awake rest, that there is no difference between the familiar track templates and the surrogate familiar templates indicates again that grid cell ensemble firing patterns do not appear to replay previous experience during later periods of rest or sleep in a way that is detectable by template matching methods.

Figure 4.3b shows the distributions of significant correlations for the four template groups examined. The distributions of significant correlations are shown in Figure 4.3b, and while they are significantly different (ANOVA: $F(3,2400) = 6.6634$, $p = 0.0002$), post-hoc tests show that the familiar and surrogate familiar distributions do not differ (Tukey's HSD, $p=0.11$), nor do the novel and surrogate novel distributions (Tukey's HSD, $p=0.98$). Once again, with only three animals with novel track experience, the novel track data were included for completeness only, and are preliminary. That we do not see differences between the familiar track template distribution and the surrogate familiar track distribution indicates that the grid cell ensemble firing patterns do not show evidence of replay of grid cell activity patterns recorded during prior experience.

Finally, I wanted to see whether there was a higher likelihood of observing larger significant correlation values between the linear track template and the rest session windows than between the shuffled template and rest session windows. Comparing the estimated cumulative probability density functions (Figure 4.3c) one can see once again that the templates from the familiar linear track behavior did not have a higher likelihood

of observing greater correlations than the shuffled templates (one sided, paired-sample K-S test, $p = 0.47$, $D = 0.03$). The results show that, as we found in overnight sleep, the grid cell firing patterns during rest do not appear to replay activity patterns from prior experience.

4.3 - Discussion

4.3.1 Evidence of grid cell ensemble replay of prior experience was not observed during rest or sleep

There was no indication in the data presented here that correlations between templates of grid cell ensemble activity during laps on a familiar linear track and firing sequences during subsequent sleep were significantly higher than correlations between surrogate data templates and sequences during subsequent sleep and rest. This differs from results reported in place cell replay papers using similar methods, during NREM sleep (Lee & Wilson 2002; Nádasdy et al. 1999) and REM sleep (Louie & Wilson 2001). Lee and Wilson found significantly higher correlations between place cells' post-behavior sleep activity and activity during traversals of a familiar or novel trajectory when compared to surrogate data controls (2002). In the data presented here, however, there was no difference between familiar track templates and surrogate familiar track templates in either the percentage of significant correlation with activity recorded during subsequent sleep or the distributions of those significant correlation values. That differences were not observed in these data seems to suggest that grid cells in the superficial layers of MEC do not exhibit replay of ensemble spiking sequences from waking behaviors during subsequent sleep and rest. However, it is possible that template matching methods such

as those used in earlier place cell studies and in this chapter are inappropriate for assessing replay in grid cells, due to the periodic firing patterns of grid cells.

It is possible that decoding methods used more recently to evaluate replay in place cells (Karlsson & Frank, 2009) would also be better suited to detect replay in grid cells also. In line with this idea, a recent study that reported significant replay of grid cell ensemble activity from waking during subsequent sleep used decoding techniques, not template matching methods (O'Neill et al., 2017). However, accurate grid cell decoding requires large numbers of simultaneously recorded grid cells, data sets that are difficult to obtain and maintain across multiple days of recording and overnight sleep.

The lack of replay also does not necessarily contradict our prior results, which showed that spike time correlations remained stable across behaviors. While we would expect to observe sequences which resembled replay more often than sequences which resembled the shuffled and uncorrelated surrogate templates (Ikegaya et al. 2004; Tsodyks et al 1999), we may be looking at timescales which are too long. The timescale at which the grid cell network activity state drifts may not be long enough for stable multi-second long sequences when sensory input is minimal, much in the same way the grid fields of rats disappear when medial septal (Brandon et al. 2011; Koenig et al. 2011) or hippocampal (Bonnevie et al 2013) input is inactivated. The previous two chapters examined correlations on the millisecond timescale, which may remain much more stable in face of reduced global input.

4.3.2 Future directions: additional studies of novel experiences and non-grid cells of the MEC

While this chapter provided evidence that grid cells in the superficial layers of the MEC do not replay activity patterns recorded during behavior during REM sleep, NREM sleep or awake rest, that does not rule out the possibility of experience-dependent replay in the MEC. We did not investigate grid cells in the deep layers of the MEC, where Olafsdottir and colleagues (2017) showed some evidence that grid cells may show replay that is coordinated with replay in place cells. With the majority of hippocampal inputs to the MEC landing in the deep layers, it is possible that place cell replay could propagate to the deep layers of the MEC and initiate replay of grid cells in those layers.

Additionally, with grid cells only making up a small fraction of the cells in the MEC (Sargolini et al 2006), there is the distinct possibility that other cell types of the MEC exhibit experience-dependent replay while grid cells do not. Other work has shown that the principal cells of the superficial layers of the MEC respond to a combination of spatial variables (Hardcastle et al 2017). These other cell types may encode unique trajectories and features that are more straightforward to parse, compared to grid cells that fire periodically in multiple spatial locations in all environments. This idea has some support in the findings of O'Neill and colleagues (2017), who found that Bayesian decoders trained using all recorded cells, not just grid cells, in the superficial layers of MEC were better able to predict an animal's current location. As such, non-grid cells may provide a separate channel through which experience-dependent replay could propagate from cortex to hippocampus.

4.4 – METHODS

For general recording and analysis methods, please refer to Appendix 1.

4.4.1 Template matching algorithm

Templates were constructed from individual laps, which were defined as the traversal from one end of the linear track to the other. Each lap was divided into bins having a duration of a quarter-theta cycle, and the spikes of each cell were then summed into each bin. The resultant template matrix (template), with each column being a quarter of a theta cycle in duration and each row containing the spikes of a single cell, was then compared in a sliding window fashion to overnight REM sleep epochs, overnight NREM sleep epochs and rest epochs which immediately followed a session on the linear track.

REM sleep epochs were divided into quarter-theta cycle time bins and the spikes from each grid cell were summed into these bins. The template could then be compared to a sub-section (window segment) of the REM epoch which had the same number of bins as the template. Once a correlation value was calculated, the process was repeated for the window starting one bin later than the previous window started. This leads to a series of comparisons which overlap by all but one bin with the previous comparison. A similar process was done for rest and NREM sleep, though based on findings in section 2.2.2, the time periods were instead split into approximately 35ms bins and then scaled by a factor of 5, such that 1 ms in the NREM window is compared to a 5 ms segment of template. Correlation values were computed using methods applied by Louie and Wilson (2001), namely calculating a correlation coefficient between the template and the window segment:

$$C_t = \frac{1}{N * C} \sum_{c=1}^{C} \sum_{n=1}^{N} (\frac{x_{nc}}{X_c} - \bar{x})(\frac{y_{nc}}{Y_c} - \bar{y}) \sigma x \sigma y$$

N is the number of time bins in a template; C is the number of grid cells in a simultaneously recorded ensemble; and x_{nc} and y_{nc} are spike counts for time bin n of cell c of the template or window, respectively. The variables $\bar{x}$ and $\bar{y}$ are the template and window average, and σ_x and σ_y are the standard deviations of the root-mean-square-normalized bin spike counts. X_c and Y_c are the root mean square amplitudes of cell c in the template and window respectively, defined as

$$X_c = \sqrt{\frac{1}{N} \sum_{n=1}^{N} x_{nc}^2} * spikes^{-1}$$

This process was repeated for each possible window of sleep or rest activity, resulting in a series of overlapping correlation values. We did not consider negative correlations ($C_t < 0$) because we were looking for forward and not reverse replay.

4.4.2 Determining putative replay events

To determine whether a putative replay event was significant, four different shuffle methods were used to create bootstrapped distributions of correlation values, and only pairings in which the original correlation was in the 95th percentile of all four shuffle methods were considered significantly correlated (Louie & Wilson, 2001).

The first shuffle method was the ID or row shuffle, in which the template rows were swapped randomly (Louie & Wilson, 2001). This modified the cell to cell correlations and firing rates, but maintained the firing rate and autocorrelations within the spike trains.

The next shuffle was the bin shuffle, in which within each row of the template, the individual bins were shuffled randomly (Louie & Wilson, 2001). This shuffling method kept each row's gross firing rate fixed but removed both autocorrelations within the spike train and the cross correlations between cells.

The third shuffle randomly re-ordered the columns of the template (Louie & Wilson, 2001). This broke the longer-term auto- and cross-correlations, but maintained the short-time scale cross correlations between cells.

Finally, the shift shuffle, in which each row was shifted by a random amount, wrapping bins that "fall off" either edge to the opposite side of the template matrix (Louie & Wilson, 2001). This method kept within-cell auto-correlations fixed, as well as the average firing rate and inter-spike interval while disrupting across-cell correlations. Each shuffle method was repeated 50 times, and for each iteration a correlation value was calculated, using the shuffled template in place of the original. The original correlation value was compared to the distribution of correlation values from this shuffled population, and if the original correlation value was greater than 95% of the probability mass of the bootstrapped distribution, the correlation was considered significant, and a putative replay event (Louie & Wilson, 2001).

4.4.3 Surrogate template controls

To investigate the likelihood of finding the amount of correlation between templates and firing sequences recorded during sleep and rest, we created surrogate control templates from shift-shuffled versions of the original data templates. For each template that was tested against a sleep period, a surrogate template was created by

independently shifting each row of the template in a circular fashion (when shifted, bins which fall off one edge are placed on the opposite edge). The shift amount was a randomly chosen integer from the range $[-1 * \mathrm{round}(0.9 * \mathrm{N}), \mathrm{round}(0.9 * \mathrm{N})]$ where N was the number of bins in the template. These surrogate templates provided a data set which maintained the same cell firing rates and mostly the same within-spike train correlations while removing the across-cell correlations. This allowed us to estimate how much of the correlations between template and sleep or rest firing sequence were due to chance or extraneous factors like mean firing rate, rather than specific firing patterns across the ensemble.

4.4.3 Statistics

Built-in MATLAB (The MathWorks, Inc., Natick, Massachusetts) functions were used for all statistical analyses performed in this chapter. CDF estimates were made using the 'ecdf' function in MATLAB. Kolmogorov-Smirnov tests were performed using the parameters "*kstest2(familiar_corr, shuffle_corr,'tail','smaller')"* to test the null hypothesis that the familiar template correlation CDF lies under the shuffled template correlation.

Chapter 5: General Discussion

5.1 - SUMMARY

I have examined the activity of grid cells during sleep to answer several important questions. First, I showed that spike timing patterns between pairs of grid cells were predicted by the relationship between their spatial responses, and that those patterns were maintained when spatial input was absent. Grid cells with overlapping fields showed high spike time correlations on short time-scales while cells with less overlapping fields showed less correlation. These findings provide further support to the hypothesis that grid cell firing patterns are a product of network connectivity, resulting in continuous attractor dynamics in their firing properties.

I next looked at whether grid cells showed changes to the spike timing relationships after novel experience. I first showed that the novel track orientation produced rate maps which were both stable from the first experience and differed from the familiar track orientation. I then showed that the novel track orientation did not appear to induce any changes in grid cell spike timing relationships during navigation or sleep. I finally investigated whether there was evidence of modification of the grid cell spike time correlation patterns during rest, REM sleep, and NREM sleep that resulted from recent experience. In all cases for which we had significant amounts of data we found the grid cell correlation patterns to be stable and show no evidence of experience-dependent change.

Finally, I looked at whether grid cell ensembles showed evidence of replaying during sleep or rest firing sequences that were recorded during behavior by comparing

ensembles of grid cell firing sequences on a familiar linear track to periods of REM sleep, NREM sleep and rest. If grid cells were replaying behavioral firing sequences during sleep it would be expected that there would be more significantly correlated sequences and a greater likelihood of highly correlated sequences during either REM sleep, NREM sleep or rest when compared to de-correlated surrogate sequences. What was observed, however, was that there were no more correlated sequences than expected by chance, indicating that grid cells may not replay behavioral firing sequences during sleep or rest. It is also possible that template matching methods used for analyzing place cell sequences are not well suited for the analysis of periodic grid cell sequences.

5.2 - DISCUSSION

Here I have showed that the spike time correlation patterns between grid cell pairs is predictable from their relative spatial phase. This result is a prediction of the continuous attractor model of grid cell field formation, with the network connections described by the model shaping grid cell firing regardless of the presence or absence of spatial input. More interestingly, it was shown that the same spatial relationship predicted the spike time correlations during sleep and rest, when spatial input is absent. These results guided the later analysis of grid cell reactivation, where I investigated whether novel activity changed grid cell correlations or if grid cell ensemble firing sequences recording during active behavior were replayed during sleep or rest. We found that grid cells showed no evidence of experience-dependent changes to their pairwise correlation patterns, nor did they appear to show during sleep or rest any replay of firing sequences from prior experience.

Other studies have performed similar analyses on head direction cells as was done on grid cells in Chapter 2 (Peyrache et al 2015). By looking at the activity of head direction cells from both the thalamus and postsubiculum during REM and NREM sleep, they observed correlated activity between cells which mimicked the correlations observed during waking behavior. Head direction cells with similar tuning directions tended to fire together even when the animal was asleep (Peyrache et al. 2015). Together these studies show two distinct components of the navigation circuit which appear to operate on the dynamics inherent in a continuous attractor system (Amari 1977). CA3 has also been hypothesized to be an attractor network (Hasselmo et al 1995; Tsodyks & Sejnowski 1995), and some experimental evidence has been provided to support the hypothesis (Colgin et al. 2010; Renno-Costa et al. 2014; Wills et al. 2005), though the details of how the attractor may be implemented is still unclear (Colgin et al. 2010; Renno-Costa et al. 2014). Our work in grid cells further promotes the idea that the continuous attractor network is a motif common to the navigation circuit.

While I have shown that place cells in CA1 do not appear to explain the stability of the grid cell correlations during non-spatial behaviors, I have not ruled out the possibility that organized inputs from other brain areas to the MEC are able to maintain the pairwise co-activity patterns I observed. Organized activity of the thalamic head direction cells (Peyrache et al. 2015), which have been shown to be required for grid cell activity (Winter et al. 2015), could also explain the continued coordination between grid cells during non-spatial behavioral states. Similar findings in other cortical areas of coordination when sensory input is absent (Ikegaya et al. 2004, Tsodyks et al. 1999), and the likelihood that yet more cortical areas could show the same properties, means that we cannot say for

certain that our observations are not a result of coordination from feed-forward inputs rather than network dynamics between grid cells.

The stable correlation patterns observed in grid cells during sleep have been shown to be stable across environments as well (Yoon et al. 2013). These stable correlations across environments and behaviors suggest that grid cells may not show experience dependent replay unless it is driven from inputs which experience plasticity. While studies have shown correlated replay between the visual system and place cells (Ji & Wilson 2007) as well as between auditory cortex and the hippocampus (Rothschild et al. 2017), none of them have looked at whether those coordinated events engage the MEC, or if they bypass the MEC via other pathways through the hippocampal formation, such as through postrhinal or perirhinal cortex (Burwell & Amaral, 1998a; Burwell & Amaral, 1998b).

Where place cells show remarkable functional plasticity, changing their firing patterns as a result of experience and maintaining those changes for hours or days at a time (Louie & Wilson, 2001), grid cell activity in the superficial layers of the MEC during sleep appears to reflect the set of possible activity patterns the network can produce, without regard of prior experience, similar to results reported *in vivo* in head direction cells (Peyrache et al. 2015) and primary visual cortex (Ikegaya et al. 2004; Tsodyks et al. 1999) as well as in slices from prefrontal cortex (Ikegaya et al. 2004). This suggests that grid cell patterns and sequences are largely shaped by the functional network in which grid cells appear to be embedded, and even when input is absent similar patterns are produced in response to random, noisy spontaneous activity. Recent studies have observed both deep layer grid cell reactivation, coordinated with hippocampal replay

(Ólafsdóttir et al. 2016) as well as replay of superficial layer grid cells which showed little to no coordination with hippocampal sharp waves or place cell replay (O'Neill et al. 2017). A missing component from each study, however, is analysis of the extent to which the replay detected is experience dependent. That experience dependence is key to determining whether grid cell replay is contributing to memory consolidation.

In this study, I began examining whether activity patterns of grid cells in the superficial layers of the MEC remained stable in the face of changing experience and across behaviors. While the results were consistent with the predictions of the continuous attractor network model of grid cell field formation, I cannot rule out the possibility that the co-activity patterns that were observed between grid cell pairs were a result of coordinated inputs, rather than network connections. I observed no experience or behavior-dependent changes in the coordination between spatial response and co-activity, though that does not mean other cells of the MEC, or grid cells in the deep layers of the MEC do not show experience-dependent changes. Additionally, while I have some preliminary results, I cannot completely rule out whether novel experience induces changes in the grid cell functional connections which could lead to experience-dependent replay. In the future, studies on whether there is replay of novel experiences in grid cells are needed, as well as what other pathways may account for the stable co-activity patterns or allow for coordinated replay between the hippocampus and both sensory cortices (Ji & Wilson, 2007; Rothschild et al. 2017) and frontal or pre-frontal cortices (Tang et al. 2017). With recent studies showing that the activity of the non-grid cells of the MEC represents complex spatial information (Hardcastle et al. 2017; O'Neill et al. 2017), it is also possible that non-grid cells in the MEC may be involved in hippocampal replay.

5.3 – Final Thoughts

In this work I have looked at the activity of grid cells during non-spatial behaviors to get a better understanding of how grid cells work and what role they play in memory. I have shown that they follow the predictions of the continuous attractor model of grid field formation, giving us a deeper understanding of how the brain is able to integrate sensory information to build a representation of an animal's position in space. By investigating whether the functional network of grid cells in the superficial layers of the MEC remains stable following experience of both novel and familiar environments, new questions have arisen as to how the cortex communicates with the hippocampus during sleep, particularly for the purpose of memory consolidation. Further study of grid cell activity after novel experiences, as well as of non-grid cells and other parallel pathways between the hippocampus and cortex, such as postrhinal and perirhinal cortex, are needed to answer these questions satisfactorily.

Appendix 1: General Methods

A1.1 Subjects

MEC and CA1 data were collected from six male Long-Evans rats weighing ~450 g to ~650 g (mean +/- std = 549 +/- 87 g) and four male Long-Evans rats weighing ~400g to ~530g (482 +/- 55 g), respectively. After surgery, animals were individually housed with several items for enrichment (e.g., cardboard tubes, wooden cubes, plastic toys). Rats were housed in custom-built acrylic cages (40 cm x 40 cm x 40 cm) on a reverse light cycle (Light: 8pm to 8am). Active waking behavior recordings were performed during the dark phase of the cycle.

Rats recovered from surgery for at least one week, with free access to food, before behavioral training resumed. During the training and data collection period, rats were food-deprived to no less than 90% of their free-feeding weight. During periods of food deprivation, food was provided ad libitum for one day per week. All experiments were conducted according to the guidelines of the United States National Institutes of Health Guide for the Care and Use of Laboratory Animals under a protocol approved by the University of Texas at Austin Institutional Animal Care and Use Committee.

A1.2 Recording drive

For animals receiving MEC recording implants, chronic “hyperdrives” (Gothard et al. 1996) (5 animals) or a Harlan Drive (Neuralynx, Bozeman, Montana, 1 animal) with 12 tetrodes and two reference electrodes or 16 tetrodes, respectively, were implanted over MEC in the right hemisphere each animal. CA1 animals were implanted with hyperdrives

above the hippocampus in the right hemisphere. Tetrodes were constructed from 17 μm polyimide-coated platinum-iridium (90/10%) wire (California Fine Wire, Grover Beach, California). Electrode tips of tetrodes designated for single unit recording were plated with platinum to reduce single channel impedances to ~150 to 300 kOhm at 1 kHz.

A1.3 SURGERY

Anesthesia was induced by placing an animal in an induction box filled with isoflurane (5%) mixed with oxygen (1.5 liters per minute). The animal was then moved to a stereotaxic frame, and isoflurane anesthesia (~1.5-3%), mixed with oxygen as above, was administered throughout surgery. Buprenorphine (0.04 mg/kg) was administered subcutaneously prior to the initial incision. Subjects also received 0.04 ml of atropine (0.54 mg/ml) injected subcutaneously prior to surgery and an additional 0.02 ml of the atropine solution after four hours of anesthesia to prevent fluid accumulation in the lungs. Sterile saline (1.00 ml, 0.90%) was administered subcutaneously prior to surgery and each hour thereafter for hydration. Subjects were checked for breathing rate and responsiveness every 15 minutes during surgery to monitor anesthesia levels.

Seven to eight bone screws were placed in the lateral, anterior, and posterior edges of rats' skulls, serving as anchors for the recording drives. Two additional screws in the anterior portion of the skull, ipsilateral to the recording drive, were used as the electrical ground reference for recording. For MEC implants, drives were positioned 4.5 mm lateral from the midline and approximately 0.2 mm anterior to the transverse sinus. The most posterior tetrode was used to position the drive according to these coordinates. For CA1 implants, drives were centered at 3.0 mm lateral to the midline and 3.8 mm

posterior to bregma. Silicon adhesive (Kwik-Sil; WPI, Sarasota, Florida) was used to fill in the exposed portion of the craniotomy, and dental cement was applied to anchor the drive to the skull and to the bone screws. At the end of surgery, subjects were given a subcutaneous injection of Rimadyl (5 mg/kg), mixed with ~1 ml of sterile saline (0.9%), for pain management.

A1.4 DATA COLLECTION

Data were recorded using a Digital Lynx system and Cheetah 5.0 recording software (Neuralynx, Bozeman, Montana). Local field potentials (LFPs) from one channel within each tetrode were continuously recorded at 2 Khz, using the built in high-pass (DC-offset filter at 0.10 Hz with 0 taps) and low pass (FIR filter at 500 Hz using 64 taps) filters. Input amplitude ranges were adjusted before each recording session to maximize resolution without signal saturation. Input ranges generally fell within +/-1600 to +/-2600 μV. Spikes were detected and recorded in the following manner. All four channels within each tetrode were filtered from 600-6000 Hz using a high pass (FIR filter at 600 Hz using 64 taps) and low pass (FIR filter at 6000 Hz using 32 taps) filter. Spikes were detected when the filtered continuous signal crossed a threshold set daily by the experimenter, which ranged from 40-75 μV. Detected events were acquired with a 32 KHz sampling rate. Signals were recorded differentially against a dedicated reference channel (see “Tetrode Positioning” section below).

Video was recorded through the Neuralynx system with a resolution of 720 x 480 pixels and a frame-rate of 29.97 frames per second. Animal position and head direction were tracked via an array of red and green LEDs on an HS-54 headstage (Neuralynx,

Bozeman, Montana) attached to a hyperdrive, or red and green LEDs connected to EIB-36-24TT headstages (Neuralynx) attached to a Harlan Drive.

A1.5 TETRODE POSITIONING

All tetrodes were initially lowered ~900 μm on the day of surgery. Thereafter, tetrodes were lowered gradually over the course of several weeks to the superficial layers of MEC or dorsal CA1 guided by the estimated depth and known electrophysiological hallmarks of MEC (e.g., prominent theta oscillations; Hafting et al. 2008; Mitchell & Ranck, 1986) and CA1 (e.g., sharp-wave ripples; Buzsaki, 1986). In the CA1 implanted rats and all but one of the MEC implanted rats, the most anterior tetrode was designated as the reference for differential recording and was targeted toward the angular bundle (MEC animals) or a quiet region of overlying cortex (CA1 animals). Due to prominent noise on the most anterior channels in one MEC rat, the most posterior tetrode was chosen as a reference instead. Tetrode positions were verified histologically after experiments were completed (see Histology section below). Reference tetrodes were continuously recorded against ground to ensure that they remained in electrically quiet locations across all days of recording. Experimental sessions and data recording began when the presence of at least four simultaneously recorded grid cells was detected (see Grid Cell Detection section below) or, in the case of CA1 recordings, when most of the tetrodes were estimated to be in the CA1 cell body layer.

A1.6 Behavioral training of MEC rats

The animals were pre-trained prior to surgery to run in multiple environments: a 1 m x 1 m square open field and a 2 m elevated linear track. In both cases the animals were motivated using sweet cereal or cookie pieces. In the open field, small pieces of cereal or cookie were lobbed in to random locations within the open field while the animal explored the environment. On linear track the animals were trained to run from one end to the other for sweet cereal or cookie pieces, which were given on either end of the track. Animals were considered ready for surgery when they ran consistently on the linear track and explored the open field with few pauses and relatively uniform coverage of the environment. After recovery from surgery rats were familiarized with the open field and linear track environments while plugged in to the recording system over several days. The first three days of familiarization consisted of open field running while the next three days consisted of linear track familiarization. Open field familiarization trials included three sessions of 20 minutes each, with rest sessions of 10 minutes each interspersed prior to and after each active session. Linear track had a similar organization but utilized 10 minute active sessions. Rest sessions were conducted in an elevated flower pot lined with towels. Following familiarization, active sessions of two 20 minute open field sessions and three 10 minute rest sessions were used to detect the prominent saw-toothed theta (6-10 Hz) oscillation of the MEC. Once it was estimated that the tetrodes were in the MEC, trials of three active sessions and four 30 minute rest sessions were conducted.

When a minimum of four grid cells were believed to be present, data collection began. On these days, rats ran on the linear track immediately prior to overnight sleep

recording beginning. At the beginning of their light cycle (~8 pm), the animals were placed in a smaller 60 cm x 60 cm open field arena long with enrichment items, any remaining food, water and towels for bedding. At approximately 8 am the next morning, rats were returned to their home cages for 2-3 hours. After spending time in their home cage, animals ran two 20 minute run sessions in the 1 m x 1 m open field (including three 10 minute sleep sessions). At the end of the day, the linear track was arranged to span the opposite diagonal as the previous day for the rotated track novel configuration. Animals again ran three 10 minute linear track sessions with four 10 minute rest sessions, then were recorded overnight beginning around 8 pm. At ~8 am the next morning, the animals were returned to their home cage, and 2-3 hours later they ran one last open field session (two 20 minute active sessions, three 10 minute rest sessions) before their tetrodes were turned a minimum of ~80 μm.

A1.7 HISTOLOGY

Histological sections were prepared in the following manner to allow for verification of tetrode positions after completion of recordings. Rats were given a lethal i.p. injection of Euthanasia III solution. This was followed by transcardial perfusion, first with physiological saline to clear blood and then with 4% formaldehyde solution to fix brain tissue. Brains from MEC-implanted rats were cut sagittally at 30 μm, and each section through the relevant portion of MEC was collected. Brains from CA1 implanted rats were cut coronally at 30 μm, and each section through the relevant portion of CA1 was collected. Sections were mounted on slides and stained with cresyl violet. Tetrode tips and tracks were localized by comparing across successive sections.

A1.8 SPIKE SORTING

MCLUST cluster-cutting software (version 3.5; A.D. Redish, University of Minnesota, Minneapolis) run in MATLAB 2014a (The MathWorks, Inc., Natick, Massachusetts) was used to sort spikes into putative single units. Spike waveforms were sorted based on peak height, waveform energy, and peak-valley difference. The valley depth of spike waveform was used as an additional feature to sort MEC units. A putative single-unit was accepted for further analysis if the associated cluster had a minimum 1 ms refractory period and shared less than 1% of its total number of spikes with any other accepted cluster.

A1.9 IDENTIFICATION OF ACTIVE WAKING AND QUIESCENT SLEEP STATES

For the initial identification of sleep epochs, videos of rats' overnight behavior were manually scored by two independent researchers trained to discriminate between sleep, stationary alertness, and consummatory behaviors. Only epochs that both researchers classified as sleep were accepted for further analysis. REM and NREM epochs were then classified during identified sleep epochs based on oscillatory activity in the LFP using the following criteria. A recording period was classified as NREM if the moving window average (5.0 s window, 0.5 s step) of the theta (6-10 Hz) power to delta (2-5 Hz) power ratio remained below 1.0 for at least 15 seconds (modified from a previous study: Csicsvari et al. 1999). Instantaneous theta and delta power were calculated via Morlet wavelet transform (Colgin et al. 2009; Tallon-Baudry et al 1997) calculated with a width parameter (σ) of 5 and a frequency resolution of 1 Hz. Recording periods were classified as REM if the moving window average of the theta-delta power ratio remained above 1.5

for at least 60 seconds (modified from previous studies: Csicsvari et al. 1999; Louie & Wilson 2001).

Recordings of active waking behaviors on the circular track (CA1 data) and in the open field (MEC data) were used to define periods of active ambulation (i.e., RUN). RUN epochs were defined as periods in which the theta-delta power ratio was above 2.0 and a rat's running speed, smoothed with a Gaussian window (radius of 133 ms or 4 video frames, standard deviation of 1), was greater than 5 cm/sec (modified from a previous study: Csicsvari et al. 1999). Thresholds were confirmed by manual examination of the power spectra and randomly chosen segments of LFP to confirm the presence or absence of theta oscillations.

A1. 10 GRID CELL DETECTION

Recordings of single unit activity in the open field environment were used to detect grid cells. First, rate maps were calculated using 3 cm spatial bins and smoothed with a Gaussian window (Hafting et al. 2005). A gridness score (Sargolini et al. 2006) was then calculated for each putative grid cell and compared to a bootstrapped distribution of gridness scores. The bootstrapped distribution consisted of 2000 shuffles in which spike trains were shifted in time by a random amount while the inter-spike intervals remained fixed. Rate maps and gridness scores were recalculated for each shuffle to create a bootstrap distribution for each putative grid cell. Units were classified as grid cells when the original gridness score met or surpassed the 95th percentile of the corresponding bootstrapped distribution. Additionally, a grid cell was only included if the same unit was identified and remained stable in an open field recording session the next day. Grid cell

stability was assessed by visual inspection of unit cluster position, inter-spike intervals, and grid field similarity.

A1.11 SPIKE TIME CORRELATIONS

Spike time cross-correlations were calculated in MATLAB using the "xcorr" function (MATLAB 2017a Signal Processing Toolbox, The MathWorks, Inc., Natick, Massachusetts). Unless otherwise stated, cross-correlations were normalized such that auto-correlations at zero lag were identically 1.0 (i.e., “coeff” normalization option in MATLAB), and correlograms were averaged across bouts of the same behavior. The exception to this is Figure 2, in which each of the un-normalized cross-correlograms, which were summed across bouts of the same behavior, were scaled by their average value (Gardner et al., SfN Abstracts 2016). This analysis was done to compare the present results with those of Gardner and colleagues, who introduced this analysis previously. Cross-correlations were calculated using spike counts in 2 ms (Figures 3-6, Supplementary Figure 1), or 5 ms, 10 ms, and 50 ms bins (Figure 2a, b, and c, respectively) to ensure that the observed results were not an artifact of the chosen bin size. All cross-correlations were calculated over +/-5000 ms lags. MEC and CA1 cell pairs that did not have a peak of at least 5 spikes in the (summed un-normalized) cross-correlation for each behavioral state were not considered. MEC cell pairs recorded simultaneously on the same tetrode were excluded if spike time correlations at zero lag were greater than the average of the correlation vector to prevent double counting of the same spikes. MEC cell pairs in which the spatial period of one cell was not within 30% of

the other were also excluded to restrict comparisons to cells within the same putative module (Yoon et al. 2013).

A1.12 RATE MAP CORRELATION COEFFICIENTS

Correlation coefficients for pairs of grid cell rate maps, which were used to sort grid cell pairs in Figure 2.2 and are shown across the x-axes in Figure 2.3a and 3.4, were calculated by the off-diagonal value returned by the "corrcoef" function in MATLAB (MATLAB 2017a, The MathWorks, Inc., Natick, Massachusetts). The values presented are the medians across the three open-field sessions. For CA1 place cells (Figure 2.3b), the rate map correlation coefficient was calculated using the 'corrcoef' function, using rate maps that were constructed from angular positions on the circular track.

A1.13 GRID CELL RATE MAP CROSS-CORRELATIONS

Rate map autocorrelations (for grid cell detection) and cross-correlations (Figures 2.4, 2.5a, 2.6; 3.5, A2.1) were performed following procedures outlined previously (Hafting et al. 2005). Briefly, the two-dimensional cross (or auto) correlation was calculated from the smoothed rate maps via:

$$R(i,j) = \frac{\sum_{m,n}(N * \boldsymbol{map1}(m,n) * \boldsymbol{map2}(m-i,n-j)) - \sum_{m,n}(\boldsymbol{map1}(m,n)) * \sum_{m,n}(\boldsymbol{map2}(m-i,n-j))}{\sqrt{N * \sum_{m,n}(\boldsymbol{map1}(m,n)^2 - \sum_{m,n}(\boldsymbol{map1}(m,n)^2))} * \sqrt{N * \sum_{m,n}(\boldsymbol{map2}(m-i,n-j)^2 - \sum_{m,n}(\boldsymbol{map2}(m-i,n-j)^2))}}$$

Where **map1** and **map2** are the smoothed firing rate maps and N is the total number of spatial bins.

A1.14 RELATIVE SPATIAL PHASE BETWEEN PAIRS OF GRID CELLS

Relative spatial phase was calculated using the rate map cross-correlation between the rate maps of two grid cells (Figures 2.4, 2.6a, 2.7, 2.8; see Figure 2.4a for a schematic explanation of the method) (similar to a previous study: Yoon et al. 2013). The peak of the cross-correlation map closest to the plot origin was identified, and spatial phase was calculated using the x and y distances from the origin to that peak. The x and y distances were then each normalized by the spatial period, calculated as the distance between the two peaks closest to the origin. Because the distance of least overlap is at one half the spatial period, phases greater than 0.5 were subtracted from 1.0 (e.g., 0.62 becomes 1.00 - 0.62 = 0.38). The phase was then divided by 0.5, giving a final relative spatial phase value that ranged from [0, 1] where [0, 0] indicated maximal overlap between grid fields and [1, 1] indicated minimal overlap between grid fields. The medians of the relative phase values calculated across the three open field sessions were used as the final relative spatial phase values shown in Figure 4. A one-dimensional measure of the relative spatial phase magnitude was also created by taking the Euclidian distance of the x and y relative phases, which spanned the range $[0, \sqrt{2}]$ (Figures 2.5, 2.6a, 2.7, 2.8, 3.5).

Cell pairs in Figure 6 were categorized as “High Overlap” (i.e., low relative spatial phase), “Low Overlap” (i.e., high relative spatial phase), or “Mid Overlap” (i.e., intermediate relative spatial phase) by comparing each cell pair’s relative spatial phase magnitude to the maximum observed relative spatial phase magnitude (which could range in value from 0 to $\sqrt{2}$). Cell pairs with a relative spatial phase magnitude that fell below 30% of the maximum relative spatial phase magnitude were labeled as High Overlap. Cell

pairs with a relative spatial phase magnitude that fell above 70% of the maximum relative spatial phase magnitude were classified as Low Overlap. Cell pairs were assigned to the Mid Overlap group if their relative spatial phase magnitude fell between 40% and 60% of the maximum relative spatial phase magnitude. Cell pairs not assigned to one of these three groups were excluded from results shown in Figure 6. Supplementary Figure 2 used the same criteria for the High Overlap and Low Overlap groups, but did not include a Mid Overlap group.

References

Abbott, L. F., & Dayan, P. (1999). The effect of correlated variability on the accuracy of a population code. *Neural Comput.*, 11(1), 91-101.

Ahmed, O. J., & Mehta, M. R. (2012). Running speed alters the frequency of hippocampal gamma oscillations. *J. Neurosci, 32(21)*, 7373-7383.

Amari, S. (1977). Dynamics of pattern formation in lateral-inhibition type neural fields. *Biol. Cybern. 27*, 77–87.

Anderson, M. I., & Jeffery, K. J. (2003). Heterogeneous modulation of place cell firing by changes in context. *J. Neurosci, 23(26)*, 8827-8835.

Aronov, D., Nevers, R., and Tank, D.W. (2017). Mapping of a non-spatial dimension by the hippocampal-entorhinal circuit. *Nature 543*, 719–722.

Barry, C., Ginzberg, L. L., O'Keefe, J., & Burgess, N. (2012). Grid cell firing patterns signal environmental novelty by expansion. *Proc. Natl. Acad. Sci. U. S. A., 109(43),* 17687-17692.

Bendor, D., & Wilson, M. A. (2012). Biasing the content of hippocampal replay during sleep. *Nat. Neurosci., 15(10)*, 1439-1444.

Bonnevie, T., Dunn, B., Fyhn, M., Hafting, T., Derdikman, D., Kubie, J. L., ... & Moser, M. B. (2013). Grid cells require excitatory drive from the hippocampus. *Nat. Neurosci., 16(3)*, 309-317.

Bostock, E., Muller, R. U., & Kubie, J. L. (1991). Experience-dependent modifications of hippocampal place cell firing. *Hippocampus, 1(2)*, 193-205.

Brandon, M. P., Bogaard, A. R., Libby, C. P., Connerney, M. A., Gupta, K., & Hasselmo, M. E. (2011). Reduction of theta rhythm dissociates grid cell spatial periodicity from directional tuning. *Science, 332(6029)*, 595-599.

Brandon, M.P., Bogaard, A.R., Andrews, C.M., and Hasselmo, M.E. (2012). Head direction cells in the postsubiculum do not show replay of prior waking sequences during sleep. *Hippocampus 22*, 604–618.

Burak, Y., and Fiete, I. (2006). Do we understand the emergent dynamics of grid cell activity? *J. Neurosci. 26*, 9352–9354.

Burak, Y., and Fiete, I.R. (2009). Accurate path integration in continuous attractor network models of grid cells. *PLoS Comput. Biol. 5*, e1000291.

Burgess, N., Barry, C., and O'Keefe, J. (2007). An oscillatory interference model of grid cell firing. *Hippocampus 17*, 801–812.

Burwell, R. D., & Amaral, D. G. (1998a). Cortical afferents of the perirhinal, postrhinal, and entorhinal cortices of the rat. *J. Comp. Neurol. , 398(2)*, 179-205.

Burwell, R. D., & Amaral, D. G. (1998b). Perirhinal and postrhinal cortices of the rat: interconnectivity and connections with the entorhinal cortex. *J. Comp. Neurol. , 391(3)*, 293-321.

Buzsáki, G., & Vanderwolf, C. H. (1983). Cellular bases of hippocampal EEG in the behaving rat. *Brain Research Reviews, 6(2)*, 139-171.

Buzsáki, G. (1986). Hippocampal sharp waves: their origin and significance. *Brain Research, 398(2)*, 242-252.

Buzsáki, G. (1989). Two-stage model of memory trace formation: a role for "noisy" brain states. *Neuroscience, 31(3),* 551-570.

Buzsáki, G. (1996). The hippocampo-neocortical dialogue. *Cerebral Cortex, 6(2)*, 81-92.

Canto, C.B., Wouterlood, F.G., and Witter, M.P. (2008). What does the anatomical organization of the entorhinal cortex tell us? *Neural Plast. 2008*, 381243.

Canto, C. B., & Witter, M. P. (2012). Cellular properties of principal neurons in the rat entorhinal cortex. II. The medial entorhinal cortex. *Hippocampus, 22(6),* 1277-1299.

Chrobak, J. J., & Buzsáki, G. (1996). High-frequency oscillations in the output networks of the hippocampal–entorhinal axis of the freely behaving rat. *J. Neurosci, 16(9)*, 3056-3066.

Colgin, L.L., Moser, E.I., and Moser, M.-B. (2008). Understanding memory through hippocampal remapping. *Trends Neurosci. 31*, 469–477.

Colgin, L. L., Denninger, T., Fyhn, M., Hafting, T., Bonnevie, T., Jensen, O., Moser, M.B. and Moser, E.I. (2009). Frequency of gamma oscillations routes flow of information in the hippocampus. *Nature, 462(7271)*, 353.

Corkin, S. (1965). Tactually-guided maze learning in man: Effects of unilateral cortical excisions and bilateral hippocampal lesions. *Neuropsychologia, 3(4)*, 339-351.

Corkin, S., Amaral, D. G., González, R. G., Johnson, K. A., & Hyman, B. T. (1997). HM's medial temporal lobe lesion: findings from magnetic resonance imaging. *J. Neurosci, 17(10)*, 3964-3979.

Csicsvari, J., Hirase, H., Czurkó, A., Mamiya, A., & Buzsáki, G. (1999). Oscillatory coupling of hippocampal pyramidal cells and interneurons in the behaving rat. *J. Neurosci, 19(1)*, 274-287.

Couey, J.J., Witoelar, A., Zhang, S.-J., Zheng, K., Ye, J., Dunn, B., Czajkowski, R., Moser, M.-B., Moser, E.I., Roudi, Y., et al. (2013). Recurrent inhibitory circuitry as a mechanism for grid formation. *Nat. Neurosci. 16*, 318–324.

Davidson, T. J., Kloosterman, F., & Wilson, M. A. (2009). Hippocampal replay of extended experience. *Neuron, 63(4)*, 497-507.

Dhillon, A., and Jones, R.S. (2000). Laminar differences in recurrent excitatory transmission in the rat entorhinal cortex in vitro. *Neuroscience 99*, 413–422.

Dolorfo, C. L., & Amaral, D. G. (1998). Entorhinal cortex of the rat: organization of intrinsic connections. *J. Comp. Neurol. , 398(1)*, 49-82.

Domnisoru, C., Kinkhabwala, A. A., & Tank, D. W. (2013). Membrane potential dynamics of grid cells. *Nature, 495(7440),* 199-204.

Dragoi, G., & Buzsáki, G. (2006). Temporal encoding of place sequences by hippocampal cell assemblies. *Neuron, 50(1)*, 145-157.

Ego-Stengel, V., & Wilson, M. A. (2010). Disruption of ripple-associated hippocampal activity during rest impairs spatial learning in the rat. *Hippocampus, 20(1),* 1-10.

Euston, D.R., Tatsuno, M., and McNaughton, B.L. (2007). Fast-forward playback of recent memory sequences in prefrontal cortex during sleep. *Science 318*, 1147–1150.

Foster, D. J., & Wilson, M. A. (2006). Reverse replay of behavioural sequences in hippocampal place cells during the awake state. *Nature, 440(7084),* 680-683.

Fuchs, E.C., Neitz, A., Pinna, R., Melzer, S., Caputi, A., and Monyer, H. (2016). Local and Distant Input Controlling Excitation in Layer II of the Medial Entorhinal Cortex. *Neuron 89*, 194–208.

Fuhs, M.C., and Touretzky, D.S. (2006). A spin glass model of path integration in rat medial entorhinal cortex. *J. Neurosci. 26*, 4266–4276.

Fyhn, M., Hafting, T., Treves, A., Moser, M.-B., and Moser, E.I. (2007). Hippocampal remapping and grid realignment in entorhinal cortex. *Nature 446*, 190–194.

Gardner, R. J., & Moser, M. (2017). Multiple mechanisms for memory replay? *Science, 355(6321)*, 131-132. doi:10.1126/science.aam5404

Geisler, C., Robbe, D., Zugaro, M., Sirota, A., and Buzsáki, G. (2007). Hippocampal place cell assemblies are speed-controlled oscillators. *Proc. Natl. Acad. Sci. U. S. A. 104*, 8149–8154.

Girardeau, G., Benchenane, K., Wiener, S. I., Buzsáki, G., & Zugaro, M. B. (2009). Selective suppression of hippocampal ripples impairs spatial memory. *Nat. Neurosci., 12(10)*, 1222-1223.

Gothard, K.M., Skaggs, W.E., Moore, K.M., and McNaughton, B.L. (1996). Binding of hippocampal CA1 neural activity to multiple reference frames in a landmark-based navigation task. *J. Neurosci. 16*, 823–835.

Grossberg, S., and Pilly, P.K. (2012). How entorhinal grid cells may learn multiple spatial scales from a dorsoventral gradient of cell response rates in a self-organizing map. *PLoS Comput. Biol. 8*, e1002648.

Guanella, A., and Verschure, P.F.M.J. (2006). A Model of Grid Cells Based on a Path Integration Mechanism. In Artificial Neural Networks – *ICANN 2006, (Springer, Berlin, Heidelberg)*, pp. 740–749.

Hafting, T., Fyhn, M., Molden, S., Moser, M.-B., and Moser, E.I. (2005). Microstructure of a spatial map in the entorhinal cortex. *Nature 436*, 801–806.

Hafting, T., Fyhn, M., Bonnevie, T., Moser, M.-B., and Moser, E.I. (2008). Hippocampus-independent phase precession in entorhinal grid cells. *Nature 453*, 1248–1252.

Hales, J. B., Schlesiger, M. I., Leutgeb, J. K., Squire, L. R., Leutgeb, S., & Clark, R. E. (2014). Medial entorhinal cortex lesions only partially disrupt hippocampal place cells and hippocampus-dependent place memory. *Cell reports, 9(3),* 893-901.

Hardcastle, K., Ganguli, S., & Giocomo, L. M. (2015). Environmental boundaries as an error correction mechanism for grid cells. *Neuron, 86(3),* 827-839.

Hardcastle, K., Maheswaranathan, N., Ganguli, S., and Giocomo, L.M. (2017). A Multiplexed, Heterogeneous, and Adaptive Code for Navigation in Medial Entorhinal Cortex. *Neuron 94*, 375–387.

Hu, Y., Zylberberg, J., & Shea-Brown, E. (2014). The sign rule and beyond: boundary effects, flexibility, and noise correlations in neural population codes. *PLoS Comput. Biol.*, 10(2), e1003469.

Ikegaya, Y., Aaron, G., Cossart, R., Aronov, D., Lampl, I., Ferster, D., & Yuste, R. (2004). Synfire chains and cortical songs: temporal modules of cortical activity. *Science, 304(5670),* 559-564.

Insausti, R., Amaral, D. G., & Cowan, W. M. (1987). The entorhinal cortex of the monkey: II. Cortical afferents. *J. Comp. Neurol. , 264(3),* 356-395.

Insausti, R., Herrero, M., & Witter, M. P. (1997). Entorhinal cortex of the rat: cytoarchitectonic subdivisions and the origin and distribution of cortical efferents. *Hippocampus, 7(2),* 146-183.

Jadhav, S. P., Kemere, C., German, P. W., & Frank, L. M. (2012). Awake hippocampal sharp-wave ripples support spatial memory. *Science, 336(6087)*, 1454-1458.

Ji, D., and Wilson, M.A. (2007). Coordinated memory replay in the visual cortex and hippocampus during sleep. *Nat. Neurosci. 10*, 100–107.

Karlsson, M. P., & Frank, L. M. (2009). Awake replay of remote experiences in the hippocampus. *Nat. Neurosci., 12(7),* 913-918.

Köhler, C. (1986). Intrinsic connections of the retrohippocampal region in the rat brain. II. The medial entorhinal area. *J. Comp. Neurol. , 246(2),* 149-169.

Killian, N.J., Jutras, M.J., and Buffalo, E.A. (2012). A map of visual space in the primate entorhinal cortex. *Nature 491*, 761–764.

Koenig, J., Linder, A. N., Leutgeb, J. K., & Leutgeb, S. (2011). The spatial periodicity of grid cells is not sustained during reduced theta oscillations. *Science, 332(6029),* 592-595.

Kraus, B.J., Brandon, M.P., Robinson, R.J., 2nd, Connerney, M.A., Hasselmo, M.E., and Eichenbaum, H. (2015). During Running in Place, Grid Cells Integrate Elapsed Time and Distance Run. *Neuron 88*, 578–589.

Kropff, E., Carmichael, J.E., Moser, M.-B., and Moser, E.I. (2015). Speed cells in the medial entorhinal cortex. *Nature 523*, 419–424.

Kudrimoti, H.S., Barnes, C.A., and McNaughton, B.L. (1999). Reactivation of hippocampal cell assemblies: effects of behavioral state, experience, and EEG dynamics. *J. Neurosci. 19*, 4090–4101.

Lee, A.K., and Wilson, M.A. (2002). Memory of sequential experience in the hippocampus during slow wave sleep. *Neuron 36*, 1183–1194.

Louie, K., and Wilson, M.A. (2001). Temporally structured replay of awake hippocampal ensemble activity during rapid eye movement sleep. *Neuron 29*, 145–156.

McNaughton, B.L., Battaglia, F.P., Jensen, O., Moser, E.I., and Moser, M.-B. (2006). Path integration and the neural basis of the “cognitive map.” *Nat. Rev. Neurosci. 7*, 663–678.

Milner, B., Corkin, S., & Teuber, H. L. (1968). Further analysis of the hippocampal amnesic syndrome: 14-year follow-up study of HM. *Neuropsychologia, 6(3),* 215-234.

Mitchell, S.J., and Ranck, J.B., Jr (1980). Generation of theta rhythm in medial entorhinal cortex of freely moving rats*. Brain Res. 189*, 49–66.

Mizuseki, K., Sirota, A., Pastalkova, E., & Buzsáki, G. (2009). Theta oscillations provide temporal windows for local circuit computation in the entorhinal-hippocampal loop. *Neuron, 64(2),* 267-280.

Morris, R. G. M., Garrud, P., Rawlins, J. A., & O'Keefe, J. (1982). Place navigation impaired in rats with hippocampal lesions. *Nature, 297(5868),* 681-683.

Moser, E., Moser, M. B., & Andersen, P. (1993). Spatial learning impairment parallels the magnitude of dorsal hippocampal lesions, but is hardly present following ventral lesions. *J. Neurosci, 13(9)*, 3916-3925.

Moser, E.I., Roudi, Y., Witter, M.P., Kentros, C., Bonhoeffer, T., and Moser, M.-B. (2014). Grid cells and cortical representation. *Nat. Rev. Neurosci. 15*, 466–481.

Muller, R. U., & Kubie, J. L. (1987). The effects of changes in the environment on the spatial firing of hippocampal complex-spike cells. *J. Neurosci, 7(7),* 1951-1968.

Nádasdy, Z., Hirase, H., Czurkó, A., Csicsvari, J., and Buzsáki, G. (1999). Replay and time compression of recurring spike sequences in the hippocampus. *J. Neurosci. 19,* 9497–9507.

Navratilova, Z., Giocomo, L.M., Fellous, J.-M., Hasselmo, M.E., and McNaughton, B.L. (2012). Phase precession and variable spatial scaling in a periodic attractor map model of medial entorhinal grid cells with realistic after-spike dynamics*. Hippocampus 22*, 772–789.

O’Keefe, J., and Dostrovsky, J. (1971). The hippocampus as a spatial map. Preliminary evidence from unit activity in the freely-moving rat. *Brain Res. 34*, 171–175.

Ólafsdóttir, H.F., Carpenter, F., and Barry, C. (2016). Coordinated grid and place cell replay during rest. *Nat. Neurosci. 19*, 792–794.

O'Neill, J., Senior, T. J., Allen, K., Huxter, J. R., & Csicsvari, J. (2008). Reactivation of experience-dependent cell assembly patterns in the hippocampus. *Nat. Neurosci., 11(2)*, 209.

O'Neill, J., Boccara, C.N., Stella, F., Schoenenberger, P., and Csicsvari, J. (2017). Superficial layers of the medial entorhinal cortex replay independently of the hippocampus. *Science 355*, 184–188.

Parkinson, J. K., Murray, E. A., & Mishkin, M. (1988). A selective mnemonic role for the hippocampus in monkeys: memory for the location of objects. *J. Neurosci, 8(11),* 4159-4167.

Pastoll, H., Solanka, L., van Rossum, M.C.W., and Nolan, M.F. (2013). Feedback Inhibition Enables Theta-Nested Gamma Oscillations and Grid Firing Fields. *Neuron 77*, 141–154.

Peyrache, A., Khamassi, M., Benchenane, K., Wiener, S. I., & Battaglia, F. P. (2009). Replay of rule-learning related neural patterns in the prefrontal cortex during sleep. *Nat. Neurosci., 12(7)*, 919-926.

Peyrache, A., Lacroix, M.M., Petersen, P.C., and Buzsáki, G. (2015). Internally organized mechanisms of the head direction sense. *Nat. Neurosci. 18*, 569–575.

Plihal, W., & Born, J. (1997). Effects of early and late nocturnal sleep on declarative and procedural memory. *Journal of Cognitive Neuroscience, 9(4)*, 534-547.

Ranck Jr, J. B. (1973). Studies on single neurons in dorsal hippocampal formation and septum in unrestrained rats: Part I. Behavioral correlates and firing repertoires. *Experimental Neurology, 41(2),* 462-531.

Rasch, B., & Born, J. (2013). About Sleep's Role in Memory. *Physiological Reviews, 93(2),* 681-766.

Rothschild, G., Eban, E., and Frank, L.M. (2017). A cortical-hippocampal-cortical loop of information processing during memory consolidation. *Nat. Neurosci. 20*, 251–259.

Sargolini, F., Fyhn, M., Hafting, T., McNaughton, B.L., Witter, M.P., Moser, M.-B., and Moser, E.I. (2006). Conjunctive representation of position, direction, and velocity in entorhinal cortex. *Science 312*, 758–762.

Saunders, R. C., & Rosene, D. L. (1988). A comparison of the afferents of the amygdala and the hippocampal formation in the rhesus monkey: I. Convergence in the entorhinal, prorhinal, and perirhinal cortices. *J. Comp. Neurol., 271(2),* 153-184.

Schmidt-Hieber, C., & Häusser, M. (2013). Cellular mechanisms of spatial navigation in the medial entorhinal cortex. *Nat. Neurosci., 16(3)*, 325-331.

Schwartz, S. P., & Coleman, P. D. (1981). Neurons of origin of the perforant path. *Experimental Neurology, 74(1),* 305-312.

Scoville, W. B., & Milner, B. (1957). Loss of recent memory after bilateral hippocampal lesions. *Journal of Neurology, Neurosurgery, and Psychiatry, 20(1)*, 11.

Sirota, A., Csicsvari, J., Buhl, D., & Buzsáki, G. (2003). Communication between neocortex and hippocampus during sleep in rodents. *Proc. Natl. Acad. Sci. U. S. A., 100(4),* 2065-2069.

Skaggs, W. E., & McNaughton, B. L. (1996). Replay of neuronal firing sequences in rat hippocampus during sleep following spatial experience. *Science, 271(5257)*, 1870.

Smith, M. L., & Milner, B. (1981). The role of the right hippocampus in the recall of spatial location. *Neuropsychologia, 19(6),* 781-793.

Solstad, T., Boccara, C.N., Kropff, E., Moser, M.-B., and Moser, E.I. (2008). Representation of geometric borders in the entorhinal cortex. *Science 322*, 1865–1868.

Squire, L. R., & Zola-Morgan, S. (1991). The medial temporal lobe memory system. *Science, 253(5026),* 1380.

Stensola, H., Stensola, T., Solstad, T., Frøland, K., Moser, M. B., & Moser, E. I. (2012). The entorhinal grid map is discretized. *Nature, 492(7427)*, 72-78.

Steward, O., and Scoville, S.A. (1976). Cells of origin of entorhinal cortical afferents to the hippocampus and fascia dentata of the rat. *J. Comp. Neurol. 169*, 347–370.

Sun, C., Kitamura, T., Yamamoto, J., Martin, J., Pignatelli, M., Kitch, L. J., ... & Tonegawa, S. (2015). Distinct speed dependence of entorhinal island and ocean cells, including respective grid cells. *Proc. Natl. Acad. Sci. U. S. A., 112(30),* 9466-9471.

Tallon-Baudry, C., Bertrand, O., Delpuech, C., & Pernier, J. (1997). Oscillatory γ-band (30–70 Hz) activity induced by a visual search task in humans. J*. Neurosci, 17(2),* 722-734.

Tang, W., Shin, J. D., Frank, L. M., & Jadhav, S. P. (2017). Hippocampal-prefrontal reactivation during learning is stronger in awake as compared to sleep states. *J. Neurosci*, 2291-17.

Taube, J.S., Muller, R.U., and Ranck, J.B., Jr (1990). Head-direction cells recorded from the postsubiculum in freely moving rats. I. Description and quantitative analysis. *J. Neurosci. 10*, 420–435.

Taylor, J. G. (1999). Neural 'bubble'dynamics in two dimensions: foundations. *Biol. Cybern*., 80(6), 393-409.

Trimper, J. B., Trettel, S. G., Hwaun, E., & Colgin, L. L. (2017). Methodological Caveats in the Detection of Coordinated Replay between Place Cells and Grid Cells. *Frontiers in Systems Neuroscience*, 11.

Tsodyks, M., Kenet, T., Grinvald, A., & Arieli, A. (1999). Linking spontaneous activity of single cortical neurons and the underlying functional architecture. *Science, 286(5446)*, 1943-1946.

Van Cauter, T., Poucet, B., & Save, E. (2008). Unstable CA1 place cell representation in rats with entorhinal cortex lesions. *European J. Neurosci, 27(8),* 1933-1946.

Van Groen, T., Van Haren, F. J., Witter, M. P., & Groenewegen, H. J. (1986). The organization of the reciprocal connections between the subiculum and the entorhinal cortex in the cat: I. A neuroanatomical tracing study. *J. Comp. Neurol., 250(4),* 485-497.

Van Groen, T., & Wyss, J. M. (1990). Extrinsic projections from area CA1 of the rat hippocampus: olfactory, cortical, subcortical, and bilateral hippocampal formation projections. *J. Comp. Neurol., 302(3),* 515-528.

Van Hoesen, G. W., Pandya, D. N., & Butters, N. (1972). Cortical afferents to the entorhinal cortex of the rhesus monkey. *Science, 175(4029),* 1471-1473.

Welinder, P.E., Burak, Y., and Fiete, I.R. (2008). Grid cells: the position code, neural network models of activity, and the problem of learning. *Hippocampus 18,* 1283–1300.

Widloski, J., & Fiete, I. R. (2015). Cortical microcircuit determination through global perturbation and sparse sampling in grid cells. *bioRxiv,* 019224.

Wilson, M.A., and McNaughton, B.L. (1994). Reactivation of hippocampal ensemble memories during sleep. *Science 265*, 676–679.

Witter, M. P., Wouterlood, F. G., Naber, P. A., & Van Haeften, T. (2000). Anatomical organization of the parahippocampal-hippocampal network. *Annals of the New York Academy of Sciences, 911(1)*, 1-24.

Yartsev, M. M., Witter, M. P., & Ulanovsky, N. (2011). Grid cells without theta oscillations in the entorhinal cortex of bats. *Nature, 479(7371),* 103-107.

Yartsev, M.M., and Ulanovsky, N. (2013). Representation of three-dimensional space in the hippocampus of flying bats. *Science 340*, 367–372.

Yoon, K., Buice, M.A., Barry, C., Hayman, R., Burgess, N., and Fiete, I.R. (2013). Specific evidence of low-dimensional continuous attractor dynamics in grid cells. *Nat. Neurosci. 16*, 1077–1084.

Yoon, K., Lewallen, S., Kinkhabwala, A.A., Tank, D.W., and Fiete, I.R. (2016). Grid Cell Responses in 1D Environments Assessed as Slices through a 2D Lattice. *Neuron 89*, 1086–1099.

Zhang, S.-J., Ye, J., Miao, C., Tsao, A., Cerniauskas, I., Ledergerber, D., Moser, M.-B., and Moser, E.I. (2013). Optogenetic dissection of entorhinal-hippocampal functional connectivity. *Science 340*, 1232627.

Zheng, C., Bieri, K. W., Trettel, S. G., & Colgin, L. L. (2015). The relationship between gamma frequency and running speed differs for slow and fast gamma rhythms in freely behaving rats. *Hippocampus, 25(8),* 924-938.